Dynamic Learning and Resource Management under Uncertainties for Smart Grid and Cognitive Radio Networks

---

A DISSERTATION

SUBMITTED TO THE FACULTY OF THE GRADUATE SCHOOL

OF THE UNIVERSITY OF MINNESOTA

BY

Nasim Yahyasoltani (Yahya Soltani)

IN PARTIAL FULFILLMENT OF THE REQUIREMENTS

FOR THE DEGREE OF

DOCTOR OF PHILOSOPHY

Professor Georgios B. Giannakis, Advisor

May 2014

Acknowledgments

First and foremost, my deepest gratitude goes to my Ph.D. advisor Prof. Georgios B. Giannakis. I would like to thank him for giving me the opportunity to pursue my Ph.D in the SPINCOM group at the University of Minnesota, a real privilege for which I am really honored. Most of what I have learned in the past four years is a direct result of his intuition, and honest critique. This would not have been possible without all his constant support and encouragement.

Due thanks go to Profs. Mostafa Kaveh, Shuzhong Zhang, Nikos Sidiropoulos, and Sairaj Dhople for agreeing to serve on my committee.

I am also grateful to Prof. William P. Robbins who gave me the opportunity to teach some classes, which were instrumental in shaping my career. I would also like to acknowledge the grants that support financially our research.

In this thesis, I have benefited from discussions with the current and former members of SPiNCOM: Prof. Seung-Jun Kim, Morteza Mardani, Brian Baingana, Prof. Gonzalo Mateos, Prof. Ketan Rajawat, Dr. Vassilis Kekatos, Dr. Eric Msechu, Dr. Pedro Forero, Dr. Juan Andrs Bazerque, Prof. Nikos Gatsis, Prof. Ioannis Schizas, Prof. Hao Zhu, Prof. Antonio G. Marques, Dr. Emiliano Dall'Anese, and Yu Zhang.

My thanks go to Dr. Shahrokh Farahmand whose help I can not forget during my first days in Minneapolis and guidance throughout the years we overlapped in Minneapolis. I would also like to extend my appreciation to Meisam Razaviyayn, Morteza Mardani, and Brian Baingana for providing me immediate help when I needed it.

I would like to thank my amazing husband, Dr. Masoud Ganji, for his love, understanding, and support throughout these four years. You have always tried your best to keep me motivated and excited - I do have fond memories of you looking for "hot" topics in my major that you excitedly discussed with me. I appreciate your patience enduring through our long-distance marriage, yet remaining a very strong pillar who has always been the source of my efficiency and productivity through the years of graduate studies. Thank you for your incessant support and devotion, I can not wait to join you in Wisconsin.

I thank my brother Navid, whom I can always count on. Thanks for all your love and support. And last, but not least I would like to express my utmost gratitude to my parents Alireza Yahya Soltani and Nayereh Mortazavi for their endless love and devotion. You gave me the love, support, and confidence to go onto this journey. In my most difficult times, a few encouraging words from you made me confident enough to proceed. I could not

imagine getting here without your love and sacrifice. I can not pay back all the sacrifices you made for me, but as the smallest token of my appreciation, I dedicate this thesis to you.

Nasim Yahyasoltani, Minneapolis, May 2014.

I dedicate this thesis to my parents:
Alireza Yahya Soltani and Nayereh Mortazavi
for all their sacrifices

Abstract

The importance of timely applications and decisions in dynamic environments, has led to the integration of intelligent networks to increase efficiency and end-user satisfaction in various application domains including telecommunication and power grid networks. Contemporary intelligent networks require advanced statistical signal processing and optimization tools to learn, infer and control their operation. This integration poses new challenges and has witnessed the emergence of novel resource management and learning techniques to cope with dynamics. In addition, in order to have implementable resource management algorithms, it is crucial to model the underlying sources of uncertainty in the optimization framework. This thesis develops algorithms for resource allocation under channel uncertainty in cognitive radio (CR) communication networks and contributes to demand coordination under uncertainty in power networks.

Demand coordination through real-time pricing is addressed first by capitalizing on the uncertainty involved in the consumption behavior of consumers. Prerequisite to the demand coordination task is learning the uncertainty present in power consumption data. The dependency of consumers' consumption behavior on the announced prices and their neighbors' behavior, is modeled through graphical models. In particular, the electric vehicle (EV) consumers are considered and the adopted model also captures dynamics of EV consumers' time-varying charging decisions. Leveraging the online convex optimization (OCO) framework, an online algorithm for tracking the model is devised. With minimal assumptions on the structure of the temporal dynamics, and while accounting for the possibly adversarial consumption behavior of consumers, the proposed online algorithm provides performance guarantees. The probability distributions obtained through the tracking algorithm are then deployed as input to stochastic economic profit maximization for real-time price setting.

Learning in the presence of missing data is a pervasive problem in statistical data analysis. Next, attention is turned to tracking the dynamic charging behavior of EV consumers, when at each time slot some of the consumers' consumption decisions are possibly missing. The problem amounts to online classification with missing labels. An online algorithm is proposed to wed real-time estimation of the missing data with learning of complete data in the OCO framework.

As regards CR networks, this thesis introduces novel resource allocation algorithms for orthogonal frequency-division multiple access (OFDMA) CR under channel uncertainty where the unique approaches can be fitted to a class of large-scale robust mixed-integer

problems. Due to the lack of cooperation of the licensed system, CRs must resort to less efficient channel estimation techniques thus incurring an inevitable channel estimation error. It is shown that CR interference constraints under channel uncertainty can be cast as chance constraints. On the other hand, instead of just modeling the user rates by logarithmic functions of transmit-powers, justified under ideal Gaussian coding, practical finite-alphabet constellations are adopted which leads to an optimization objective of a weighted sum of mutual information. When multiple users are present, due to the combinatorial search for optimal subcarrier assignment, the problem is non-convex and hard to solve, as the optimization variables are coupled across all subcarriers. To circumvent the resulting computational hurdle, tight and conservative approximations of the chance constraint are introduced to break the coupling and enforce separability per subcarrier. The *separable* problem across subcarriers opens the door to the dual decomposition approach, which leads to a near-optimal and computationally efficient solution.

Contents

List of Figures

List of Tables

Chapter 1

Introduction

1.1 Motivation and Context

Resource management is a vital task in different application domains, including power grid and telecommunication networks, because it is concerned with the utilization and allocation of available resources.

Under the assumption that the system model parameters and input data are certain, the optimal solution to resource allocation offers what one could term as "nominal" solution. However, in practice, the input data and the model parameters are obtained from measurements or predictions that inevitably incur errors and uncertainty. Hence, deploying the nominal solutions into real-world scenarios makes the implementation infeasible.

There are two main approaches that are typically considered for optimization with uncertain parameters [37]. When the uncertain parameters are regarded as random, statistical knowledge such as their mean and covariance, or their distribution is assumed, which leads to probabilistic formulations. A deterministic alternative is to adopt a robust optimization framework, where a bounded uncertainty region is postulated. In certain cases, the two approaches can be shown to be intimately related [5]. In addition, to capture the stochastic nature and interdependencies of data, a general methodology is built upon probabilistic models that can accommodate uncertainty and statistical errors associated with the data. Probabilistic graphical models combine graph theory with probability theory to yield an

encompassing multivariate statistical modeling approach [55].

Recent advances in the so-termed smart grid embrace information technologies for the electrical power network to address the aging infrastructure challenges. The objective and features of the smart grid vision are fourfold: (a) two-way communication; (b) advanced monitoring and optimization; (c) integration of renewables and electric vehicles (EVs); and (d) environmental awareness and sustainability. Through a two-way communication, the utility company aims at an optimal coordination of the generation and load demand to ensure high consumer satisfaction and guaranteed reliability in addition to making some revenue. Prerequisite to the demand coordination task is availability of reliable analytics, i.e., it is instrumental to learn the consumers' consumption patterns and model the uncertainty in power consumption data. In addition, the consumption patterns of the consumers are time-varying which needs to be accounted for in order to obtain a reliable demand coordination.

By the same token, growing demands for higher data rate in wireless communications to support high quality-of-service multimedia applications, necessitate an optimal management of resources. In order to utilize a large swath of bandwidth efficiently, the intelligent technology of cognitive radio (CR) networks has been introduced. CRs can be unlicensed users that need to acquire the information of the RF operational environment in order to smartly coordinate, manage resources and follow the spectral changes in order to mitigate any interference caused to the spectrum license holders. Furthermore, as the license holder system is usually unaware of CRs operation, there is no cooperation from the primary user (PU) system in the channel estimation which leads to some channel uncertainty. The literature in CR resource management is extensive [67], [65], [14], [58]. However, deploying orthogonal frequency-division multiple access (OFDMA) as an efficient technique for CR technology, makes the resource allocation under uncertainty a non-trivial task.

This thesis develops models and algorithms for efficient resource management under uncertainty in both smart power grid and CR networks. In addition, online algorithms are devised to learn the temporal variations and the dynamics of the underlying network structure. The particular motivation, context, tools, and contributions of this thesis are

described in Section 1.2 for the smart power grid context, and in Section 1.3 for the CR network paradigm.

1.2 Resource Allocation in Power Grid Networks

The power grid consists of three major functional components: (i) the electricity generation facilities; (ii) the transmission lines, which transfer electricity from the generation part to the neighborhoods; and (iii) the distribution network, which uses distribution lines to bring electricity to the customers. The connections between these parts are made at the substations. The main feature of the smart grid is the existence of a two-way communication between the utility company and the customers. In fact, through smart meters in consumers premises the utility company is updated of the detailed consumption information such as time-of-use.

Recently, there has been also growing interest in electric vehicles (EVs), which are expected to be widely deployed by 2050 [28]. EV penetration may contribute to alleviating dependence on fossil fuel and drastically reducing greenhouse gas emissions. EV owners may also benefit from lower energy cost in the face of spiking gasoline prices.

Currently, there are three levels of charging EVs. Level 1 charging is the slowest and supports 120V sockets for charging. Level 2 is faster and uses 240V sockets. Level 1 and 2 are both considered as AC chargers. Level 3, also known as fast charging, is much faster than the other two levels. In level 3 a DC charger converts AC to DC off the car [68].

Despite the fact that the EVs are considered as elastic load in the network (since, their charging time can be quite flexible), uncoordinated EV charging can aggravate load peaks due to, e.g., concentrated charging demand before commuting hours, resulting in higher generation cost for the utility company to avoid shortages. EV charging impacts on the power grid have been addressed in [39], [33], [13].

Clearly, it is advantageous for the utility company to have EV consumers charge their vehicles during periods that the renewable generation output is high. Therefore, charging coordination of EVs in the smart grid network is a crucial task.

1.2.1 Online Learning of Consumption Behavior of EV Consumer

Charging coordination of EVs is vital for the smart grid network operation. In order to elicit desirable electricity consumption patterns, various time-based pricing schemes have been proposed. By allowing the electricity price to vary over different hours of a day, consumers are encouraged to shift inessential loads to the periods of low prices, which generally correspond to off-peak hours [38]. There is extensive literature on scheduling the time and rate of EV charging [17–19, 36, 45, 46, 53]. Generation and EV charging costs were minimized in [46] under power flow constraints. With the goal of shifting EV loads to fill the overnight demand valley, a distributed algorithm for day-ahead charging rate schedules was proposed in [18]. The EV charging schedule was optimized in [53] by minimizing load variance and maximizing load factor.

Prerequisite to the demand coordination task is availability of reliable analytics. In addition to essential loads and price forecasting, it is instrumental also to learn the consumers' behavioral patterns. In [22], smart grid consumers' price elasticity was estimated using a linear regression model with price changes as regressors and the corresponding shift in total demand as the response. The price responsiveness is useful, for instance, when one desires to set the prices optimally with various objectives such as minimizing the generation cost or maximizing revenue of the utility company.

However, existing techniques for acquiring price elasticity fall short of capturing the following important aspects. First, the dynamics of consumer preferences over time have been not accounted for. In practice, price elasticity might change abruptly and even in an adversarial manner, as the consumers may also react so as to maximize their own profit. Secondly, the spatial dependencies of consumer behaviors, e.g., the correlations present in the behaviors of consumers in geographic proximity, have not been exploited.

Chapter 2 addresses the problem of estimating the probability with which each consumer will charge his/her EV, paying the announced price and given all the past prices and the corresponding observed behaviors, while accounting for possible spatial dependencies among consumption behavior of consumers. The adopted model captures the dependency of EV consumers' charging decisions on the announced electricity price. As the charging

decisions can be best described by discrete values (e.g., "charging" or "not charging"), a logistic regression-type framework is employed. To capture the stochastic nature and interdependencies of consumption behavior of consumers, the dependency structure is encoded as a graph, and the overall model corresponds to a conditional random field (CRF) [32].

CRF model

Graphical models are powerful tools for analyzing the interdependencies among a large number of random variables defined over graphs to represent their conditional dependence. Consider an undirected graph $G = (V, E)$, where the vertex set $V := \{1, 2, \ldots, M\}$ corresponds to the nodes in the graph, and edges $(i, j) \in E$ capture the proximity between nodes i and j. Collect in vectors $\mathbf{b}^t$ and $\boldsymbol{\rho}^t$ variables $\{b_i^t\}_{i=1}^M$ as labels and $\{\rho_i^t\}_{i=1}^M$ as input features, respectively. The CRF models the conditional probability distribution function (*pdf*) $p(\mathbf{b}^t|\boldsymbol{\rho}^t)$. In short, $p(\mathbf{b}^t|\boldsymbol{\rho}^t)$ is a CRF with respect to G if it obeys the Markov property for every $\boldsymbol{\rho}^t$. This means that conditioned on $\boldsymbol{\rho}^t$, for any $i, j \in V$, label b_i^t is independent of label b_j^t given the neighbors $\{b_k^t : (i, k) \in E\}$. Intuitively, this means that given the features $\boldsymbol{\rho}^t$, the neighbors of b_i^t contain all the information needed for predicting b_i^t, and other variables are irrelevant.

Let $\boldsymbol{\psi}_{i,j}(b_i^t, b_j^t)$ denote feature functions quantifying the dependency between nodes i and j. In addition, functions $\boldsymbol{\phi}_i(b_i^t, \rho_i^t)$ model the dependency of b_i^t on the input variable ρ_i^t. Parameters $\boldsymbol{\theta}_i^t$ and $\boldsymbol{\theta}_{i,j}^t$ are introduced for $\boldsymbol{\phi}_i$ and $\boldsymbol{\psi}_{i,j}$, respectively, to capture the strengths of these dependencies. With $\boldsymbol{\theta}^t := [\boldsymbol{\theta}_i^t, \boldsymbol{\theta}_{i,j}^t]$, the conditional *pdf* can thus be modeled as

$$p_{\boldsymbol{\theta}^t}(\mathbf{b}^t|\boldsymbol{\rho}^t) = \frac{1}{Z(\boldsymbol{\rho}^t)} \prod_{i \in V} e^{\langle \boldsymbol{\theta}_i^t, \boldsymbol{\phi}_{\boldsymbol{i}}(b_i^t, \rho_i^t) \rangle} \prod_{(i,j) \in E} e^{\langle \boldsymbol{\theta}_{i,j}^t, \boldsymbol{\psi}_{i,j}(b_i^t, b_j^t) \rangle} \tag{1.1}$$

where $\langle \cdot, \cdot \rangle$ denotes the inner product, and

$$Z(\boldsymbol{\rho}^t) := \sum_{\mathbf{b}^t \in \mathcal{S}^{\mathcal{N}}} \prod_{i \in V} e^{\langle \boldsymbol{\theta}_i^t, \boldsymbol{\phi}_{\boldsymbol{i}}(b_i^t, \rho_i^t) \rangle} \prod_{(i,j) \in E} e^{\langle \boldsymbol{\theta}_{i,j}^t, \boldsymbol{\psi}_{i,j}(b_i^t, b_j^t) \rangle} \tag{1.2}$$

is a normalization factor, also known as the partition function. Computing the partition function incurs high computational complexity, especially as the number of nodes increases. For instance, in a binary labeling case, the computation of the partition function involves a summation of 2^M terms. However, there are techniques for approximating the partition function in an efficient manner [61].

In terms of algorithm implementation, online algorithms are preferred over batch alternatives for real-time streaming analytics. In addition, as the consumers may also act strategically to maximize their own benefit (and mend their price responsiveness accordingly), the online algorithm should provide performance guarantee even in an "adversarial" setting. Furthermore, the consumers' charging decisions are typically correlated across time in practice. In this thesis, an online algorithm is developed to estimate the relevant model parameters, based on an online convex optimization (OCO) framework, which provides performance guarantees with minimal assumptions on the structure of temporal dynamics [44]. The proposed algorithm yields probability distributions and a belief propagation (BP) iteration to effect a message passing algorithm for efficient computation of marginal probabilities. As explained next, the probability distributions are then used as input for stochastic economic dispatch or revenue maximization.

1.2.2 Real-time Price Setting

Chapter 2, introduced models and algorithms to capture the consumers' charging decisions. Since the CRF model provides the probability distribution of the charging decisions given the prices, one can subsequently formulate a risk-limiting stochastic optimization problem to tailor the EV charging demand in some desirable fashion. Here, for simplicity, a price setting formulation is considered to maximize the utility's net profit, which is the utility's revenue collected from the customers minus the power generation cost.

There are prior works on stochastic revenue maximization accounting for elasticity and load uncertainty in real-time pricing [62], [56]. A demand elasticity model is considered in [62] to optimize the utility function (area under price-demand curve) and minimize the generation costs for real-time pricing. However, in addition to ignoring consumption dependencies of consumers, the parameters of the load elasticity model are assumed to be known and are not learned over time. Real-time pricing in [56] entails maximization of utility minus cost functions. To capture load uncertainty however, the load is modeled with a typical load plus a random variable. By online learning of the consumers' price responsiveness and their consumption dependency, while allowing for strategic action of consumers, Chapter 2

introduces a new approach for an optimal control of consumers total charging consumption with the pertinent goal of maximizing revenue.

1.2.3 Online Learning with Missing Data

Chapter 3 deals with the case when some of the consumers' charging decisions are missing. Missing data occur in a broad range of application domains including the smart grid. In practice, due to experimental limitations and errors only a portion of the data of large networks can be observed. Hence, it is instrumental to develop algorithms that can learn from partially observed data. CRF models are usually trained by maximizing the log-likelihood of completely labeled training data (pairs of input and output). Missing data are problematic and the most common approach is to drop the variables with missing labels in the algorithm. In practice, this is restrictive as it may result in biased results.

This chapter adopts a CRF framework to model the dependency of EV consumers' charging decisions as in Chapter 2. It is assumed that incomplete charging decisions of consumers which belong to an associated set of binary decisions (e.g., "charging" or "not charging") are sequentially observed by the utility company. At each time step, the observed charging decisions include misses, where the number and locations of the misses may even change over time. Then, with an inference of the misses per time t, an online learning algorithm in an OCO framework is developed to estimate the relevant model parameters, which allows for strategic behavior of consumers [44].

1.3 Resource Allocation in Uncertain CR-OFDMA Networks

Due to the increasing demand for high-speed wireless data access, efficient utilization of the limited frequency spectrum has become crucial. The cognitive radio (CR) technology puts forth a promising proposal to mitigate the scarcity of spectral resources by allowing unlicensed transmitters to use underutilized licensed bands in an opportunistic fashion. To avoid interfering licensed primary user (PU) systems and capture spectrum opportunities

efficiently, CRs must adapt to the spectrum occupancy dynamically and intelligently.

There are a number of coexistence models to implement the CR concept [66]. In the so-called spectrum overlay scenario (also termed *interweave* in [21]), CRs detect frequency bands unoccupied by PUs through spectrum sensing, and exploit those "spectrum holes" using dynamic resource allocation. Under a spectrum underlay model, CRs may transmit concurrently with PUs sharing the same bands, provided that the interference experienced by the PUs is controlled to a tolerable level, say, comparable to that of the ambient noise and interference.

In order to utilize a broad swath of spectrum flexibly, CR systems often employ multi-channel architectures such as orthogonal frequency-division multiple access (OFDMA). Key resource allocation (RA) issues in OFDMA radios include optimal assignment of subcarriers to individual users, and optimal power loading across the subcarriers. Extensive research has been carried out on this important topic, with recent applications to CR scenarios. A heuristic algorithm based on the multi-dimensional knapsack problem was proposed for OFDM CRs in [64]. A weighted sum-rate maximization problem has been considered in [2].

Channel estimation in CR systems is challenging, since the CRs gain access to the medium only intermittently, and the incumbent PU system often does not explicitly support channel estimation for CR systems. In addition, CRs might not have prior knowledge of PU signal characteristics, and thus are forced to resort to less efficient channel estimation techniques. Nevertheless, PU transmissions must be strictly protected from the interference due to CRs. Therefore, it is widely recognized that RA for CRs must account for channel uncertainty.

There are a couple of approaches that are typically considered for optimization with uncertain parameters [37].

Typically, uncertainty in the parameters of an optimization problem is captured either deterministically or statistically [5]. Under the deterministic approach, bounded-uncertainty parameter sets are assumed, and the worst-case solution immunized to all elements in the uncertainty set is sought. When the parameters are viewed as random, chance constraints are constructed from the distributions of the parameters. It can be shown that a determin-

istic robust optimization approach is intimately related to the chance-constrained approach under special circumstances.

Specifically, let $\sum_{n=1}^{N} g^{(n)}p^{(n)} \leq I_{\max}$ denote the constraint of interest, where $I_{\max} \geq 0$ is a given constant, $p^{(n)}$ for all n are deterministic and the uncertainty in vector $\mathbf{g} := [g^{(1)}\ g^{(2)}\ \ldots\ g^{(N)}]^T$ is captured by an ellipsoidal uncertainty region given by

$$\mathcal{G} := \left\{\bar{\mathbf{g}} + \Delta\mathbf{g} : \Delta\mathbf{g}^T\mathbf{C}_g^{-1}\Delta\mathbf{g} \leq \Omega^2\right\} \tag{1.3}$$

where $\bar{\mathbf{g}}$ is the nominal value of $\mathbf{g}$, $\Delta\mathbf{g}$ the deviation from the nominal value, $\mathbf{C}_g$ a symmetric positive definite matrix, and $\Omega \geq 0$ a given constant. Then, a robust constraint guarantees $\sum_{n=1}^{N} g^{(n)}p^{(n)} \leq I_{\max}$ for all possible $\mathbf{g} \in \mathcal{G}$; that is,

$$\sum_{n=1}^{N} g^{(n)}p^{(n)} \leq I_{\max} \text{ for all } \mathbf{g} \in \mathcal{G}. \tag{1.4}$$

Alternatively, one can note that (1.4) is equivalent to

$$\bar{\mathbf{g}}^T\mathbf{p} + \max_{\Delta\mathbf{g}:\Delta\mathbf{g}^T\mathbf{C}_g^{-1}\Delta\mathbf{g}\leq\Omega^2} \Delta\mathbf{g}^T\mathbf{p} \leq I_{\max}. \tag{1.5}$$

Upon defining$\Delta\tilde{\mathbf{g}} := \mathbf{C}_g^{-\frac{1}{2}}\Delta\mathbf{g}$, and invoking Cauchy-Schwarz's inequality as

$$\Delta\mathbf{g}^T\mathbf{p} = \Delta\tilde{\mathbf{g}}^T\mathbf{C}_g^{\frac{1}{2}}\mathbf{p} \leq ||\Delta\tilde{\mathbf{g}}||_2||\mathbf{C}_g^{\frac{1}{2}}\mathbf{p}||_2 \leq \Omega\sqrt{\mathbf{p}^T\mathbf{C}_g\mathbf{p}}, \tag{1.6}$$

one can easily confirm that (1.4) is equivalent to

$$\mathbf{p} \in \mathcal{C} := \left\{\mathbf{p}\middle| I_{\max} - \bar{\mathbf{g}}^T\mathbf{p} \geq \Omega\sqrt{\mathbf{p}^T\mathbf{C}_g\mathbf{p}}\right\} \tag{1.7}$$

which is a second-order cone constraint [5].

Also, one can arrive at (1.7) by assuming that $\mathbf{g}$ is jointly Gaussian with mean $\bar{\mathbf{g}}$ and covariance $\mathbf{C}_g$, and considering the chance constraint given by

$$\Pr\left\{\sum_{n=1}^{N} g^{(n)}p^{(n)} > I_{\max}\right\} \leq \epsilon \tag{1.8}$$

which enforces the probability that $\sum_{n=1}^{N} g^{(n)}p^{(n)}$ exceeds $I_{\max}$ is at most ϵ.

Yet another connection to the chance-constrained problem can be made by assuming that $\{g^{(n)}\}$ are random and independent of one another, and have finite support such that $g^{(n)} - \bar{g}^{(n)} \in [-\hat{g}^{(n)}, \hat{g}^{(n)}]$ for all n. Then, a conservative approximation of (1.8) is again given by (1.7) with $\mathbf{C}_g$ being a diagonal matrix whose n-th diagonal entry equals to $(\hat{g}^{(n)})^2$, and $\Omega := \sqrt{2\log\left(\frac{1}{\epsilon}\right)}$ [37].

CR interference constraints under channel uncertainty can be cast as chance constraints. The upshot is that the chance-constrained framework can embrace a rather broad range of modeling perspectives, based on either statistical or deterministic approaches. Thus, the formulation and solution methodology in this thesis can readily accommodate practical system requirements and deployment scenarios.

However, chance constraints are typically more difficult to handle than their deterministic counterparts, as they may be either nonconvex, or tough to verify as being convex. Moreover, it is sometimes difficult to express these constraints in closed form. In such cases, convex approximation of chance constraints is of practical merit.

Probabilistic interference constraints were considered for a CR power control problem in [15], where uncertainty in composite fading channels comprising shadowing and Nakagami fading was accounted for. RA problems for generic OFDMA systems with channel uncertainty have also been investigated extensively [1, 59]. However, not many works have addressed the RA problems for OFDMA-based CRs under channel uncertainty. A heuristic RA algorithm for OFDMA CR systems has been reported in [26], where the sum rate was maximized under power, interference, and average bit error rate constraints. However, the algorithm accounted for uncertainties only in the channels between the CR base station (BS) and the CR mobile stations (MSs), but not between the CR-BS and the PU. CR-PU channel uncertainty was considered in an OFDM setup by [52], but the subcarrier assignment issue for OFDMA was not addressed. Both channel estimation and spectrum sensing errors were taken into account for OFDMA CRs in [58] under a spectrum overlay model, in which the bands occupied by the PUs are completely avoided.

Chapters 4 and 5 introduce novel resource allocation algorithms for OFDMA CRs under channel uncertainty. Although important components of the proposed algorithms, such as

the Lagrange relaxation technique, robust optimization, and rate maximization for practical constellations, have received much attention in the literature, it must be emphasized that bringing these together for OFDMA CR RA under channel uncertainty incurs significant and novel challenges. On a high level, the contributions can be put in the following perspective. It is widely accepted that the Lagrange relaxation technique is a powerful tool for OFDMA RA. It is also generally recognized that robust optimization is an important framework to address RA problems with uncertain data. The critical question is whether it is possible to combine these two to tackle the challenging OFDMA RA problem for CRs. Chapters 4 and 5 offer a positive answer to this intriguing query, with associated trade-offs carefully examined. Moreover, the resulting contributions may have impact beyond the particular RA task treated here, as they can further be used to efficiently tackle a class of large-scale robust mixed-integer programming problems involving second-order cone constraints.

1.3.1 Resource Allocation in OFDMA CR Uplink

Chapter 4 addresses the RA task for OFDMA uplink CRs with uncertain CR-to-PU channels. A weighted sum-rate maximization problem is formulated subject to a probabilistic interference constraint and maximum transmit-power constraints for the CR users. The Bernstein method is adopted to approximate the probabilistic constraint by a convex constraint. Even after the approximation, the overall problem is still nonconvex due to the combinatorial assignment of users to each subcarrier. By employing appropriate bounds, the approximation emerging from the interference constraint can be further made *separable* across subcarriers. This opens the door to the dual decomposition approach, which leads to a near-optimal and computationally efficient solution [35]

1.3.2 Resource Allocation in OFDMA CR Downlink

The work in Chapter 5 considers an OFDMA CR network operating in a spectrum underlay set-up. A weighted sum rate maximization problem is formulated for a CR-BS that transmits to a set of CR-MSs, while respecting a strict interference constraint to protect PUs when the channel estimate between the CR-BS and the PU receiver contains uncer-

tainty. It turns out that the interference constraint can be converted to a second-order cone constraint, which is convex. However, the overall optimization problem is still non-convex in general due to the combinatorial search necessary for subcarrier assignment. It is well known that when an OFDMA RA problem has separable structure, the duality gap vanishes as the number of subcarriers grows large [35, 43]. To induce such a separable structure, a tight linear approximation for the interference constraint is introduced at a modest (polynomial) increase in the problem dimension. The approximated problem can then be readily solved using the dual decomposition method, which leads to a near-optimal, computationally efficient algorithm.

Different from Chapter 4, in which the user rates are modeled by logarithmic functions of transmit-powers, justified under ideal Gaussian coding, practical finite-alphabet constellations are adopted in Chapter 5. The optimization objective is a weighted sum of mutual information for individual CR-MSs. As the rate does not grow without bound even when the transmit-power is increased, a mercury/water-filling step is introduced rather than the conventional water-filling step [34]. The dual problem is solved using the relationship between the minimum mean-square error (MMSE) and the derivative of mutual information [23]. Instead of the chance-constrained formulation pursued in Chapter 4, a robust optimization framework is adopted in Chapter 5, and the close relationship between the two is delineated. A suboptimal benchmark algorithm is also considered, which aims at a locally optimal solution. A time complexity analysis for the proposed algorithm is provided as well.

Chapter 4 tackles OFDMA *uplink* problem was tackled, which entails a significantly different set of challenges than the *downlink* case. While conservative approximations of probabilistic interference constraints with strictly positive gaps are employed in Chapter 4, Chapter 5 pursues an arbitrarily tight approximation of robust interference constraints.

Chapter 2

Online Learning and Price Setting for EV Charging Response

In this chapter, the spatial dependence of the of EV consumers' charging decisions on the announced electricity price, are modeled using a CRF where the dependency structure is encoded a graph. Subsequently, an online algorithm is developed to estimate the relevant model parameters, based on OCO framework. The proposed algorithm yields probability distributions suitable for stochastic economic dispatch or revenue maximization, which are then used for the optimal the real-time price setting. The proposed model and algorithm are verified using synthetic and semi-real charging data. The material in this chapter draws from [51], [50].

2.1 Modeling and Problem Statement

The goal of a load serving entity is to shape the EV charging load imposed to the distribution grid in some desirable way, so as to minimize the generation cost, or maximize the net profit. One way of achieving this is to set the electricity prices for individual consumers appropriately in order to influence the consumers' EV charging behavior. For this, it is first necessary to estimate how responsive individual consumers are at each time to different prices presented to them.

Consider M EV owners, who desire to charge their EVs via a distribution network. Let $b_i^t \in \mathcal{S} := \{0, 1\}$ indicate the charging behavior of consumer i at time t; i.e., $b_i^t = 1$ when consumer i is charging his EV at time t, and $b_i^t = 0$, otherwise.[1] Similarly, ρ_i^t denotes the electricity price during time slot t for consumer i. To capture spatial dependence (e.g., behavioral dependence of consumers living in the same neighborhood, or having similar income levels), an undirected graph $G = (V, E)$ is introduced, where the vertex set $V := \{1, 2, \ldots, M\}$ corresponds to the consumers, and edges $(i, j) \in E$ capture the dependence between consumers i and j. Since the edges are undirected, it is assumed that $(i, j) \in E$ if $(j, i) \in E$.

It is assumed that the customer premises are equipped with smart meters so that bi-directional communication between the utility and the consumers is feasible. Leveraging such an advanced metering infrastructure, the utility announces prices $\{\rho_i^t\}$ to all consumers $i \in V$ at the beginning of slot $t = 1, 2, \ldots$. Subsequently, the charging decisions $\{b_i^t\}$ of the consumers are reported back to the utility at the end of slot t.

In this context, the following problem is of interest: estimate the probability with which each consumer $i \in V$ will charge the EV at time t paying for price $\{\rho_i^t\}$, given past prices $\{\rho_i^\tau, i \in V, \tau = 1, \ldots, t-1\}$, and the corresponding observed charging behaviors $\{b_i^\tau, i \in V, \tau = 1, \ldots, t-1\}$, while accounting for possible spatial dependencies in $\{b_i^t\}$ captured by G.

A CRF model for EV charging behavior To solve the aforementioned problem, the framework of CRF is adopted [32]. Collect in vectors $\mathbf{b}^t$ and $\boldsymbol{\rho}^t$ variables $\{b_i^t\}_{i=1}^M$ and $\{\rho_i^t\}_{i=1}^M$, respectively. The CRF models the conditional probability distribution function (*pdf*) $p(\mathbf{b}^t|\boldsymbol{\rho}^t)$. In short, $p(\mathbf{b}^t|\boldsymbol{\rho}^t)$ is a CRF with respect to G if it obeys the Markov property for every $\boldsymbol{\rho}^t$. This means that conditioned on $\boldsymbol{\rho}^t$, for any node pair $(i, j) \in V$, behavior b_i^t is independent of b_j^t given the neighbors $b_k^t \in N(i) := \{k : (i, k) \in E\}$.

Let $\psi_{i,j}(b_i^t, b_j^t)$ denote the feature functions quantifying the dependency in charging behavior of consumers i and j. In addition, functions $\phi_i(b_i^t, \rho_i^t)$ model the dependency of b_i^t

[1]Multiple charging rates can be accommodated straightforwardly by increasing the number of labels in $\mathcal{S}$.

on price ρ_i^t. Parameters θ_i^t and $\theta_{i,j}^t$ are introduced for ϕ_i and $\psi_{i,j}$, respectively, to capture the strengths of these dependencies. With $\boldsymbol{\theta}^t := [\theta_i^t, i \in V; \theta_{i,j}^t, (i,j) \in E]$, the price-conditional behavior *pdf* can be modeled as

$$p_{\boldsymbol{\theta}^t}(\mathbf{b}^t|\boldsymbol{\rho}^t) = \frac{1}{Z(\boldsymbol{\rho}^t)} \prod_{i \in V} e^{\theta_i^t \phi_i(b_i^t, \rho_i^t)} \prod_{(i,j) \in E} e^{\theta_{i,j}^t \psi_{i,j}(b_i^t, b_j^t)} \tag{2.1a}$$

$$Z(\boldsymbol{\rho}^t) := \sum_{\mathbf{b}^t \in \mathcal{S}^M} \prod_{i \in V} e^{\theta_i^t \phi_i(b_i^t, \rho_i^t)} \prod_{(i,j) \in E} e^{\theta_{i,j}^t \psi_{i,j}(b_i^t, b_j^t)} \tag{2.1b}$$

where $Z(\boldsymbol{\rho}^t)$ is a normalization factor, also known as the partition function. Motivated by the CRF model *pdf* involved with logistic regression, we adopt the function

$$\phi_i(b_i^t, \rho_i^t) := b_i^t \rho_i^t. \tag{2.2}$$

Furthermore, inspired by the Ising model for modeling dependencies of binary random variables [57],

$$\psi_{i,j}(b_i^t, b_j^t) := b_i^t b_j^t \tag{2.3}$$

is chosen. Now the problem of finding $p_{\boldsymbol{\theta}^t}(\mathbf{b}^t|\boldsymbol{\rho}^t)$ given $\{\rho_i^\tau, b_i^\tau, i \in V, \tau = 1, \ldots, t-1\}$ translates to estimating $\boldsymbol{\theta}^t$ at each time t.

2.2 Online Learning of Load Elasticity

Compared to batch algorithms that process the entire collection of data to obtain the desired estimates, online algorithms feature the capability to process data one by one in a sequential fashion. To develop an online algorithm for estimating $\boldsymbol{\theta}^t$, the approach here utilizes OCO, which requires minimal assumptions on the temporal dynamics of $\boldsymbol{\theta}^t$, and can provide provable performance guarantees even in adversarial settings [44], [24], [69]. Such guarantees against adversarial players are meaningful because the consumers may act strategically to maximize their own benefit (and mend their price responsiveness accordingly). Next, OCO framework is outlined.

2.2.1 OCO Framework

OCO can be viewed as a multi-round game with a forecaster and an adversary. The loss functions $\ell^t(\cdot)$ associated with the forecasts for $t = 1, 2, \ldots, T$, and the feasible set $\boldsymbol{\Theta}$ are assumed convex. In round t, the forecaster chooses $\hat{\boldsymbol{\theta}}^t \in \boldsymbol{\Theta}$, after which the adversary reveals $\ell^t(\cdot)$, incurring loss $\ell^t(\hat{\boldsymbol{\theta}}^t)$ for the t-th round. Performance of the online actions $\{\hat{\boldsymbol{\theta}}^t\}$ is assessed through the so-termed *regret* given by

$$R_T = \sum_{t=1}^{T} \ell^t(\hat{\boldsymbol{\theta}}^t) - \min_{\boldsymbol{\theta}\in\boldsymbol{\Theta}} \sum_{t=1}^{T} \ell^t(\boldsymbol{\theta}) \tag{2.4}$$

which represents the relative cumulative loss of the *online* forecaster after T rounds, compared to an optimal *offline* minimizer, which has the advantage of hindsight. Online convex programming algorithms provide ways to generate the sequence $\{\hat{\boldsymbol{\theta}}^t\}_{t=1}^T$ to achieve a regret that is sublinear in T.

2.2.2 Online Learning of Load Elasticity

In our context, the forecaster is the utility company and the adversaries are the EV owners. The loss is represented by the negative log-likelihood function

$$\ell^t(\boldsymbol{\theta}^t) := -\log p_{\boldsymbol{\theta}^t}(\mathbf{b}^t|\boldsymbol{\rho}^t) \tag{2.5}$$

which is not revealed to the utility company until the utility predicts $\hat{\boldsymbol{\theta}}^t$ and announces $\boldsymbol{\rho}^t$ based on $\hat{\boldsymbol{\theta}}^t$, since only then can the consumers respond with their charging decisions $\mathbf{b}^t$.

Note that the chosen loss $\ell^t(\boldsymbol{\theta}^t)$ in (2.5) with $p_{\boldsymbol{\theta}^t}(\mathbf{b}^t|\boldsymbol{\rho}^t)$ as in (2.1a) is convex [40]. A popular online convex programming algorithm relies on the online mirror descent (OMD) iteration, which is a projected subgradient method with the Bregman divergence used as a proximal term. It yields an efficient first-order algorithm with sublinear convergence rate [54]. Vector $\hat{\boldsymbol{\theta}}^{t+1}$ is obtained recursively in OMD as

$$\hat{\boldsymbol{\theta}}^{t+1} = \arg\min_{\boldsymbol{\theta}} \langle \nabla\ell^t(\hat{\boldsymbol{\theta}}^t), \boldsymbol{\theta}\rangle + \frac{1}{\mu^t} D(\hat{\boldsymbol{\theta}}^t \| \boldsymbol{\theta}) \tag{2.6}$$

where μ^t denotes a step size, and $D(\cdot\|\cdot)$ represents the Bregman divergence. The Bregman divergence associated with the ℓ_2-norm is simply given by $D(\hat{\boldsymbol{\theta}}^t\|\boldsymbol{\theta}) = \frac{1}{2}\|\boldsymbol{\theta} - \hat{\boldsymbol{\theta}}^t\|^2$. Upon

substituting this into (2.6), the OMD update boils down to an online gradient descent given by

$$\hat{\boldsymbol{\theta}}^{t+1} = \hat{\boldsymbol{\theta}}^{t} - \mu^{t} \nabla \ell^{t}(\hat{\boldsymbol{\theta}}^{t}). \tag{2.7}$$

To evaluate the gradient in (3.2), for the likelihood in (2.5) and the *pdf* in (2.1a), it is shown in Appendix 2.6.1 that

$$\frac{\partial \ell^{t}}{\partial \theta_{i}^{t}} = \mathrm{E}\{b_{i}^{t}\rho_{i}^{t}|\boldsymbol{\rho}^{t}\} - b_{i}^{t}\rho_{i}^{t}, \qquad \forall i \in V \tag{2.8}$$

$$\frac{\partial \ell^{t}}{\partial \theta_{i,j}^{t}} = \mathrm{E}\{b_{i}^{t}b_{j}^{t}|\boldsymbol{\rho}^{t}\} - b_{i}^{t}b_{j}^{t}, \qquad \forall (i,j) \in E \tag{2.9}$$

where the expectation is with respect to $p_{\hat{\boldsymbol{\theta}}^{t}}(\mathbf{b}^{t}|\boldsymbol{\rho}^{t})$.

Since b_{i}^{t} is a Bernoulli variable, it follows that

$$\mathrm{E}\{b_{i}^{t}\rho_{i}^{t}|\boldsymbol{\rho}^{t}\} = \rho_{i}^{t} p_{\hat{\boldsymbol{\theta}}^{t}}(b_{i}^{t} = 1|\boldsymbol{\rho}^{t}) \tag{2.10}$$

$$\mathrm{E}\{b_{i}^{t}b_{j}^{t}|\boldsymbol{\rho}^{t}\} = p_{\hat{\boldsymbol{\theta}}^{t}}(b_{i}^{t} = 1, b_{j}^{t} = 1|\boldsymbol{\rho}^{t}). \tag{2.11}$$

These marginal conditional probabilities can be efficiently evaluated by employing the belief propagation (BP) algorithm [61]. Starting with some initial messages, the BP algorithm performs message passing between nodes. The messages are updated iteratively till convergence or for a fixed number of iterations. The obtained messages can then be used for computing exact marginal probabilities for tree structured graphs. In graphs with loops, one needs to resort to the loopy belief propagation (LBP) algorithm [61], which often yields good approximations of marginals.

Let $m_{ij}(b_{i}^{t})$ denote the message passed from node i to node j for $(i,j) \in E$. Then, based on the standard BP update rules, the updated messages $m_{ij}(b_{j}^{t})$ and the marginals $p(b_{i}^{t}|\boldsymbol{\rho}^{t})$ and $p(b_{i}^{t}, b_{j}^{t}|\boldsymbol{\rho}^{t})$ are obtained as summarized in Table 2.1 [61]. The main computational burden of the BP algorithm lies in the message update step, which is $\mathcal{O}(|\mathcal{S}|^{2})$ for each pair of nodes. This is considerably better than the $\mathcal{O}(|\mathcal{S}|^{M})$ complexity incurred by computing marginals through direct summation over all variables.

The overall online algorithm for estimating $\boldsymbol{\theta}^{t+1}$ is summarized in Table 2.2. Steps 5 and 6 confirm that $\hat{\boldsymbol{\theta}}^{t+1}$ is dependent on past values of $\{\boldsymbol{\theta}^{\tau}\}_{\tau=1}^{t}$, and thus on $\{\mathbf{b}^{\tau}, \boldsymbol{\rho}^{\tau}\}_{\tau=1}^{t}$ as

1: Initialize $m_{ij}^{(0)}(b_j^t) = 1$ for all $i, j \in V$ and $b_j^t \in \mathcal{S}$.

2: For $n = 1, 2, ..., \mathsf{MAX\_ITER}$

Perform for all $i, j \in V$ and $b_j^t \in \mathcal{S}$:

3: Update: $m_{ij}^{(n)}(b_j^t) \leftarrow \sum_{b_i^t \in \mathcal{S}} \exp\left(\theta_i^t \phi_i(b_i^t, \rho_i^t)\right) \exp\left(\theta_{i,j}^t \psi_{i,j}(b_i^t, b_j^t)\right) \prod_{\nu \in N(i)\setminus\{j\}} m_{\nu i}^{(n-1)}(b_i^t)$

4: Normalize: $m_{ij}^{(n)}(b_j^t) \leftarrow \zeta_1^{-1} m_{ij}^{(n)}(b_j^t)$, where $\zeta_1 := \sum_{b_j^t \in \mathcal{S}} m_{ij}^{(n)}(b_j^t)$

5: Next n

6: Set $m_{ij}(b_j^t) = m_{ij}^{(\mathsf{MAX\_ITER})}(b_j^t)$ for all $i, j \in V$ and $b_j^t \in \mathcal{S}$.

7: Compute beliefs:

$$\tilde{p}(b_i^t|\boldsymbol{\rho}^t) = \exp\left(\theta_i^t \phi_i(b_i^t, \rho_i^t)\right) \prod_{j \in N(i)} m_{ji}(b_i^t)$$

$$\tilde{p}(b_i^t, b_j^t|\boldsymbol{\rho}^t) = \exp\left(\theta_i^t \phi_i(b_i^t, \rho_i^t)\right) \exp\left(\theta_j^t \phi_j(b_j^t, \rho_j^t)\right) \exp\left(\theta_{i,j}^t \psi_{i,j}(b_i^t, b_j^t)\right) \prod_{\nu \in N(j)\setminus\{i\}} m_{\nu j}(b_j^t) \prod_{o \in N(i)\setminus\{j\}} m_{oi}(b_i^t)$$

8: Normalize:

$$p(b_i^t|\boldsymbol{\rho}^t) = \zeta_2^{-1} \tilde{p}(b_i^t|\boldsymbol{\rho}^t), \text{ where } \zeta_2 := \sum_{b_i^t \in \mathcal{S}} \tilde{p}(b_i^t|\boldsymbol{\rho}^t)$$

$$p(b_i^t, b_j^t|\boldsymbol{\rho}^t) = \zeta_3^{-1} \tilde{p}(b_i^t, b_j^t|\boldsymbol{\rho}^t), \text{ where } \zeta_3 := \frac{\sum_{b_i^t \in \mathcal{S}} \tilde{p}(b_i^t, b_j^t|\boldsymbol{\rho}^t)}{p(b_j^t|\boldsymbol{\rho}^t)}$$

Table 2.1: A BP algorithm for computing $\{p(b_i^t|\boldsymbol{\rho}^t)\}$ and $\{p(b_i^t, b_j^t|\boldsymbol{\rho}^t)\}$.

well. Therefore, (3.2) makes use of the information in the entire input history. An instance of price setting algorithm for step 3 will be discussed in Sec. 2.3.

Clearly, consumers' charging decisions are correlated across time in practice. Compared to stochastic approximation alternatives [31], the novel algorithm based on online convex programming requires minimal assumptions on the structure of temporal correlation of data (charging decisions). In addition, the framework accommodates strategic actions of the consumers [44].

2.2.3 Performance Analysis

The algorithm in Table 2.2 yields a regret bound that is sublinear in T, as described in the following proposition.

Proposition 2.1 *Let $N_e := |E|$ denote the number of edges in E. If $\max\{|\theta_i^t|, |\theta_{i,j}^t|\} \leq \theta_0$ and $|\rho_i^t| \leq \rho_0$ for all t, $i \in V$, and $(i,j) \in E$, then for $\{\hat{\boldsymbol{\theta}}^t\}$ obtained from the algorithm in Table 2.2, it holds that*

$$R_T \leq \theta_0 \sqrt{2(M\rho_0^2 + N_e)T} = O(\sqrt{T}). \tag{2.12}$$

Proof: See Appendix 2.6.2. Regarding practicality of the assumptions, it is natural to assume that the prices are bounded. In addition, to account for consumers that do not respond to price changes (corresponding to $\theta_i^t = \pm\infty$), one can use a sufficiently large bound for $\max\{|\theta_i^t|, |\theta_{i,j}^t|\}$ in practice. Thus, the conditions in Proposition 1 can be readily satisfied.

2.2.4 Dynamic Logistic Regression Benchmark

If one neglects the spatial dependencies by setting $\theta_{i,j} = 0$ for $(i,j) \in E$, the CRF model reduces to M parallel logistic regression models; that is [cf. (2.1a)]

$$p_{\boldsymbol{\theta}^t}(\mathbf{b}^t|\boldsymbol{\rho}^t) = \frac{1}{Z(\boldsymbol{\rho}^t)} \exp\left(\sum_{i\in V} \theta_i^t b_i^t \rho_i^t\right) = \prod_{i=1}^{M} \frac{e^{\theta_i^t b_i^t \rho_i^t}}{1 + e^{\theta_i^t \rho_i^t}} \ . \tag{2.13}$$

To obtain online estimates of $\{\theta_i^t\}$, the algorithm in Table 2.2 is again applicable, but the gradient evaluation can be performed without using BP, simply as

$$\frac{\partial \ell^t}{\partial \theta_i^t} = \frac{\rho_i^t e^{\theta_i^t \rho_i^t}}{1 + e^{\theta_i^t \rho_i^t}} - b_i^t \rho_i^t, \qquad i \in V. \tag{2.14}$$

2.3 CRF-Based Real-Time Price Setting

So far, we have developed models and algorithms to capture consumers' EV charging decisions. Since the CRF model provides the probability distribution of the charging decisions

1: Initialize $\hat{\boldsymbol{\theta}}^1$
2: For $t = 1, 2, \ldots$ do
3: Set prices $\boldsymbol{\rho}^t$ based on $\hat{\boldsymbol{\theta}}^t$.
4: Collect EV charging decisions $\mathbf{b}^t$.
5: Compute $\nabla \ell^t(\hat{\boldsymbol{\theta}}^t)$ using BP.
6: Update $\hat{\boldsymbol{\theta}}^{t+1} = \hat{\boldsymbol{\theta}}^t - \mu_t \nabla \ell^t(\hat{\boldsymbol{\theta}}^t)$
7: Next t

Table 2.2: Overall online algorithm.

given the prices, one can now formulate a risk-limiting stochastic optimization problem to tailor the EV charging demand in some desirable fashion. Here, a price setting formulation for maximizing the utility's net profit is considered, where the profit equals the revenue collected from customers minus power generation cost.

Let P_{EV} denote the charging rate for a single EV, and η_i^t represent the aggregate base load of household i at time t. Then,

$$d_{tot}^t := \sum_{i=1}^{M} (P_{EV} b_i^t + \eta_i^t) \tag{2.15}$$

$$u_{tot}^t := \sum_{i=1}^{M} \rho_i^t (P_{EV} b_i^t + \eta_i^t) \tag{2.16}$$

correspond to the total demand and payment due to M consumers at time t, respectively.

The generation cost is modeled as quadratic in total power P as $\alpha P^2 + \beta P + \gamma$, where α, β and γ are constants. Then, the problem of interest is to maximize the expected net profit while the chance of the total load exceeding certain threshold is smaller than a specified risk level. Formally, this corresponds to

$$\text{(P1)} \qquad \max_{\mathbf{0} \preceq \boldsymbol{\rho}^t \preceq \bar{\boldsymbol{\rho}}} \mathrm{E}\{u_{tot}^t - [\alpha (d_{tot}^t)^2 + \beta d_{tot}^t + \gamma] | \boldsymbol{\rho}^t\} \tag{2.17a}$$

$$\text{subject to } \Pr\{d_{tot}^t > P_{\max} | \boldsymbol{\rho}^t\} \leq \epsilon \tag{2.17b}$$

where the expectation is with respect to $p_{\hat{\boldsymbol{\theta}}^t}(\mathbf{b}^t | \boldsymbol{\rho}^t)$ and $\bar{\boldsymbol{\rho}}$ is the vector of maximum allowable prices. Eq. (2.17b) ensures that the probability of aggregate load exceeding $P_{\max}$ is less than

ϵ. The expectation in (2.17a) can be evaluated as

$$\begin{aligned} U^t(\boldsymbol{\rho}^t) &:= \mathrm{E}\{u_{tot}^t - [\alpha(d_{tot}^t)^2 + \beta d_{tot}^t + \gamma] | \boldsymbol{\rho}^t\} \\ &= \sum_{i=1}^{M} \left[\rho_i^t P_{EV} - \alpha \left(P_{EV}^2 + 2P_{EV} \sum_{j=1}^{M} \eta_j^t \right) - \beta P_{EV} \right] p_{\hat{\boldsymbol{\theta}}^t}(b_i^t = 1 | \boldsymbol{\rho}^t) \\ &- \alpha \sum_{i=1}^{M} \sum_{\substack{j=1 \\ j \neq i}}^{M} P_{EV}^2 p_{\hat{\boldsymbol{\theta}}^t}(b_i^t = 1, b_j^t = 1 | \boldsymbol{\rho}^t) + \sum_{i=1}^{M} (\rho_i^t - \beta)\eta_i^t - \alpha \left(\sum_{i=1}^{M} \eta_i^t \right)^2 - \gamma \end{aligned} \tag{2.18}$$

using the marginal probabilities $p_{\hat{\boldsymbol{\theta}}^t}(b_i^t = 1 | \boldsymbol{\rho}^t)$ and $p_{\hat{\boldsymbol{\theta}}^t}(b_i^t = 1, b_j^t = 1 | \boldsymbol{\rho}^t)$ obtained from the BP algorithm.

In order to obtain a tractable closed-form approximation of the risk constraint (2.17b), the central limit theorem is invoked, which holds for a sum of dependent random variables under appropriate mixing conditions [7,9,41]. Specifically, d_{tot}^t is approximated as Gaussian-distributed with mean and variance given as

$$\bar{\mu}^t(M) := \mathrm{E}\{d_{tot}^t | \boldsymbol{\rho}^t\} = \sum_{i=1}^{M} \left[p_{\hat{\boldsymbol{\theta}}^t}(b_i^t = 1 | \boldsymbol{\rho}^t) P_{EV} + \eta_i^t \right] \tag{2.19}$$

$$\begin{aligned} \left(\sigma^t(M)\right)^2 &:= \mathrm{var}\{d_{tot}^t | \boldsymbol{\rho}^t\} \\ &= P_{EV}^2 \sum_{i=1}^{M} \left[p_{\hat{\boldsymbol{\theta}}^t}(b_i^t = 1 | \boldsymbol{\rho}^t) + \sum_{\substack{j=1 \\ j \neq i}}^{M} p_{\hat{\boldsymbol{\theta}}^t}(b_i^t = 1, b_j^t = 1 | \boldsymbol{\rho}^t) - \sum_{j=1}^{M} p_{\hat{\boldsymbol{\theta}}^t}(b_i^t = 1 | \boldsymbol{\rho}^t) p_{\hat{\boldsymbol{\theta}}^t}(b_j^t = 1 | \boldsymbol{\rho}^t) \right] \end{aligned} \tag{2.20}$$

respectively. Based on this approximation, one can replace (2.17b) with

$$\bar{\mu}^t(M) - P_{\max} + \sigma^t(M) Q^{-1}(\epsilon) \leq 0 \tag{2.21}$$

where $Q(\cdot)$ is the standard Gaussian tail function. Thus, the optimization problem to solve is

$$\text{(P2)} \qquad \max_{\mathbf{0} \preceq \boldsymbol{\rho}^t \preceq \bar{\boldsymbol{\rho}}} U^t(\boldsymbol{\rho}^t) \text{ subject to (2.21).} \tag{2.22}$$

Since the conditional marginals are log-concave with respect to $\boldsymbol{\rho}^t$ [3], (P2) is not convex in general. In the next section, locally optimal solutions to (P2) are sought using the "fmincon" function in the MATLAB package.

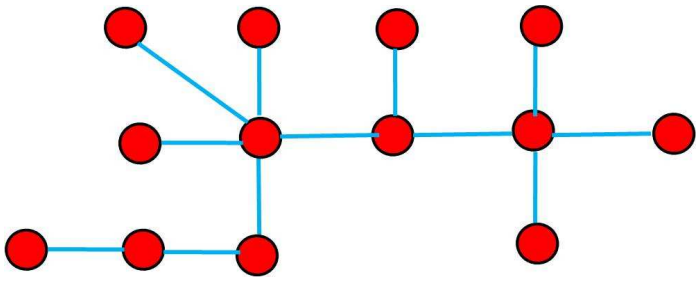

Figure 2.1: Spatial dependency graph for the simulated test.

2.4 Numerical Tests

The performance of the proposed algorithm was verified via numerical tests. Both fully simulated data and semi-real data were utilized.

2.4.1 Simulated Data

A set of 13 EV owners was considered, whose spatial dependencies were captured by graph G in Fig. 2.1. Given the true CRF parameters $\boldsymbol{\theta}^{*t}$, the charging decisions $\mathbf{b}^t$ were the samples from the CRF model in (2.1a)–(2.3), with $\boldsymbol{\rho}^t$ chosen as explained next. The values of $\boldsymbol{\theta}^{*t}$ were changed occasionally but otherwise were kept fixed over time; see Fig. 2.2(a), which depicts $\boldsymbol{\theta}^{*t}$. To test the tracking performance of the proposed method, three simple strategies for selecting $\boldsymbol{\rho}^t$ independent of estimated parameters are considered here: s1) constant prices; s2) time-of-use (ToU) prices; and s3) random prices. For the constant pricing setup, ρ_i^t was set to 1 for all consumers and held constant across time. For ToU pricing, the following was used:

$$\rho_i^t = \begin{cases} \$0.508, & \text{7am-2pm} \\ \$0.880, & \text{2pm-8pm} \\ \$0.722, & \text{8pm-11pm} \\ \$0.508, & \text{11pm-7am} \end{cases} \qquad \forall i \in V. \tag{2.23}$$

In random pricing, the prices were randomly selected from a uniform distribution over $[0, 1]$. Prices were updated every 12 minutes, which corresponds to the duration of one time slot.

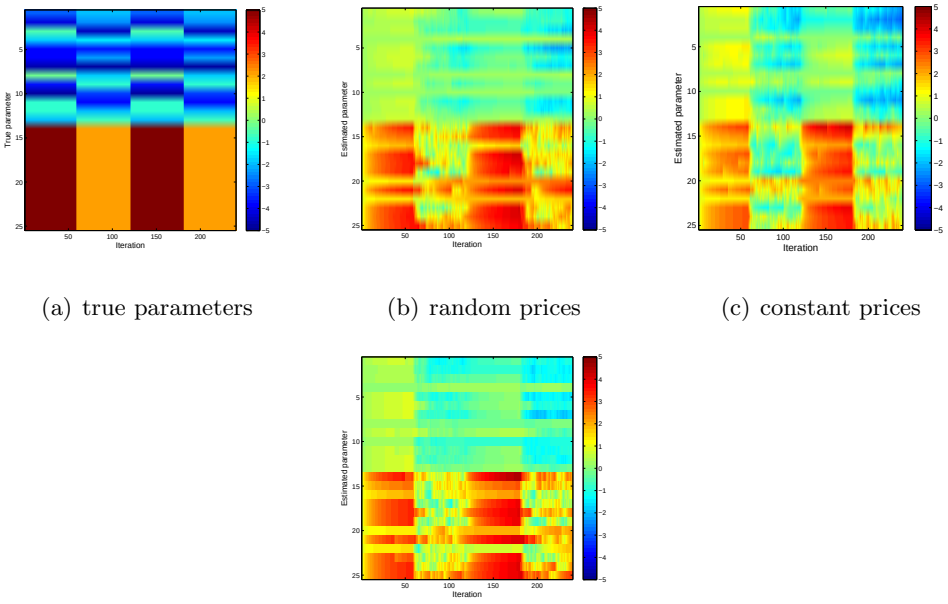

(a) true parameters (b) random prices (c) constant prices

(d) ToU prices

Figure 2.2: True and estimated model parameters $\boldsymbol{\theta}^t$.

A step size $\mu^t = 0.72$ was used. Fig. 2.2 shows true and estimated parameters for the different pricing strategies. It can be seen that the parameters are tracked approximately.

Fig. 2.3 depicts the squared prediction error of the parameters, averaged over $M + N_e = 25$ parameters. For all price setting mechanisms, the errors tend to decrease as iterations progress, while sharp changes in the prediction error result whenever the parameter values are changed abruptly.

A comparison of $p_{\hat{\theta}^t}(\mathbf{b}^t_{\text{revealed}}|\boldsymbol{\rho}^t)$ with $p_{\boldsymbol{\theta}^{*t}}(\mathbf{b}^t_{\text{revealed}}|\boldsymbol{\rho}^t)$ per iteration is shown in Fig. 2.4. It can be seen that the joint probability of the charging decisions is tracked very well.

Once the joint probabilities $p(\mathbf{b}^t|\boldsymbol{\rho}^t)$ have been estimated, the expected value of the total load can be readily found as $\bar{P}^t_{tot} := P_{EV} \sum_{i=1}^{M} p_{\hat{\boldsymbol{\theta}}^t}(b^t_i = 1|\boldsymbol{\rho}^t)$. The predicted total loads are depicted in Fig. 2.5, where the CRF-based estimates and the logistic regression-based ones are plotted together for comparison. The CRF-based algorithm achieves the performance gain by incorporating spatial dependencies.

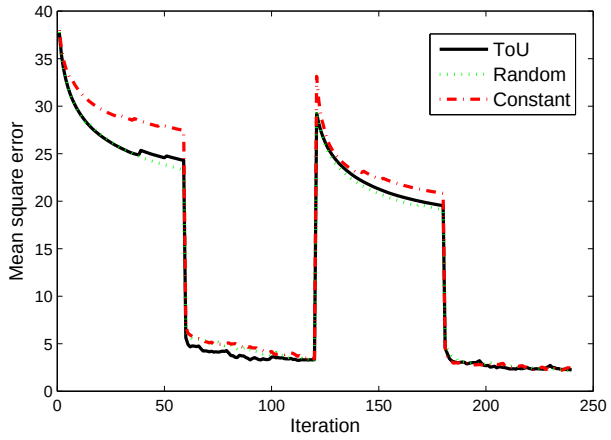

Figure 2.3: Average squared prediction error for CRF parameters.

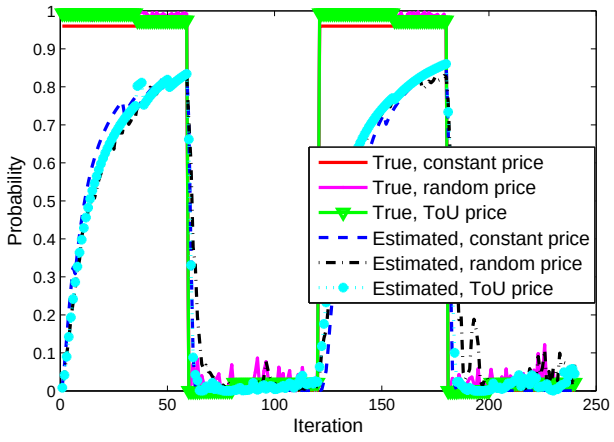

Figure 2.4: Joint probability of consumer charging decisions.

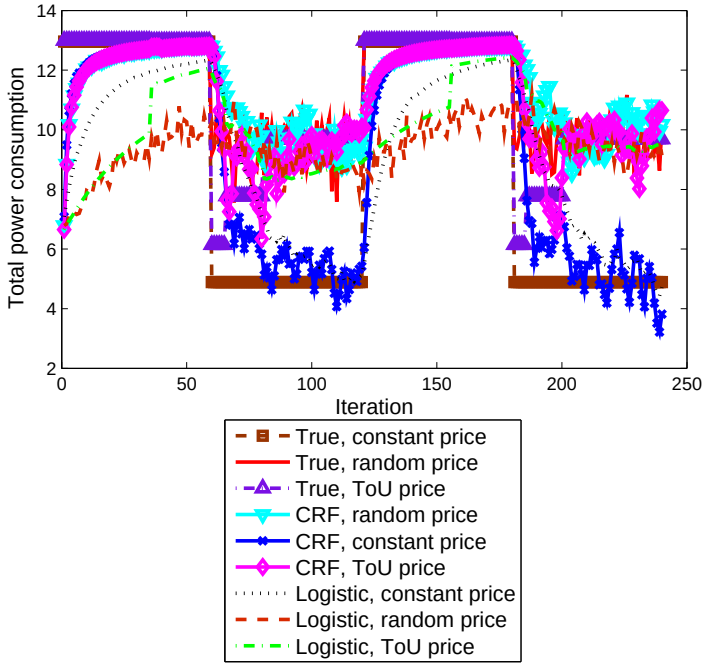

Figure 2.5: Predicted total EV charging load $\bar{P}^t_{tot}$.

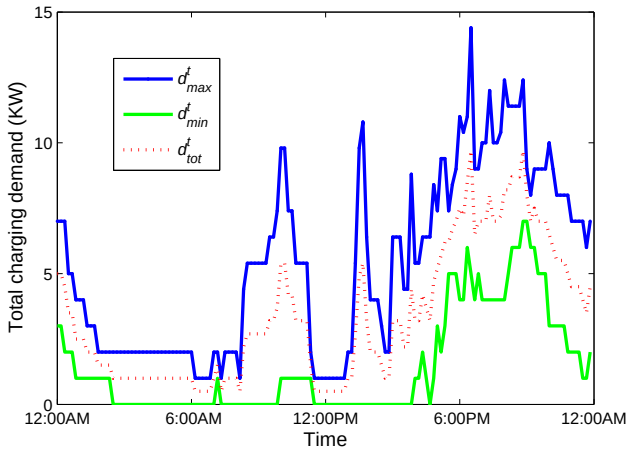

Figure 2.6: Charging demand of 25 households [16].

2.4.2 Semi-real Data

To validate the proposed methods in a more realistic setting, the experimental data of charging demand collected from 25 Northern California households in [16] were used in the tests. The project ran from August 2008 to April 2010, and the collected data have been aggregated to a single summary week. The charging power flow of EV, was assumed to be $P_{EV} = 1.4$ kW in all the experiments. Fig. 2.6 depicts the daily total demand data collected every 10 minutes with the price held equal at all times and for all consumers; that is, $\rho_i^t = 1, \forall i, t$. The three curves in Fig. 2.6 correspond to the highest demand $d^t_{\max}$ at each time t, the lowest demand $d^t_{\min}$, and their average

$$\bar{d}^t_{tot} := \frac{d^t_{\max} + d^t_{\min}}{2}. \tag{2.24}$$

To evaluate the proposed model, data that capture consumers' charging behaviors in response to price changes are necessary. For this, a reasonable consumer behavioral model is concocted as delineated next, which is then fitted such that when the prices are held fixed at $\rho_i^t = 1$, the total demand curves as shown in Fig. 2.6 are obtained.

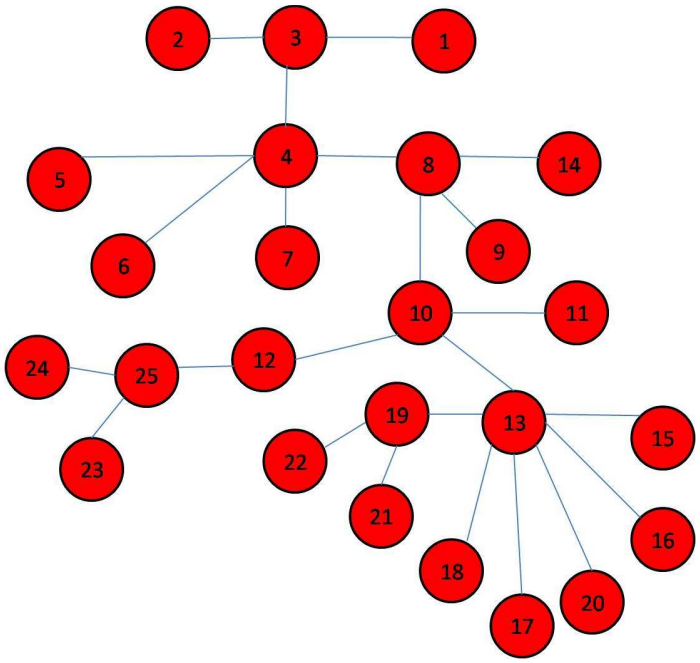

Figure 2.7: Spatial dependency graph for semi-real data.

Consumer behavior model

A simple consumer behavior model is adopted, where consumer i charges when the price ρ_i^t is less than some threshold τ_i^t. That is, b_i^t is modeled as

$$b_i^t = \begin{cases} 1, & \text{if } \rho_i^t < \tau_i^t \\ 0, & \text{otherwise} \end{cases} \tag{2.25}$$

for $i \in V$ and $t = 1, 2, \ldots$. Note that $\tau_i^t < 0$ can model the case where the EV i is fully charged.

Let $\boldsymbol{\tau}^t := [\tau_1^t, \ldots, \tau_M^t]$ and $P_{tot}^t := P_{EV} \sum_{i=1}^M b_i^t$. In order to capture the spatial dependency of charging behaviors, $\boldsymbol{\tau}^t$ is sampled from a Gaussian distribution with mean $\boldsymbol{\mu}^t$ and covariance $\boldsymbol{\Sigma}^t$, where $\boldsymbol{\Sigma}^t$ encodes the dependency graph G shown in Fig. 2.7, via

$$[\boldsymbol{\Sigma}^t]_{ij} = \begin{cases} r_{ij}^t, & \text{if } (i,j) \in E \\ r_{ii}^t, & \text{if } i = j \\ 0, & \text{otherwise} \end{cases} \tag{2.26}$$

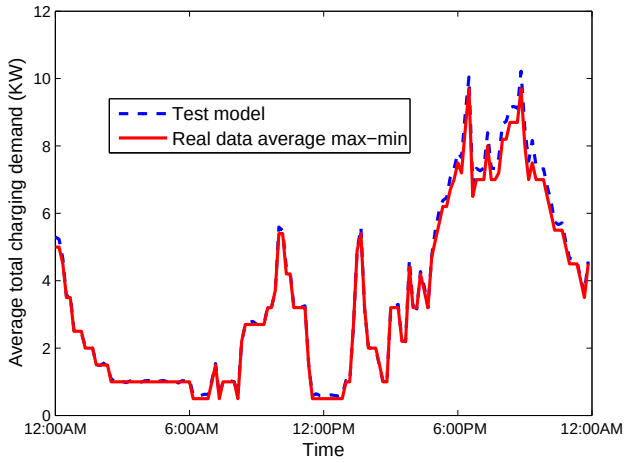

Figure 2.8: Real and simulated total charging demands.

with $r_{ij}^t > 0$ for $i, j \in V$. Using again the central limit theorem for dependent random variables, P_{tot}^t can be approximated to follow a Gaussian distribution with mean μ_S^t and variance $(\sigma_S^t)^2$. To fit the model to the real data when $\rho_i^t = 1$ for all i, t, the positive definiteness of $\mathbf{\Sigma}^t$ as well as the following relations are used to determine parameters $\{r_{ij}^t\}$:

$$\mu_S^t = \bar{d}_{tot}^t \tag{2.27}$$

$$\sigma_S^t = \frac{d_{\max}^t - d_{\min}^t}{4}. \tag{2.28}$$

Fig. 2.8 shows the result of the fitting. The dotted curve shows the total charging demand obtained through the model in (2.25)–(2.26) averaged over 28 realizations, and the solid curve represents $\bar{d}_{tot}^t$ due to the real data. It can be seen that real charging demand matches well with the value obtained from the proposed behavior model.

Online model parameter learning

The performance of the proposed online learning algorithm was tested using the semi-real data. Fig. 2.9 shows the average predicted total charging demands $\bar{P}_{tot}^t$ (averaged over 28 realizations) using the CRF and logistic regression models, based on the input generated from the model in (2.25)–(2.26) under constant pricing. The model parameters $\{\boldsymbol{\theta}^t\}$ were tracked using the algorithm in Table 2.2. It can be seen that the prediction is very accurate

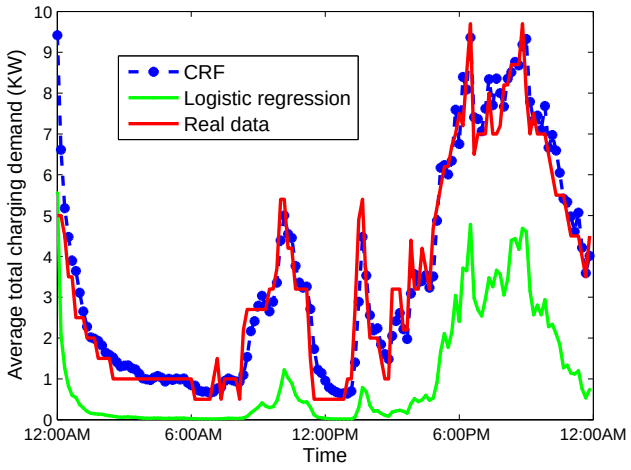

Figure 2.9: Predicted average total charging demands.

when the CRF model is used. However, similar to the case of simulated data, the logistic regression model produces predictions that are quite off from the true values. Note that the initial performance degradation seen in the CRF curve is due to the transient effect in tracking, which depends on the initial value of $\boldsymbol{\theta}^t$.

Real-time pricing

Finally, the real-time price setting formulation discussed in Sec. 2.3 is tested. Here, $\epsilon = 0.001$ and $P_{\max}$ was set to 5 kW, and $\bar{\boldsymbol{\rho}} = [2, 2, \ldots, 2]$ was used. The case of zero base load was considered; i.e. $\eta_i^t = 0$ for all i and t. The generator parameters were chosen to be $\alpha = 0.15$, $\beta = 0.4$ and $\gamma = 0$. In addition to the most general price setting formulation (P2), a special case of setting the prices equal to all consumers was also considered. That is,

$$\rho_1 = \rho_2 = \cdots = \rho_M^t = \rho^t \tag{2.29}$$

was enforced in (P2) at each time t. Fig. 2.10 depicts the net profit and the total EV charging load under real-time pricing. The dash-dot curve in Fig. 2.10(a) is the net profit obtained from model (2.25) when prices are set through (P2), and the dashed curve corresponds to the case of equal pricing under (2.29). For comparison, the net profit under fixed pricing at $\rho_i^t = 1$ for all i and t as in the real data is also plotted in the solid curve. From Fig. 2.10(a), it

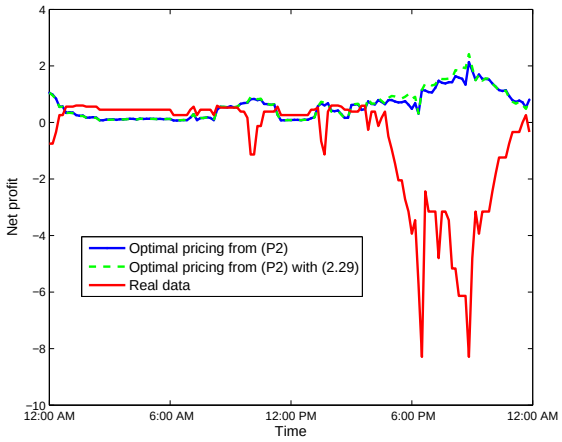

(a) net profit

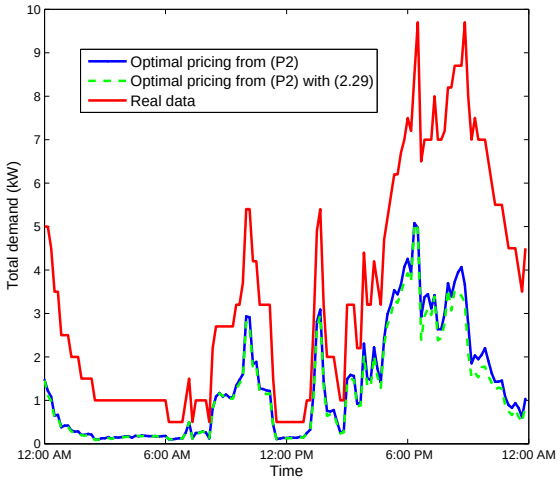

(b) total charging demand

Figure 2.10: Net profit and total charging demand under real-time pricing.

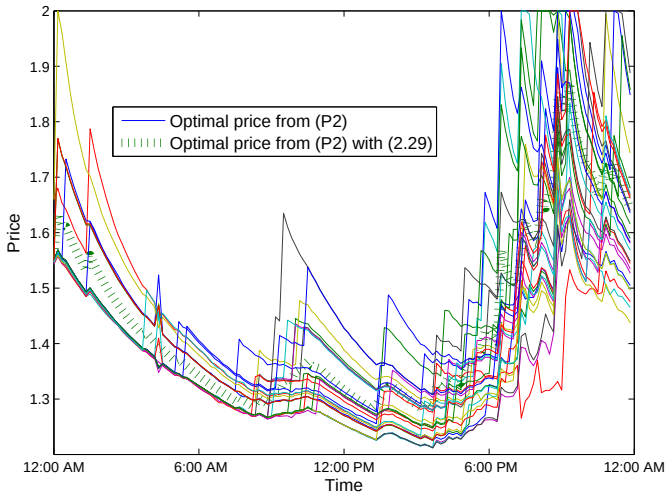

Figure 2.11: Real-time prices.

can be observed that the profit is generally much improved by employing real-time pricing, compared to the curve for which fixed pricing was used. However, since the tracking is not perfect, and the solutions to (P2) may suffer from local optima, the profit does not always stay at the optimum. The load curve in Fig. 2.10(b) clearly shows that the demand is flattened by real-time pricing, as the economically favorable operating point is tracked. Interestingly, it is noted that adopting identical prices across customers incurs almost no performance loss.

Fig. 2.11 depicts $\{\rho_i^{*t}\}$ for the individual customers $i \in V$ from solving (P2) in the solid curves, as well as ρ^t from (P2) with the additional constraint (2.29) in the thick dashed curve. Neglecting the initial transient, it can be seen that the prices increase at high demand and decrease at low demand as expected.

2.5 Conclusions

An algorithm to track the elasticity of individual EV charging loads was developed. Such information is essential for setting the electricity prices in real time to coordinate EV charging. The probabilities with which individual EV consumers charge their vehicles when presented

with real-time prices were obtained based on a CRF model, in which the spatial dependency of the customers' behavior was captured. Without explicit models for temporal dynamics, an online learning algorithm to estimate the CRF parameters was derived in the framework of OCO. The CRF model was then applied as an input to an stochastic profit maximization problem for real-time price setting. The performance of the proposed algorithms was corroborated using simulated and semi-real data.

2.6 Appendices

2.6.1 Derivation of (2.8) and (2.9)

Differentiating the $-\log$ of the *pdf* in (2.1) yields

$$\frac{\partial \ell^t}{\partial \theta_i^t} = \frac{\partial \log Z(\boldsymbol{\rho}^t)}{\partial \theta_i^t} - b_i^t \rho_i^t, \qquad \forall i \in V$$
$$\frac{\partial \ell^t}{\partial \theta_{i,j}^t} = \frac{\partial \log Z(\boldsymbol{\rho}^t)}{\partial \theta_{i,j}^t} - b_i^t b_j^t, \qquad \forall (i,j) \in E$$

where after substituting $Z(\boldsymbol{\rho}^t)$ from (2.1b), it follows

$$\begin{aligned}\frac{\partial \log Z(\boldsymbol{\rho}^t)}{\partial \theta_i^t} &= \frac{1}{Z(\boldsymbol{\rho}^t)} \sum_{\mathbf{b}^t} b_i^t \rho_i^t \exp\left(\sum_{i=1}^N \theta_i^t b_i^t \rho_i^t + \sum_{i,j\in E} \theta_{i,j}^t b_i^t b_j^t\right) \\ &= \mathrm{E}\{b_i^t \rho_i^t | \boldsymbol{\rho}^t\}, \qquad \forall i \in V \\ \frac{\partial \log Z(\boldsymbol{\rho}^t)}{\partial \theta_{i,j}^t} &= \frac{1}{Z(\boldsymbol{\rho}^t)} \sum_{\mathbf{b}^t} b_i^t b_j^t \exp\left(\sum_{i=1}^N \theta_i^t b_i^t b_j^t + \sum_{i,j\in E} \theta_{i,j}^t b_i^t \rho_i^t\right) \\ &= \mathrm{E}\{b_i^t b_j^t | \boldsymbol{\rho}^t\}, \qquad \forall (i,j) \in E\end{aligned}$$

thus completing the proof.

2.6.2 Proof of Proposition 2.1

The regret of online gradient descent algorithm for convex loss function, $\ell^t(\boldsymbol{\theta}^t)$, is bounded by [44]

$$R_T(\boldsymbol{\theta}) := \sum_{t=1}^T \ell^t(\boldsymbol{\theta}^t) - \sum_{t=1}^T \ell^t(\boldsymbol{\theta}) \leq \frac{1}{2\mu_t}\|\boldsymbol{\theta}\|^2 + \mu_t \sum_{t=1}^T \|\nabla \ell^t\|^2. \tag{2.30}$$

Since $b_i^t \in \{0,1\}$, $0 \leq p_{\boldsymbol{\theta}^t}(b_i^t = 1|\boldsymbol{\rho}^t) \leq 1$, and $0 \leq p_{\boldsymbol{\theta}^t}(b_i^t = 1, b_j^t = 1|\boldsymbol{\rho}^t) \leq 1$, it follows from (2.9) and (2.8) that the gradients are bounded as

$$-\rho_i^t \leq \frac{\partial \ell^t}{\partial \theta_i^t} \leq \rho_i^t \qquad \forall i \in V \tag{2.31a}$$
$$-1 \leq \frac{\partial \ell^t}{\partial \theta_{i,j}^t} \leq 1 \qquad \forall (i,j) \in E. \tag{2.31b}$$

Upon assuming that the price is bounded, i.e., $|\rho_i^t| \leq \rho_0$ for all t, $i \in V$, it follows that $\|\boldsymbol{\rho}^t\|^2 \leq M\rho_0^2$. Letting $N_e := |E|$ denote the number of edges in E, it then holds that $\|\nabla \ell^t\|^2 \leq M\rho_0^2 + N_e$. If $\max\{|\theta_i^t|, |\theta_{i,j}^t|\} \leq \theta_0$ and we further choose $\mu_t = \frac{\theta_0}{\sqrt{(2(M\rho_0^2+N_e)T}}$, the regret boils down to

$$R_T \leq \theta_0 \sqrt{2(M\rho_0^2 + N_e)T} = O(\sqrt{T}). \tag{2.32}$$

Chapter 3

Online Learning of EV Consumers' Charging Behavior with Missing Data

This chapter adopts a conditional random field model to capture the dependency of EV consumers' charging decisions [51]. It is assumed that even incomplete charging decisions of consumers which belong to an associated set of binary decisions (e.g., "charging" or "not charging") are sequentially observed by the utility company. At each time step, the observed charging decisions may include misses, where the number and locations of the misses may change over time. Then, an online learning algorithm in the OCO framework is developed to infer missing data and subsequently estimate the relevant model parameters, which allows for strategic behavior of consumers [44]. The material in this chapter draws from [47].

3.1 Problem Statement

Consider N EV consumers in the distribution network. Suppose that any two consumers are connected with an edge if they are geographically adjacent, thus forming the graph $G(V, E)$, where V and E represent the set of vertices and edges, respectively. It is further assumed

that the consumers are equipped with smart meters so that they can communicate with the utility company and thus respond to price variations. Let $\mathcal{S} \triangleq\{0,1\}$, with $\{b_i^t \in \mathcal{S}, i \in V\}$ indicating the charging behavior of EV consumer i at time t, i.e., $b_i^t = 1$ if the consumer is charging, and zero otherwise. Suppose that the time horizon consists of T slots, where T is a finite positive integer. At the beginning of time slot $t \in \{1, 2, ..., T\}$, the utility announces a price ρ_i^t for consumer i over time slot $[t, t+1)$.

Motivated by the CRF model *pdf* involved with logistic regression, we adopt a scalar function $\boldsymbol{\phi}_i(b_i^t, \rho_i^t) = b_i^t \rho_i^t$. Furthermore, inspired by the Ising model for modeling dependencies of binary random variables, we choose $\boldsymbol{\psi}_{i,j}(b_i^t, b_j^t) = b_i^t b_j^t$ [57].

With $\boldsymbol{\theta}^t \triangleq [\theta_i^t, i \in V; \theta_{i,j}^t, (i,j) \in E]$, $\boldsymbol{\alpha}^t \triangleq \{\rho_i^t \theta_i^t\}_{i \in V}$, $\boldsymbol{\Phi}^t \triangleq \{\theta_{i,j}^t\}_{i \in V, j \in V}$, (2.1a) can be rewritten as

$$p_{\boldsymbol{\theta}^t}(\mathbf{b}^t | \boldsymbol{\rho}^t) = \frac{e^{\boldsymbol{\alpha}^{t\,T} \mathbf{b}^t + \mathbf{b}^{t\,T} \boldsymbol{\Phi}^t \mathbf{b}^t}}{Z(\boldsymbol{\rho}^t, \boldsymbol{\theta}^t)}. \tag{3.1}$$

It is assumed that there are no self-loops (self-dependency) in the graph, which corresponds to setting the diagonal elements of $\boldsymbol{\Phi}^t$ to zero. The problem of interest is to estimate the probability with which each consumer $i \in V$ will charge his EV at time $t+1$ paying price $\{\rho_i^{t+1}\}$, given past prices $\{\rho_i^\tau, i \in V, \tau = 1, \ldots, t\}$, and partially observed corresponding charging behavior $\{b_i^\tau, i \in \mathcal{O}^\tau, \tau = 1, \ldots, t\}$, where $\mathcal{O}^\tau$ denotes the set of consumers with observed charging decisions. Similarly, let $\mathcal{M}^\tau$ represent the set of consumers whose charging decisions are missing.

3.2 Dynamic Learning of CRF with Misses using OCO

It was shown in Chapter 2 that when all $\mathbf{b}^t$ are known, then an estimate of $\boldsymbol{\theta}^{t+1}$ is simply obtained by

$$\hat{\boldsymbol{\theta}}^{t+1} = \hat{\boldsymbol{\theta}}^t - \mu_t \nabla \ell^t(\hat{\boldsymbol{\theta}}^t). \tag{3.2}$$

However, if some of $\mathbf{b}^t$ are unknown, then $\mathbf{b}^t$ consists of $\mathbf{b}_o^t = \{b_o^t \in \mathcal{S},\ o \in \mathcal{O}^t\}$, and $\mathbf{b}_m^t = \{b_m^t \in \mathcal{S},\ m \in \mathcal{M}^t\}$, where $\mathbf{b}_o^t$ and $\mathbf{b}_m^t$ denote the observed and missing charging

decisions of consumers, respectively. Then, $\ell^t(\boldsymbol{\theta}^t)$ cannot be evaluated since it depends on missing data.

An approach to dealing with misses is based on past data to obtain an estimate of $\mathbf{b}_m^t$. To this end, an online approach for estimation and prediction of $\mathbf{b}_m^t$ and $\boldsymbol{\theta}^{t+1}$, is proposed which is briefed next.

3.2.1 Online Learning with Sequential Estimation of Missing Data

This section addresses online missing data estimation and CRF parameter learning. The number and locations of the missing data are allowed to be time varying. Acquiring the predicted $\hat{\boldsymbol{\theta}}^t$ from time $t-1$, $\boldsymbol{\rho}^t$, and $\mathbf{b}_o^t$, the problem of estimating $\mathbf{b}_m^t$ is

$$\hat{\mathbf{b}}_m^t = \arg \max_{\mathbf{u}\in\{0,1\}^{|\mathcal{M}^t|}} \log p_{\hat{\boldsymbol{\theta}}^t}(\mathbf{b}_o^t, \mathbf{u}|\boldsymbol{\rho}^t, \hat{\boldsymbol{\theta}}^t). \tag{3.3}$$

Upon defining $\hat{\ell}^t := -\log p_{\boldsymbol{\theta}^t}(\mathbf{b}_o^t, \hat{\mathbf{b}}_m^t|\boldsymbol{\rho}^t)$, the vector $\hat{\boldsymbol{\theta}}^{t+1}$ is obtained from

$$\hat{\boldsymbol{\theta}}^{t+1} = \hat{\boldsymbol{\theta}}^t - \mu_t \nabla \hat{\ell}^t(\hat{\boldsymbol{\theta}}^t). \tag{3.4}$$

With $\mathbf{P}^t$ denoting an orthonormal permutation matrix (or any permutation operator), for which $[\mathbf{b}_o^t, \mathbf{b}_m^t]^T = \mathbf{P}^t\mathbf{b}^t$, the charging data can be sorted as observed and missed. Accordingly, define

$$\begin{aligned}
\boldsymbol{\alpha}_P^t &:= \mathbf{P}^t\boldsymbol{\alpha}^t \\
\hat{\mathbf{b}}_P &:= \mathbf{P}^t\hat{\mathbf{b}}^{t-1} \\
\boldsymbol{\Phi}_P^t &:= \mathbf{P}^t\boldsymbol{\Phi}^t{\mathbf{P}^t}^T
\end{aligned} \tag{3.5}$$

where $\hat{\mathbf{b}}^{t-1}$ is the vector of consumers' charging behavior at time $t-1$, including the estimated misses. Then, ${\mathbf{b}^t}^T\boldsymbol{\Phi}^t\mathbf{b}^t$ in (3.1) can be substituted by $[\mathbf{b}_o^t, \mathbf{b}_m^t]\boldsymbol{\Phi}_{\boldsymbol{P}}^t[\mathbf{b}_o^t, \mathbf{b}_m^t]^T$. Assuming that $\boldsymbol{\Phi}^t$ is symmetric,[1] it can be easily shown that $\boldsymbol{\Phi}_{\boldsymbol{P}}^t$ preserves symmetry. Then (3.3) can be equivalently written as

$$\hat{\mathbf{b}}_m^t = \arg \max_{\mathbf{u}\in\{0,1\}^{|\mathcal{M}^t|}} {\boldsymbol{\alpha}_{\boldsymbol{m}}^t}^T\mathbf{u} + 2{\mathbf{b}_o^t}^T\boldsymbol{\Phi}_{\boldsymbol{om}}^t\mathbf{u} + \mathbf{u}^T\boldsymbol{\Phi}_{\boldsymbol{mm}}^t\mathbf{u} \tag{3.6}$$

[1]Even if not symmetric, one can symmetrize it by substituting the matrix $\boldsymbol{\Phi}^t$ entries by $\acute{\theta}_{i,j} = (\theta_{i,j} + \theta_{j,i})/2, \quad \forall i, j \in V$.

where using MATLAB notations, $\boldsymbol{\Phi}^t_{\boldsymbol{om}}$, $\boldsymbol{\Phi}^t_{\boldsymbol{mm}}$, $\boldsymbol{\alpha}^t_{\boldsymbol{m}}$, and $\mathbf{u}^*_{\mathbf{m}}$ are given by

$$\boldsymbol{\Phi}^t_{\boldsymbol{om}} := \boldsymbol{\Phi}^t_P(1 : |\mathcal{O}|, N - |\mathcal{O}| + 1 : N) \tag{3.7}$$

$$\boldsymbol{\Phi}^t_{\boldsymbol{mm}} := \boldsymbol{\Phi}^t_P(N - |\mathcal{O}| + 1 : N, N - |\mathcal{O}| + 1 : N) \tag{3.8}$$

$$\mathbf{u}^*_{\mathbf{m}} := \hat{\mathbf{b}}_P(N - |\mathcal{O}| + 1 : N) \tag{3.9}$$

$$\boldsymbol{\alpha}^t_{\boldsymbol{m}} := \boldsymbol{\alpha}^t_{\boldsymbol{P}}(N - |\mathcal{O}| + 1 : N). \tag{3.10}$$

The optimization in (3.6) is an integer programming problem and in general non-convex, as the entries of $\mathbf{u}$ are constrained to be binary. A common approach to avoid the hurdle of binary assignment is to relax the constraint $\mathbf{u} \in \{0, 1\}^{|\mathcal{M}^t|}$ with $\mathbf{0} \preceq \mathbf{u} \preceq \mathbf{1}$, where the vector inequality is element-wise. However, under the assumption that there are no self-loops in the graph, the diagonal elements of $\boldsymbol{\Phi}^t$ are zero and $\boldsymbol{\Phi}^t$(similarly, $\boldsymbol{\Phi}^t_{\boldsymbol{mm}}$) is in general non-positive definite. Therefore, due to the quadratic term in (3.6), the overall optimization problem with relaxed constraint is still non-convex. To tackle this non-convexity, we resort to an approximation of the quadratic function.

The second-order Taylor approximation of the quadratic function, $\mathbf{u}^T\boldsymbol{\Phi}^t_{\boldsymbol{mm}}\mathbf{u}$, at any point in its domain, e.g., $\bar{\mathbf{b}}$, is obtained from

$$\mathbf{u}^T\boldsymbol{\Phi}^t_{\boldsymbol{mm}}\mathbf{u} \approxeq \bar{\mathbf{b}}^T\boldsymbol{\Phi}^t_{\boldsymbol{mm}}\bar{\mathbf{b}} + 2\langle \mathbf{u} - \bar{\mathbf{b}}, \boldsymbol{\Phi}^t_{\boldsymbol{mm}}\bar{\mathbf{b}}\rangle + (\mathbf{u} - \bar{\mathbf{b}})^T\boldsymbol{\Phi}^t_{\boldsymbol{mm}}(\mathbf{u} - \bar{\mathbf{b}}) \tag{3.11}$$

From (3.11), it can be easily shown that $\mathbf{u}^T\boldsymbol{\Phi}^t_{\boldsymbol{mm}}\mathbf{u}$ can be lower-bounded by

$$\mathbf{u}^T\boldsymbol{\Phi}^t_{\boldsymbol{mm}}\mathbf{u} \geq \bar{\mathbf{b}}^T\boldsymbol{\Phi}^t_{\boldsymbol{mm}}\bar{\mathbf{b}} + 2\langle \mathbf{u} - \bar{\mathbf{b}}, \boldsymbol{\Phi}^t_{\boldsymbol{mm}}\bar{\mathbf{b}}\rangle - \gamma\|\mathbf{u} - \bar{\mathbf{b}}\|^2 \tag{3.12}$$

where $\gamma := \max\{|\lambda_{\min}(\Phi^t_{mm})|, |\lambda_{\max}(\Phi^t_{mm})|\}$, and $\lambda_{\min}(\Phi^t_{mm})$ and $\lambda_{\max}(\Phi^t_{mm})$ are the smallest and largest eigenvalues of Φ^t_{mm}, respectively.

Employing the lowerbound in (3.12) and relaxing the constraint $\mathbf{u} \in \{0, 1\}^{|\mathcal{M}^t}$ with $\mathbf{0} \preceq \mathbf{u} \preceq \mathbf{1}$, estimates of the misses follows

$$\hat{\mathbf{b}}^t_m = \arg \max_{\mathbf{0} \preceq \mathbf{u} \preceq \mathbf{1}} \boldsymbol{\alpha}^{t\ T}_{\boldsymbol{m}}\mathbf{u} + 2\mathbf{b}^{t\ T}_o\boldsymbol{\Phi}^t_{\boldsymbol{om}}\mathbf{u} + 2\mathbf{u}^T\boldsymbol{\Phi}^t_{\boldsymbol{mm}}\bar{\mathbf{b}} - \gamma\|\mathbf{u} - \bar{\mathbf{b}}\|^{\mathbf{2}}. \tag{3.13}$$

Then, a closed-form solution of $\mathbf{u}$ can be obtained as

$$[\hat{\mathbf{u}}]_i = [t_i]^1_0, \quad i \in \mathcal{M}^t \tag{3.14}$$

1: Initialize $\boldsymbol{\alpha}^0 = 0$, $\boldsymbol{\Phi}^0 = 0 \times \boldsymbol{I}$, $\mathbf{b}^0 = \mathbf{1}_{N\times 1}$
2: For t=1,2,... do
3: Acquire $\boldsymbol{\rho}^t$ and $\mathbf{b}^t$ and find the locations of misses in $\mathbf{b}^t$
4: Based on step 3, form the permutation matrix $\mathbf{P}^t$
5: Find $\boldsymbol{\Phi}^t_{\boldsymbol{om}}$, $\boldsymbol{\Phi}^t_{\boldsymbol{mm}}$, $\mathbf{u}^*_m$, and $\boldsymbol{\alpha}^t_{\boldsymbol{m}}$ using (3.7)-(3.10)
6: $\bar{\mathbf{b}} = \mathbf{u}^*_m$
7: Obtain $\hat{\mathbf{b}}^t_m$ from (3.14) and evaluate $\nabla\hat{\ell}^t(\hat{\boldsymbol{\theta}}^t)$
8: Update $\hat{\boldsymbol{\theta}}^{t+1} = \hat{\boldsymbol{\theta}}^t - \mu_t\nabla\hat{\ell}^t(\hat{\boldsymbol{\theta}}^t)$

Table 3.1: Overall algorithm.

where

$$t_i := \left[\frac{0.5\boldsymbol{\alpha}^t_{\boldsymbol{m}} + \boldsymbol{\Phi}^t_{\boldsymbol{om}}{}^T\mathbf{b}^t_o + \boldsymbol{\Phi}^t_{\boldsymbol{mm}}\bar{\mathbf{b}} + \gamma\bar{\mathbf{b}}}{\gamma}\right]_i, \quad i \in \mathcal{M}^t \tag{3.15}$$

and $[u]^b_a \triangleq \min\{\max\{u, a\}, b\}$. Using $\hat{\mathbf{b}}^t_m$ from (3.14), $\hat{\boldsymbol{\theta}}^{t+1}$ can then be obtained by (3.4).

The overall algorithm based on the approximation of the quadratic term is given in Table 5.1.

3.3 Expectation-maximization Benchmark

When estimates of the misses are not available, the marginal distribution of the observed data can be obtained by simply discarding the missing data. Therefore, analogous to the case with complete data, $\hat{\boldsymbol{\theta}}^{t+1}$ can be estimated using (3.2) except that the loss function ℓ^t is replaced by

$$\ell^t_{partial}(\boldsymbol{\theta}^t) := -\log p_{\boldsymbol{\theta}^t}(\mathbf{b}^t_o|\boldsymbol{\rho}^t) \tag{3.16}$$

where $p_{\boldsymbol{\theta}^t}(\mathbf{b}^t_o|\boldsymbol{\rho}^t) = \sum_{\mathbf{b}^t_m} p_{\boldsymbol{\theta}^t}(\mathbf{b}^t_o, \mathbf{b}^t_m|\boldsymbol{\rho}^t)$. One can rewrite $\ell^t_{partial}(\boldsymbol{\theta}^t)$ as

$$\ell^t_{partial}(\boldsymbol{\theta}^t) = -\log \sum_{\mathbf{b}^t_m} \frac{p_{\boldsymbol{\theta}^t}(\mathbf{b}^t_o, \mathbf{b}^t_m|\boldsymbol{\rho}^t)}{p_{\hat{\boldsymbol{\theta}}^t}(\mathbf{b}^t_m|\boldsymbol{\rho}^t, \mathbf{b}^t_o)} p_{\hat{\boldsymbol{\theta}}^t}(\mathbf{b}^t_m|\boldsymbol{\rho}^t, \mathbf{b}^t_o)$$
$$= -E_{p_{\hat{\boldsymbol{\theta}}^t}(\mathbf{b}^t_m|\boldsymbol{\rho}^t, \mathbf{b}^t_o)}\{\log \sum_{\mathbf{b}^t_m} \frac{p_{\boldsymbol{\theta}^t}(\mathbf{b}^t_o, \mathbf{b}^t_m|\boldsymbol{\rho}^t)}{p_{\hat{\boldsymbol{\theta}}^t}(\mathbf{b}^t_m|\boldsymbol{\rho}^t, \mathbf{b}^t_o)}\}. \tag{3.17}$$

Upon invoking Jensen's inequality a lower bound of the marginal log-likelihood, can be obtained as

$$\log \sum_{\mathbf{b}^t_m} \frac{p_{\boldsymbol{\theta}^t}(\mathbf{b}^t_o, \mathbf{b}^t_m|\boldsymbol{\rho}^t)}{p_{\hat{\boldsymbol{\theta}}^t}(\mathbf{b}^t_m|\boldsymbol{\rho}^t, \mathbf{b}^t_o)} p_{\hat{\boldsymbol{\theta}}^t}(\mathbf{b}^t_m|\boldsymbol{\rho}^t, \mathbf{b}^t_o)$$
$$\geq \sum_{\mathbf{b}^t_m} [\log p_{\boldsymbol{\theta}^t}(\mathbf{b}^t_o, \mathbf{b}^t_m|\boldsymbol{\rho}^t) - \log p_{\hat{\boldsymbol{\theta}}^t}(\mathbf{b}^t_m|\boldsymbol{\rho}^t, \mathbf{b}^t_o)] p_{\hat{\boldsymbol{\theta}}^t}(\mathbf{b}^t_m|\boldsymbol{\rho}^t, \mathbf{b}^t_o). \tag{3.18}$$

It can be seen that the term $\log p_{\hat{\boldsymbol{\theta}}^t}(\mathbf{b}^t_m|\boldsymbol{\rho}^t, \mathbf{b}^t_o) p_{\hat{\boldsymbol{\theta}}^t}(\mathbf{b}^t_m|\boldsymbol{\rho}^t, \mathbf{b}^t_o)$ can be evaluated at $\hat{\boldsymbol{\theta}}^t$ and is not involved in $\boldsymbol{\theta}^t$ estimation. Then, the prediction of $\boldsymbol{\theta}^{t+1}$, boils down to an expectation maximization (EM) step with the following loss function and gradient

$$\ell^t_{EM}(\boldsymbol{\theta}^t) := -\sum_{\mathbf{b}^t_m} \log p_{\boldsymbol{\theta}^t}(\mathbf{b}^t_o, \mathbf{b}^t_m|\boldsymbol{\rho}^t) p_{\hat{\boldsymbol{\theta}}^t}(\mathbf{b}^t_m|\boldsymbol{\rho}^t, \mathbf{b}^t_o) \tag{3.19a}$$

$$\nabla \ell^t_{EM}(\boldsymbol{\theta}^t) = -\sum_{\mathbf{b}^t_m} \nabla \log p_{\boldsymbol{\theta}^t}(\mathbf{b}^t_o, \mathbf{b}^t_m|\boldsymbol{\rho}^t) p_{\hat{\boldsymbol{\theta}}^t}(\mathbf{b}^t_m|\boldsymbol{\rho}^t, \mathbf{b}^t_o). \tag{3.19b}$$

Intuitively, EM first fills in the misses with probability $p_{\hat{\boldsymbol{\theta}}^t}(\mathbf{b}^t_m|\boldsymbol{\rho}^t, \mathbf{b}^t_o)$, and then applies an online learning algorithm to filled-in data.

It is worth noting that in addition to the computational complexity of evaluating $p_{\boldsymbol{\theta}^t}(\mathbf{b}^t_m|\boldsymbol{\rho}^t, \mathbf{b}^t_o)$, the summation required to incorporate all possible values for the misses in the parameter estimation renders EM algorithm computationally expensive, especially when the number of misses and the dimension of the problem increases.

3.4 Numerical Tests

3.4.1 Synthetic Data

The performance of the proposed algorithm was verified via numerical tests. A set of 10 EV owners was considered, whose spatial dependencies were captured by the graph G shown in

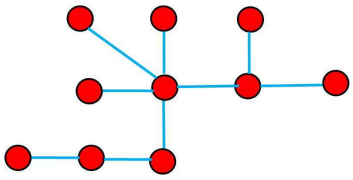

Figure 3.1: Spatial dependency graph for synthetic data.

Fig. 3.1. The set of consumers whose charging decisions was not collected, namely, $\mathcal{M}^t$, was uniformly sampled from V. The price $\boldsymbol{\rho}^t$ was set to 1 for all consumers and held constant. It is assumed that $\boldsymbol{\theta}^t$ changes at $t = 110$ and $t = 220$, and remains fixed for the rest of iterations.

Fig. 3.2 depicts the normalized prediction error of the parameters of the *pdf* in (3.1), averaged over 20 realizations. It is observed that when 70% of data are missing, with the proposed online algorithm, the errors tend to decrease as iterations progress, while sharp increases in the prediction error result whenever the parameter values are changed abruptly. Similar trend can be seen when 30% of the data are missing. However, as expected the case with 30% misses has a small gap with the error obtained with full data case, while the gap is larger when there are 70% misses. It can be also seen that the EM-based online algorithm exhibits performance similar to proposed algorithm when only 30% of data are missing, but incurs more errors than the proposed one when the number of misses increases. In addition, the EM-based online algorithm does not track the abrupt parameter changes, adequately.

The expected value of the total charging load is given by

$$P_{tot}^t := P_{EV} \sum_{i=1}^{N} p_{\hat{\boldsymbol{\theta}}^t}(b_i^t = 1 | \boldsymbol{\rho}^t) \tag{3.20}$$

where $P_{EV} = 1\text{kW}$ is the load due to charging of a single EV. The predicted total charging loads are depicted in Fig. 3.3, where the proposed and EM-based algorithms are plotted together for comparison purposes. It can be seen that both EM and the proposed algorithm track the true total consumption when 30% of data are missing. However, with 70% misses the proposed algorithm outperforms the EM-based algorithm.

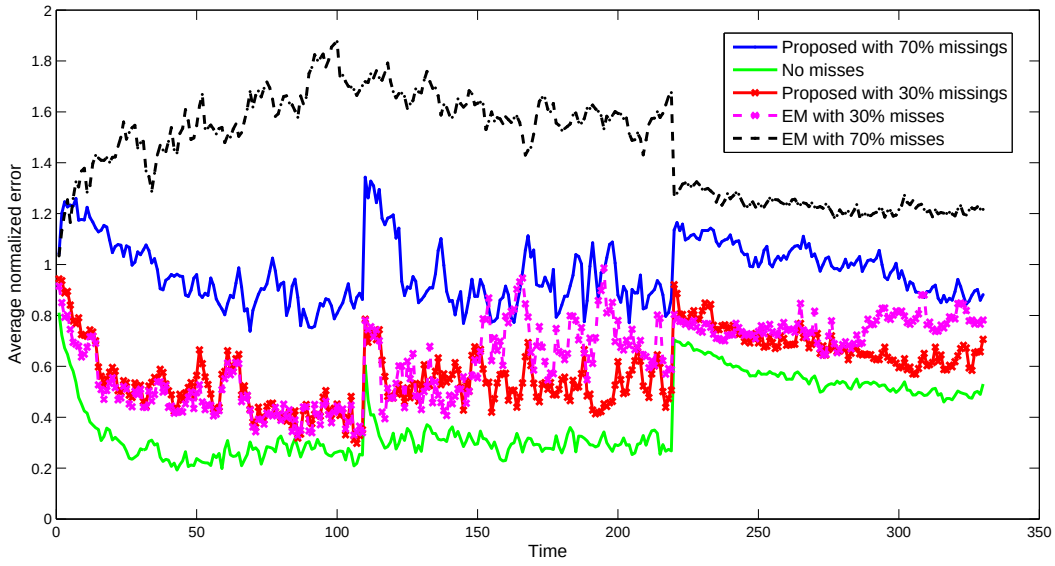

Figure 3.2: Normalized prediction error.

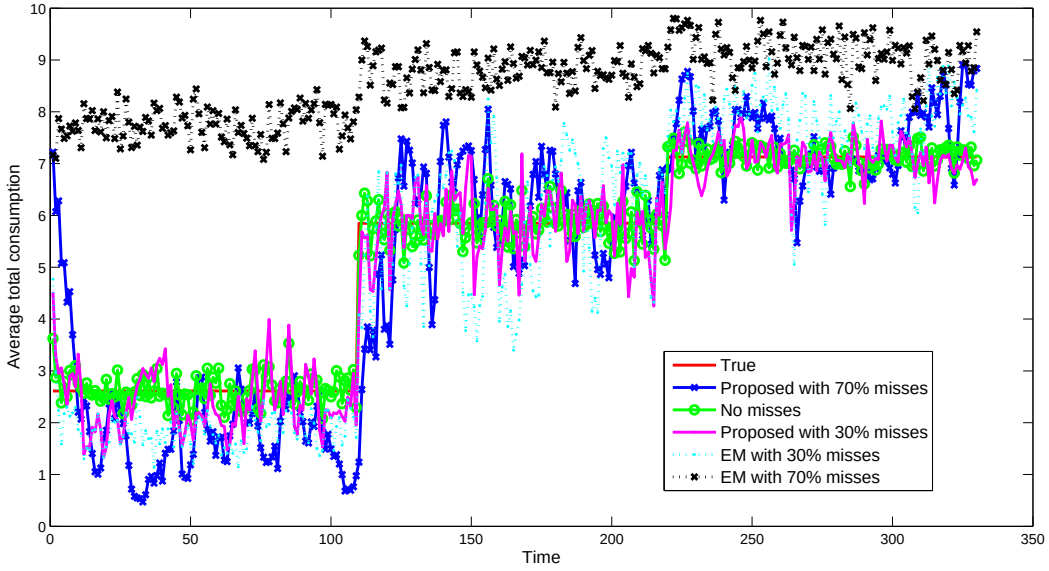

Figure 3.3: Total charging load

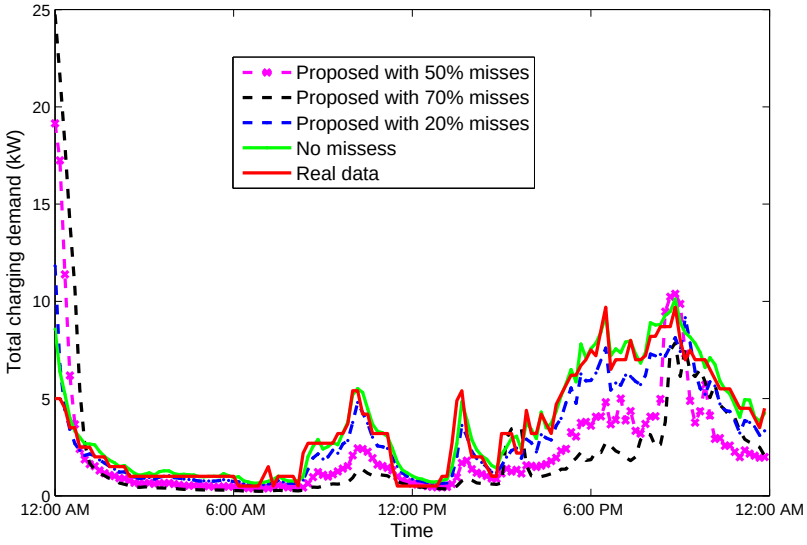

Figure 3.4: Total charging demand with missing data

3.4.2 Semi-real Data

The experimental data of total home charging power demand for 25 Northern California households as shown in Figures 2.6 and 2.8 is used. As explained in Chapter 2, the consumers' decisions at each time are sampled from

$$b_i^t = \begin{cases} 1, & \text{if } \rho_i^t < \tau_i^t \\ 0, & \text{otherwise} \end{cases} \qquad \forall i \in V. \tag{3.21}$$

It is assumed that $P_{EV} = 1.4$ and the set of consumers whose charging decisions was not collected, namely, $\mathcal{M}^t$ is uniformly sampled from V. Fig. 3.4 depicts the total estimated charging of consumers when there are misses in the consumers' charging decisions. It can be seen that the predicted demand using the CRF-based model with no misses fits well the true charging demand. It is further observed that the proposed algorithm with the misses being replaced by their estimates, tracks well the true demand, while the gap between the predicted demand with 20% misses and the true demand is small. However, the gap grows as the number of misses increases, as expected.

In Fig. 3.5 the solid line depicts the predicted total charging demand obtained by the proposed algorithm when the number of misses changes, while the dashed line and the

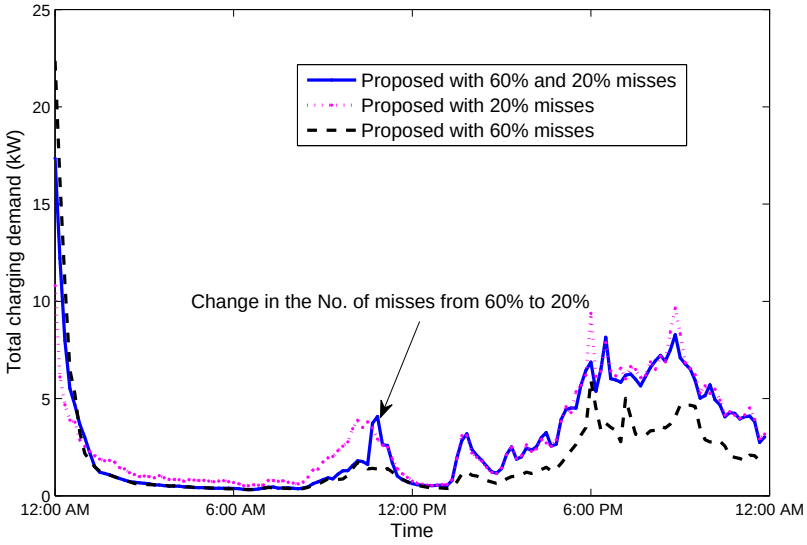

Figure 3.5: Total charging demand with a change in the number of misses

dotted dash line represent the predicted total charging demand with the number of misses fixed at 60% and 20%, respectively. It can be seen that when the number of misses changes, the predicted total charging demand tracks the changes in the missing data and touches the right curve.

3.5 Conclusions

The problem of learning the consumers' charging behavior with missing data was considered. A CRF-based model for capturing the probabilities with which individual EV consumers charge their vehicles was introduced. The collected charging data from individual customers were allowed to include misses, which is natural to expect in the charging data collected from the network of consumers. Then, instead of neglecting the misses or filling them with all possible values, an estimate of the misses was first obtained. Incorporating the estimates and without explicit models for the temporal dynamics of consumption behavior, an online algorithm for learning the consumers dependency network parameters and elasticity was developed. The performance of the proposed algorithm was verified by numerical tests using synthetic and semi-real data.

Chapter 4

Resource Allocation for OFDMA CR under Channel Uncertainty in uplink

This chapter addresses the RA task for OFDMA uplink CRs with uncertain CR-to-PU channels. A weighted sum-rate maximization problem is formulated under a probabilistic interference constraint and maximum transmit-power constraints for the CR users. The Bernstein method is adopted to approximate the probabilistic constraint by a convex constraint. Even after the approximation, the overall problem is still nonconvex due to the combinatorial assignment of users to each subcarrier. By employing appropriate bounds, the approximation emerging from the interference constraint can be further made *separable* across subcarriers. This opens the door to the dual decomposition approach, which leads to a near-optimal and computationally efficient solution [35]. The material in this chapter draws from [48], [49].

4.1 Modeling and Problem Statement

Consider the uplink mode of a network comprising K CR users communicating with their BS using OFDMA over N subcarriers. The instantaneous channel gain $\tilde{g}_k^{(n)}$ between CR

user $k \in \mathcal{K} \triangleq \{1, 2, \ldots, K\}$ and the CR BS on subcarrier $n \in \mathcal{N} \triangleq \{1, 2, \ldots, N\}$ is assumed to be acquired accurately via conventional channel estimation techniques. It is further assumed that during the spectrum sensing phase, the presence of an active PU has been detected. It is straightforward to handle multiple PUs in the framework to be proposed. In order to limit the interference inflicted to the PU, the channels from the CR users to the PU must be known. Let $g_k^{(n)}$ denote the channel gain from the k-th CR to the PU receiver on subcarrier n. Due to lack of cooperation from the PU system, it is difficult to estimate $g_k^{(n)}$ precisely. To capture this uncertainty, $g_k^{(n)}$ is modeled as a random variable.

A relevant RA problem is to maximize the weighted sum of all CR throughputs under the transmit-power constraints (one per CR), and the PU interference constraint. Let $p^{(n)}$ denote the transmit-power loaded on subcarrier n, where $0 \leq p^{(n)} \leq P_{\max}^{(n)}$. Let $\mathbf{p}$ and $\mathbf{P}_{\max}$ be the vectorized versions of $\{p^{(n)}\}$ and $\{P_{\max}^{(n)}\}$, respectively. Also, let $k(n) \in \mathcal{K}$ represent the index of the user served on subcarrier n, and define $\mathbf{k} \triangleq [k(1), \ldots, k(N)]^T$. With w_k denoting the positive weight for user $k \in \mathcal{K}$, the following chance-constrained optimization problem is of interest.

$$\text{(P1)} \qquad \max_{0 \preceq \mathbf{p} \preceq \mathbf{P}_{\max}, \mathbf{k} \in \mathcal{K}^N} \sum_{n \in \mathcal{N}} w_{k(n)} \log\left(1 + \tilde{g}_{k(n)}^{(n)} p^{(n)}\right) \tag{4.1}$$

$$\text{subject to} \sum_{n \in \mathcal{N}: k(n) = k} p^{(n)} \leq P_{k,\max}, \quad k \in \mathcal{K} \tag{4.2}$$

$$\Pr\left\{\sum_{n \in \mathcal{N}} g_{k(n)}^{(n)} p^{(n)} < I_{\max}\right\} \geq 1 - \epsilon \tag{4.3}$$

where (5.6) is the per-CR power constraint, and (4.3) enforces that the interference power at the PU stays below $I_{\max}$ with probability no less than $1 - \epsilon$ with $\epsilon \in (0, 1)$ denoting the desired upper-bound on the probability that the interference threshold is exceeded. In case of more than one PUs present, multiple PU protection constraints analogous to (4.3) can be imposed. The widely accepted constraint is to control the "interference temperature" such that the interference experienced by the PU system is below a certain threshold on the order of the background noise and interference.

The feasible set of (4.3) can be either convex or nonconvex, depending on the distribution of $g_k^{(n)}$ [37]. For example, $\Pr\left\{\mathbf{a}^T\mathbf{u} < \mathbf{b}\right\} \geq 1 - \epsilon$ is convex for $\epsilon < 1/2$, if $[\mathbf{a}^T \ \mathbf{b}^T]^T$ has a

symmetric logarithmically concave density [37]. However, even if (4.3) is convex, it may not be straightforward to express it in closed form, rendering the optimization problem intractable. Moreover, the overall problem would be still nonconvex due to the combinatorial search over $\mathbf{k}$ needed for the subcarrier assignment to CR users.

In the following, a convex approximation of (4.3) is advocated. In particular, the approximation is made conservative in the sense that the approximate constraint implies the original constraint (4.3). This will be achieved by using the Bernstein method [5, 37]. By judiciously choosing the form of the approximation, one can also ensure that the approximate constraint is separable in n. Then, an efficient near-optimal solution will be obtained via dual decomposition [12, 35].

4.2 Approximation of Chance Constraints

4.2.1 Bernstein Approximation

A useful class of approximation techniques for chance constraints known as Bernstein approximations is briefly reviewed in the present context [5, 37]. Consider a chance constraint of the form

$$\Pr\left\{ f_0(\mathbf{p}) + \sum_{n=1}^{N} \zeta_n f_n(\mathbf{p}) < 0 \right\} \geq 1 - \epsilon \tag{4.4}$$

where $\mathbf{p}$ is a deterministic parameter vector, and $\{\zeta_n\}$ are random variables with marginal distributions denoted as $\{\pi_n\}$. Suppose that one desires to meet this constraint for a given family of $\{\zeta_n\}$ distributions, under the following assumptions.

as1) $\{f_n(\mathbf{p})\}$ are affine in $\mathbf{p}$ for $n = 0, 1, \ldots, N$;

as2) $\{\zeta_n\}$ are independent of each other; and

as3) $\{\pi_n\}$ have a common bounded support of $[-1, 1]$; that is, $-1 \leq \zeta_n \leq 1$ for all $n = 1, \ldots, N$.

Under these assumptions, the following constraint constitutes a conservative substitute and thus implies (4.4)

$$\inf_{\rho>0}\left[f_0(\mathbf{p})+\rho\sum_{n=1}^{N}\Omega_n\left(\rho^{-1}f_n(\mathbf{p})\right)+\rho\log\left(\frac{1}{\epsilon}\right)\right]\leq 0 \tag{4.5}$$

where $\Omega_n(y)\triangleq\max_{\pi_n}\log\left(\int\exp(xy)d\pi_n(x)\right)$. Moreover, it is guaranteed that (4.5) is convex [5, 37]. The approximation is useful when $\{\Omega_n(y)\}$ can be evaluated efficiently. In general, one can consider an upper-bound for $\Omega_n(y)$ given by

$$\Omega_n(y)\leq\max\{\mu_n^-y,\mu_n^+y\}+\frac{\sigma_n^2}{2}y^2,\quad n=1,\ldots,N \tag{4.6}$$

where μ_n^-, μ_n^+ with $-1\leq\mu_n^-\leq\mu_n^+\leq 1$ and $\sigma_n\geq 0$ are constants that depend on the given families of probability distributions. Some examples are given in [5, Table 1], where the useful prior knowledge includes the support, unimodality (with respect to the center of the support), and symmetry of the distribution, as well as the ranges of the first- and the second-order moments. Using more prior knowledge leads to tighter approximation. Replacing $\Omega_n(\cdot)$ in (4.5) with this upper-bound, and invoking the arithmetic-geometric inequality, yields

$$f_0(\mathbf{p})+\sum_{n=1}^{N}\max\{\mu_n^-f_n(\mathbf{p}),\mu_n^+f_n(\mathbf{p})\}+\sqrt{2\log\frac{1}{\epsilon}}\left(\sum_{n=1}^{N}\sigma_n^2f_n(\mathbf{p})^2\right)^{\frac{1}{2}}\leq 0 \tag{4.7}$$

as a convex conservative surrogate for (4.4).

Suppose now that the distributions of $g_k^{(n)}$ have bounded supports $[a_k^{(n)},b_k^{(n)}]$.[1] The case with unbounded supports will be treated in Sec. 4.2.2. Introduce constants $\alpha_k^{(n)}\triangleq\frac{1}{2}(b_k^{(n)}-a_k^{(n)})\neq 0$ and $\beta_k^{(n)}\triangleq\frac{1}{2}(b_k^{(n)}+a_k^{(n)})$ to normalize the supports to $[-1,1]$ per as3); that is,

$$\zeta_k^{(n)}\triangleq\frac{g_k^{(n)}-\beta_k^{(n)}}{\alpha_k^{(n)}}\in[-1,1]. \tag{4.8}$$

Then, letting $f_0(\mathbf{p})=-I_{\max}+\sum_{n=1}^{N}\beta_{k(n)}^{(n)}p^{(n)}$ and $f_n(\mathbf{p})=\alpha_{k(n)}^{(n)}p^{(n)}$ for $n\in\mathcal{N}$, it follows that (4.4) is equivalent to (4.3). Thus, substituting these into (4.7), and noting that $p^{(n)}\geq 0$,

[1] In practice, the channel estimation techniques often yield not only the channel gain estimates, but also the associated confidence interval, from which one can effectively bound the channel gains.

one obtains

$$-I_{\max}+\sum_{n=1}^{N}\beta_{k(n)}^{(n)}p^{(n)}+\sum_{n=1}^{N}\mu_{k(n)}^{(n)+}\alpha_{k(n)}^{(n)}p^{(n)}+\sqrt{2\log\frac{1}{\epsilon}}\left(\sum_{n=1}^{N}\left(\sigma_{k(n)}^{(n)}\alpha_{k(n)}^{(n)}p^{(n)}\right)^2\right)^{\frac{1}{2}}\leq 0. \tag{4.9}$$

The overall RA problem corresponding to (P1) with (4.3) replaced by (4.9) is still nonconvex due to the combinatorial search for the optimal $\mathbf{k}$ over $\mathcal{K}^N$, which is a nonconvex set. In fact, as the variables $p^{(n)}$ are coupled nonlinearly through the last term in (4.9), the search complexity grows rapidly as N increases. To mitigate these issues, we consider adopting the dual decomposition method, which is applicable when the problem has a separable structure; that is, after relaxing coupling constraints through Lagrange relaxation, the problem must decompose into subproblems that can be solved independently. To bring about such a separable structure, we further approximate (4.9) by noting that the last term in (4.9) involves the ℓ_2-norm of the vector $[\sigma_{k(1)}^{(1)}\alpha_{k(1)}^{(1)}p^{(1)},\ldots,\sigma_{k(N)}^{(N)}\alpha_{k(N)}^{(N)}p^{(N)}]$, and that $\|\mathbf{x}\|_2\leq\sqrt{N}\|\mathbf{x}\|_\infty$ for any $\mathbf{x}\in\mathbb{R}^N$. Thus, the constraint becomes

$$\sum_{n=1}^{N}\gamma_{k(n)}^{(n)}p^{(n)}+\sqrt{2N\log\frac{1}{\epsilon}}\max_{n\in\mathcal{N}}\sigma_{k(n)}^{(n)}\alpha_{k(n)}^{(n)}p^{(n)}\leq I_{\max} \tag{4.10}$$

where $\gamma_{k(n)}^{(n)}\triangleq\mu_{k(n)}^{(n)+}\alpha_{k(n)}^{(n)}+\beta_{k(n)}^{(n)}$.

Alternatively, one can appeal to the fact that $\|\mathbf{x}\|_2\leq\|\mathbf{x}\|_1$ to obtain yet another substitute for (4.3) as

$$\sum_{n=1}^{N}\gamma_{k(n)}^{(n)}p^{(n)}+\sqrt{2\log\frac{1}{\epsilon}}\sum_{n=1}^{N}|\sigma_{k(n)}^{(n)}\alpha_{k(n)}^{(n)}p^{(n)}|\leq I_{\max}. \tag{4.11}$$

Both (4.10) and (4.11) are amenable to dual decomposition, as will be discussed in Sec. 5.3. In the sequel, (P1) with (4.3) replaced by (4.9), (4.10) and (4.11) will be referred to as the ℓ_2-, ℓ_∞-, and ℓ_1-*approximate problems*, respectively.

Even when the channel distribution is known, if the corresponding chance constraint is nonconvex or hard to express analytically, it may be reasonable to apply Bernstein approximation for tractability, as long as conditions as1)–as3) are met, which include boundedness of the support of the distribution. The case of distributions with an unbounded support is discussed next.

4.2.2 Extensions to Channels with Unbounded Support

In the preceding discussion, Bernstein approximations were applied to bounded channel gains. While this may be reasonable considering the finite dynamic ranges of the A/D converters in the radios, presuming too large a range for the uncertain parameters might lead to a very loose approximation of the chance constraint. An alternative approach is developed here when the channel distributions are known (as opposed to the preceding case where the *family* of possible distributions was assumed to be known.)

Upon defining $I \triangleq \sum_n g_{k(n)}^{(n)} p^{(n)}$, it is possible to express $\Pr\{I < I_{\max}\}$ in (4.3) as

$$\begin{aligned} &\Pr\{I < I_{\max} | \mathbf{a} \le \mathbf{g} \le \mathbf{b}\} \Pr\{\mathbf{a} \le \mathbf{g} \le \mathbf{b}\} \\ &+ \Pr\{I < I_{\max} | \mathbf{g} < \mathbf{a} \text{ or } \mathbf{g} > \mathbf{b}\} \Pr\{\mathbf{g} < \mathbf{a} \text{ or } \mathbf{g} > \mathbf{b}\} \end{aligned} \tag{4.12}$$

where $\mathbf{g} \triangleq [g_{k(1)}^{(1)}, ..., g_{k(N)}^{(N)}]^T$, $\mathbf{a} \triangleq [a_{k(1)}^{(1)}, ..., a_{k(N)}^{(N)}]^T$ and $\mathbf{b} \triangleq [b_{k(1)}^{(1)}, ..., b_{k(N)}^{(N)}]^T$ are appropriate constants determined such that

$$\delta \triangleq \Pr\{\mathbf{a} \le \mathbf{g} \le \mathbf{b}\} \in (1 - \epsilon, 1). \tag{4.13}$$

Then, noting that the second term in (4.12) is no larger than $(1 - \delta)$, and thus neglecting this term, (4.3) can be approximated conservatively as

$$\Pr\{I < I_{\max} \, | \mathbf{a} \le \mathbf{g} \le \mathbf{b}\} \ge \frac{1 - \epsilon}{\Pr\{\mathbf{a} \le \mathbf{g} \le \mathbf{b}\}} = \frac{1 - \epsilon}{\delta} \triangleq 1 - \epsilon' \tag{4.14}$$

which can now be approximated by (4.10) or (4.11) with ϵ replaced by ϵ'. For concreteness, consider the cases with and without channel estimation over Rayleigh fading channels.

Without Channel Estimation

Suppose first that channel estimation is not attempted. Then, one has only the prior knowledge that the probability density function (*p.d.f.*) of $g_k^{(n)}$ is exponential with mean $\bar{g}_k^{(n)}$ as

$$f_{g_k^{(n)}}(x) = \frac{1}{\bar{g}_k^{(n)}} \exp\left(-\frac{x}{\bar{g}_k^{(n)}}\right). \tag{4.15}$$

It then follows from the independence assumption that

$$\Pr\{\mathbf{a} \leq \mathbf{g} \leq \mathbf{b}\} = \prod_{n=1}^{N} \Pr\left\{a_{k(n)}^{(n)} \leq g_{k(n)}^{(n)} \leq b_{k(n)}^{(n)}\right\}$$
$$= \prod_{n=1}^{N} \left[\exp\left(-\frac{a_{k(n)}^{(n)}}{\bar{g}_{k(n)}^{(n)}}\right) - \exp\left(-\frac{b_{k(n)}^{(n)}}{\bar{g}_{k(n)}^{(n)}}\right)\right] = \delta. \tag{4.16}$$

Since the peak of the *p.d.f.* of $g_k^{(n)}$ is located at the origin, it is natural to choose the lower-bound as $\mathbf{a} = \mathbf{0}$. To determine $\mathbf{b}$, $\Pr\left\{0 \leq g_{k(n)}^{(n)} \leq b_{k(n)}^{(n)}\right\}$ is enforced to be constant across n. Then, $\mathbf{b}$ is obtained as

$$b_{k(n)}^{(n)} = \bar{g}_{k(n)}^{(n)} \log \frac{1}{1 - \delta^{\frac{1}{N}}}, \quad n \in \mathcal{N}\ . \tag{4.17}$$

With Channel Estimation

Consider now that OFDM channel estimation is performed using the minimum mean-square error (MMSE) estimator under Rayleigh fading [60]. The complex channel coefficient vector of the k-th user, $\mathbf{h}_k = \{h_k^{(n)}\}_{n=1}^{N}$, can be modeled as

$$\mathbf{h}_k = \hat{\mathbf{h}}_k + \tilde{\mathbf{h}}_k \tag{4.18}$$

where $\hat{\mathbf{h}}_k$ is the channel estimate, and $\tilde{\mathbf{h}}_k$ zero-mean Gaussian-distributed estimation error. The covariance matrix of $\tilde{\mathbf{h}}_k$ is given by [60]

$$\mathbf{\Sigma}_{\tilde{\mathbf{h}}_k} = \frac{N\sigma_h^2}{L+1}\mathbf{F}_L\mathbf{F}_L^H \tag{4.19}$$

where $(L+1)$ is the number of paths in the fading channel, σ_h^2 is a parameter that depends on the system parameters including Doppler spread and the noise variance at the receiver, and $\mathbf{F}_L$ is the $N \times (L+1)$ DFT matrix with (n,ℓ)-th entry given by $\frac{1}{\sqrt{N}}e^{-j\frac{2\pi}{N}(n-1)(\ell-1)}$. Therefore, $\mathbf{h}_k$ is distributed as circularly symmetric complex Gaussian with mean $\hat{\mathbf{h}}_k$ and covariance $\mathbf{\Sigma}_{\tilde{\mathbf{h}}_k}$. It is assumed that $\mathbf{h}_k$ is independent across k.

Upon defining $\hat{g}_k^{(n)} \triangleq \left|\hat{h}_k^{(n)}\right|^2$, the random variable $g_k^{(n)} = \left|h_k^{(n)}\right|^2$ is non-central Chi-square with two degrees of freedom and non-centrality parameter $\frac{2\hat{g}_k^{(n)}}{\sigma_h^2}$, with its *p.d.f.* given by

$$f_{g_k^{(n)}}(x) = \frac{1}{\sigma_h^2}\exp\left(-\frac{\hat{g}_k^{(n)} + x}{\sigma_h^2}\right) I_0\left(\frac{2}{\sigma_h^2}\sqrt{\hat{g}_k^{(n)}x}\right). \tag{4.20}$$

To apply Bernstein's approximation, it is further assumed here that $\{h_k^{(n)}\}$ are independent across n. This essentially holds true when the number of subchannels is close to the number of paths. However, even if this is not the case, the numerical tests in Sec. 5 will verify that the interference constraints are approximated conservatively. Proceeding under the assumption, one obtains

$$\begin{aligned}\Pr\{\mathbf{a} \le \mathbf{g} \le \mathbf{b}\} &= \prod_{n=1}^{N} \Pr\left\{a_{k(n)}^{(n)} \le g_{k(n)}^{(n)} \le b_{k(n)}^{(n)}\right\} \\ &= \prod_{n=1}^{N} \left[Q\left(\sqrt{\frac{2\hat{g}_{k(n)}^{(n)}}{\sigma_h^2}}, \sqrt{\frac{2a_{k(n)}^{(n)}}{\sigma_h^2}} \right) - Q\left(\sqrt{\frac{2\hat{g}_{k(n)}^{(n)}}{\sigma_h^2}}, \sqrt{\frac{2b_{k(n)}^{(n)}}{\sigma_h^2}} \right) \right] = \delta \end{aligned} \tag{4.21}$$

where $Q(\cdot,\cdot)$ is Marcum's Q-function. Similar to the case without channel estimation, we choose to set the factors in the product in (4.21) equal across n. Since the mode of the distribution of $g_{k(n)}^{(n)}$ is tightly upper-bounded by $\hat{g}_{k(n)}^{(n)}$ [42], it is natural to set $a_{k(n)}^{(n)} = \hat{g}_{k(n)}^{(n)} - \check{g}_{k(n)}^{(n)}$ and $b_{k(n)}^{(n)} = \hat{g}_{k(n)}^{(n)} + \check{g}_{k(n)}^{(n)}$ for $0 \le \check{g}_{k(n)}^{(n)} \le \hat{g}_{k(n)}^{(n)}$ such that

$$Q\left(\sqrt{\frac{2\hat{g}_{k(n)}^{(n)}}{\sigma_h^2}}, \sqrt{\frac{2(\hat{g}_{k(n)}^{(n)} - \check{g}_{k(n)}^{(n)})}{\sigma_h^2}} \right) - Q\left(\sqrt{\frac{2\hat{g}_{k(n)}^{(n)}}{\sigma_h^2}}, \sqrt{\frac{2(\hat{g}_{k(n)}^{(n)} + \check{g}_{k(n)}^{(n)})}{\sigma_h^2}} \right) = \delta^{\frac{1}{N}} \tag{4.22}$$

is satisfied. If such $\check{g}_{k(n)}^{(n)}$ does not exist due to small $\frac{2\hat{g}_{k(n)}^{(n)}}{\sigma_h^2}$ (or, equivalently, large channel uncertainty), it is prudent to choose $a_{k(n)}^{(n)} = 0$ and find $b_{k(n)}^{(n)}$ from

$$Q\left(\sqrt{\frac{2\hat{g}_{k(n)}^{(n)}}{\sigma_h^2}}, \sqrt{\frac{2b_{k(n)}^{(n)}}{\sigma_h^2}} \right) = 1 - \delta^{\frac{1}{N}}. \tag{4.23}$$

It is worth noting that even if the channel *p.d.f.*'s are known to be either exponential or non-central Chi-square, it is not straightforward to express the *p.d.f.* of I in closed form [10, 11], which underlines the usefulness of the proposed approach.

Remark 4.1 It can be checked that when the channel estimation error vanishes, the approximated chance-constraints (4.9)–(4.11) fall back to the desired deterministic interference constraint, namely, $\sum_{n\in\mathcal{N}} \hat{g}_{k(n)}^{(n)} p^{(n)} \le I_{\max}$. To see this, first note that $\check{g}_{k(n)}^{(n)} \to 0$ as $\sigma_h^2 \to 0$ from (4.22). Thus, $\alpha_{k(n)}^{(n)}$ and $\beta_{k(n)}^{(n)}$ approach 0 and $\hat{g}_{k(n)}^{(n)}$, respectively. Substituting these into (4.9)–(4.11) yields the desired result.

4.3 Resource Allocation Algorithms

The OFDMA RA problems with separable structure can be tackled efficiently in the dual domain. In this approach, the overall problem is divided into multiple smaller per-subcarrier subproblems, which can be solved separately, coordinated by the range multipliers. Moreover, it can be shown that the duality gap vanishes as the number of subcarriers increases. This approach has been widely applied to the RA problems for multi-carrier systems [12, 35, 63].

The ℓ_1-approximate problem is clearly separable in n. As for the ℓ_∞-approximate problem, by introducing auxiliary variables $\mathbf{u} \triangleq [u_1, \ldots, u_N]^T$, the following separable constraints can be shown to be equivalent to (4.10).

$$\sum_{n=1}^{N} \gamma_{k(n)}^{(n)} p^{(n)} + \sqrt{2 \log \frac{1}{\epsilon}} \sum_{n=1}^{N} u_n \leq I_{\max} \tag{4.24}$$

$$\sqrt{N} \sigma_{k(n)}^{(n)} \alpha_{k(n)}^{(n)} p^{(n)} \leq \sum_{n'=1}^{N} u_{n'}, \quad n \in \mathcal{N} \tag{4.25}$$

This can be seen from the following argument. Suppose that (4.25) is slack for all $n \in \mathcal{N}$ at the optimum. Then, the sum $\sum_{n'=1}^{N} u_{n'}$ can be decreased by small amount without any penalty in the objective. However, this makes (4.24) less tight, leading to net increase in the objective (unless the power constraint (5.6) is already tight), which contradicts the initial assumption of being at the optimum.

We continue the derivation of the RA algorithm using (4.24) and (4.25). The case of the ℓ_1-approximation will be discussed briefly in Sec. 4.3.2.

4.3.1 Algorithm for the ℓ_∞-Approximate Problem

Introducing dual variables $\boldsymbol{\lambda} \triangleq [\lambda_1, \lambda_2, \ldots, \lambda_N]^T \geq \mathbf{0}$, $\boldsymbol{\mu} \triangleq [\mu_1, \mu_2, \ldots, \mu_K]^T \geq \mathbf{0}$ and $\nu \geq 0$ to relax (4.25), (5.6), and (4.24), respectively, one can write the Lagrangian as

$$\begin{aligned} L(\mathbf{p}, \mathbf{u}; \boldsymbol{\lambda}, \boldsymbol{\mu}, \nu) = \sum_{n \in \mathcal{N}} w_{k(n)} \Big[& \log\left(1 + \tilde{g}_k^{(n)} p^{(n)}\right) \\ & - \left(\nu \gamma_{k(n)}^{(n)} + \mu_{k(n)} + \lambda_n \sqrt{N} \sigma_{k(n)}^{(n)} \alpha_{k(n)}^{(n)}\right) p^{(n)} \\ & + \left(\sum_{n' \in \mathcal{N}} \lambda_{n'} - \nu \sqrt{2 \log \frac{1}{\epsilon}}\right) u_n \Big] + \nu I_{\max} + \sum_{k \in \mathcal{K}} \mu_k P_{k,\max} \end{aligned} \tag{4.26}$$

Therefore, the dual function is

$$\begin{aligned} D(\boldsymbol{\lambda}, \boldsymbol{\mu}) &= \sup_{\mathbf{0} \preceq \mathbf{p} \preceq \mathbf{P}_{\max}, \mathbf{u}, \mathbf{k} \in \mathcal{K}^N} L(\mathbf{p}, \mathbf{u}; \boldsymbol{\lambda}, \boldsymbol{\mu}, \nu) \\ &= \sup_{\substack{\mathbf{0} \preceq \mathbf{p} \preceq \mathbf{P}_{\max} \\ \mathbf{k} \in \mathcal{K}^N}} \sum_{n \in \mathcal{N}} L_n(p^{(n)}, k(n)) + \nu I_{\max} + \sum_{k \in \mathcal{K}} \mu_k P_{k,\max} \end{aligned}$$

where

$$L_n(p^{(n)}, k) \triangleq w_k \log\left(1 + \tilde{g}_k^{(n)} p^{(n)}\right) - t_k^{(n)} p^{(n)} \tag{4.27}$$

$$t_k^{(n)} \triangleq \nu \gamma_k^{(n)} + \mu_k + \lambda_n \sqrt{N} \sigma_k^{(n)} \alpha_k^{(n)} \tag{4.28}$$

and $\nu := \left(2 \log \frac{1}{\epsilon}\right)^{-\frac{1}{2}} \sum_{n' \in \mathcal{N}} \lambda_{n'}$. The dual problem is thus

$$\inf_{\boldsymbol{\lambda} \succeq \mathbf{0}, \boldsymbol{\mu} \succeq \mathbf{0}} D(\boldsymbol{\lambda}, \boldsymbol{\mu}) \ . \tag{4.29}$$

It can be seen from (5.27) that the optimization can be decoupled to per-tone problems given by

$$\max_{0 \leq p^{(n)} \leq P_{\max}^{(n)}, k(n) \in \mathcal{K}} L_n(p^{(n)}, k(n)). \tag{4.30}$$

If $k(n) = k$, the optimal power loading $p^{*(n)}[k]$ can be shown to be

$$p^{*(n)}[k] = \left[\frac{w_k}{t_k^{(n)}} - \frac{1}{\tilde{g}_k^{(n)}}\right]_0^{P_{\max}^{(n)}}, \quad n \in \mathcal{N} \tag{4.31}$$

where $[\cdot]_a^b \triangleq \min\{\max\{0, a\}, b\}$. The optimal user allocation $\mathbf{k}^*$ is then given by

$$k^*(n) \in \arg\max_{k \in \mathcal{K}} L_n(p^{*(n)}[k], k), \quad n \in \mathcal{N} \tag{4.32}$$

and the optimal power loading by

$$p^{*(n)} = p^{*(n)}[k^*(n)], \quad n \in \mathcal{N} \ . \tag{4.33}$$

The dual problem (5.28) can be solved using, e.g., the subgradient method, or the ellipsoid method, which require the subgradient of $D(\cdot)$ w.r.t. $[\boldsymbol{\mu}^T \boldsymbol{\lambda}^T]^T$. One such subgradient is

$$- \begin{bmatrix} \sum_{n \in \mathcal{N}: k(n)=1} p^{(n)} - P_{1,\max} \\ \vdots \\ \sum_{n \in \mathcal{N}: k(n)=K} p^{(n)} - P_{K,\max} \\ \frac{-I_{\max} + \sum_{n \in \mathcal{N}} \gamma_{k(n)}^{(n)} p^{(n)}}{\sqrt{2 \log \frac{1}{\epsilon}}} + \sqrt{N} \sigma_{k(n)}^{(1)} \alpha_{k(n)}^{(1)} p^{(1)} \\ \vdots \\ \frac{-I_{\max} + \sum_{n \in \mathcal{N}} \gamma_{k(n)}^{(n)} p^{(n)}}{\sqrt{2 \log \frac{1}{\epsilon}}} + \sqrt{N} \sigma_{k(N)}^{(N)} \alpha_{k(N)}^{(N)} p^{(N)} \end{bmatrix} . \tag{4.34}$$

The overall RA algorithm based on the ellipsoid method is described in the following.

Algorithm 1:

1: Initialize $\mathbf{\Sigma}$ and $\boldsymbol{\theta} \triangleq [\boldsymbol{\mu}^T \ \boldsymbol{\lambda}^T]^T$;
and set $V = N + K$ for the ℓ_∞-approximation.
[Alternatively, $\boldsymbol{\theta} \triangleq [\boldsymbol{\mu}^T \ \nu]^T$, and set $V = K + 1$
for the ℓ_1-approximation].
Set tolerance τ
2: Repeat
3: If $\boldsymbol{\theta} < 0$ for some entries $i \in \mathcal{I}$
set $\mathbf{d} = \sum_{i\in\mathcal{I}} \mathbf{e}_i$ ($\mathbf{e}_i$ is the i-th canonical basis)
4: Otherwise:
5: Find $\mathbf{k}^*$ and $\mathbf{p}^*$ from (4.31)–(4.32)
[Alternatively use (4.35)–(4.36)]
6: Set $\mathbf{d}$ as (5.35) [Alternatively, use (4.37)]
7: If $\sqrt{\mathbf{d}^T\mathbf{\Sigma}\mathbf{d}} < \tau$, stop.
8: Perform the ellipsoid update:
9: $\mathbf{d} \leftarrow \mathbf{d}/\sqrt{\mathbf{d}^T\mathbf{\Sigma}\mathbf{d}}$
10: $\boldsymbol{\theta} \leftarrow \boldsymbol{\theta} - \mathbf{\Sigma}\mathbf{d}/(V+1)$
11: $\mathbf{\Sigma} \leftarrow \frac{V^2}{V^2-1}\left(\mathbf{\Sigma} - \frac{2}{V+1}\mathbf{\Sigma}\mathbf{d}\mathbf{d}^T\mathbf{\Sigma}\right)$

4.3.2 Algorithm for the ℓ_1-Approximate Problem

The ℓ_1-approximate problem can be similarly solved by the dual method. Introduce $(K+1)$ dual variables $\boldsymbol{\mu}$ and ν to relax (5.6) and (4.11), respectively, and let $s_k^{(n)} \triangleq \nu\left(\gamma_k^{(n)} + \sqrt{2\log\frac{1}{\epsilon}}\sigma_k^{(n)}\alpha_k^{(n)}\right) + \mu_k$. Then, one can obtain the optimal power loading as

$$p^{*(n)}[k] = \left[\frac{w_k}{s_k^{(n)}} - \frac{1}{\tilde{g}_k^{(n)}}\right]_0^{P_{\max}^{(n)}}, \quad n \in \mathcal{N} \tag{4.35}$$

and the optimal user allocation $\mathbf{k}^*$ as

$$k^*(n) \in \arg\max_{k\in\mathcal{K}} \log(1 + \tilde{g}_k^{(n)}p^{(n)}) - s_k^{(n)}p^{*(n)}[k], \qquad n \in \mathcal{N}. \tag{4.36}$$

A subgradient of the dual function w.r.t. $[\boldsymbol{\mu}^T \ \nu]^T$ is given by

$$-\begin{bmatrix} \sum_{n\in\mathcal{N}:k(n)=1} p^{(n)} - P_{1,\max} \\ \vdots \\ \sum_{n\in\mathcal{N}:k(n)=K} p^{(n)} - P_{K,\max} \\ -I_{\max} + \sum_{n\in\mathcal{N}} \left(\gamma_{k(n)}^{(n)} + \sqrt{2\log\frac{1}{\epsilon}}\sigma_{k(n)}^{(n)}\alpha_{k(n)}^{(n)}\right) p^{(n)} \end{bmatrix}. \tag{4.37}$$

The overall algorithm is implemented by following the alternative steps in the brackets in Algorithm 1 presented in Sec. 4.3.1.

Remark 4.2 A discussion on the complexity order of the proposed algorithms is in order. One must consider the total number of operations per iteration multiplied by the number of iterations required for convergence. The number of iterations needed to obtain an ϵ-optimal solution using the ellipsoid method with V variables is $\mathcal{O}\left(V^2 \log\frac{1}{\epsilon}\right)$ [8]. In the algorithm for the ℓ_∞-approximation problem, the number of variables is $(N+K)$. At each iteration, (4.31) and (4.32) need to be performed KN times, in addition to $(N+K)^2$ operations needed for the ellipsoid update. The overall complexity order is thus $\mathcal{O}((N+K)^4)$. On the other hand, the algorithm for the ℓ_1-approximate problem involves $(K+1)$ dual variables, leading to a complexity order of $\mathcal{O}(K^3N + K^4)$.

4.3.3 Suboptimal Algorithm

To obtain a performance benchmark, a suboptimal RA algorithm based on alternating maximization is derived. A suboptimal algorithm is a reasonable alternative used in a number of works such as [27]. Note that the algorithm still aims to solve the ℓ_2-, ℓ_∞-, and ℓ_1-approximate problems that result from applying the Bernstein method. The algorithm involves the following steps.

1) Initialize the power loading; e.g., set $p^{(n)} := \min\{\frac{1}{N}\min_k P_{k,\max}, P_{\max}^{(n)}\}$, $n \in \mathcal{N}$.

2) For each subcarrier $n \in \mathcal{N}$, find the user k^* that maximizes $w_k \log(1 + \tilde{g}_k^{(n)} p^{(n)})$ and allocate subcarrier n to that user, i.e., $k(n) := k^*$

3) For fixed $\mathbf{k}$ obtained from step (2), optimize over $\mathbf{p}$ by solving the convex problem, using e.g., the interior-point method or the subgradient method

4) Repeat steps (2)–(3) until convergence.

It can be shown easily that the objective function does not decrease per iteration, thus guaranteeing convergence.

4.3.4 Algorithms Based on the Central Limit Theorem

A yet another set of algorithms are derived here to approximately solve (5.5)–(4.3) without resorting to Bernstein's approximation when the mean $\hat{g}_k^{(n)}$ and the variance $(v_k^{(n)})^2$ of the channel gains $g_k^{(n)}$ are known. They will be useful in Sec. 5.4 to characterize the performance degradation due to the conservatism introduced by Bernstein's approximation. The idea is to apply the central limit theorem to the interference power $\sum_{n\in\mathcal{N}} g_{k(n)}^{(n)} p^{(n)}$ in (4.3) and approximate it as a Gaussian random variable with mean $\sum_{n\in\mathcal{N}} \hat{g}_{k(n)}^{(n)} p^{(n)}$ and variance $\sum_{n\in\mathcal{N}} (v_{k(n)}^{(n)} p^{(n)})^2$ (again assuming independence). Then, (4.3) can be expressed as

$$-I_{\max} + \sum_{n\in\mathcal{N}} \hat{g}_{k(n)}^{(n)} p^{(n)} + Q^{-1}(\epsilon) \left(\sum_{n\in\mathcal{N}} (v_{k(n)}^{(n)} p^{(n)})^2 \right)^{\frac{1}{2}} \leq 0 \tag{4.38}$$

Note the resemblance of (4.38) and (4.9). In particular, they both involve the ℓ_2-norm of vector $[v_{k(1)}^{(1)} p^{(1)}, \ldots, v_{k(N)}^{(N)} p^{(N)}]$. Thus, one can readily derive separable surrogates based on the ℓ_∞- and the ℓ_1-norms, given by [cf. (4.10) and (4.11)]

$$\sum_{n\in\mathcal{N}} \hat{g}_{k(n)}^{(n)} p^{(n)} + Q^{-1}(\epsilon) \max_{n\in\mathcal{N}} v_{k(n)}^{(n)} p^{(n)} \leq I_{\max} \tag{4.39}$$

$$\sum_{n\in\mathcal{N}} \hat{g}_{k(n)}^{(n)} p^{(n)} + Q^{-1}(\epsilon) \sum_{n\in\mathcal{N}} |v_{k(n)}^{(n)} p^{(n)}| \leq I_{\max} \tag{4.40}$$

respectively.

4.4 Numerical Tests

The proposed RA algorithms were tested via numerical experiments. The wideband channels $\tilde{g}_k^{(n)}$ and $g_k^{(n)}$ were simulated as 4-path Rayleigh fading channels. The pathloss exponent

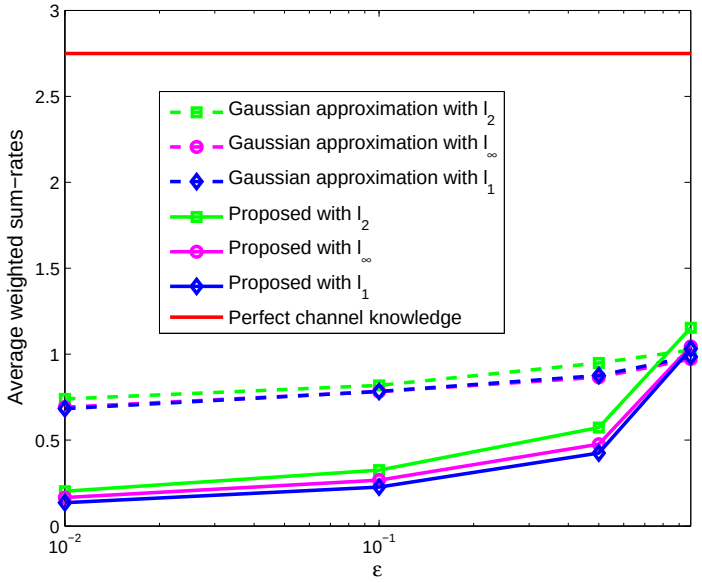

Figure 4.1: Average weighted sum-rates without channel estimation.

was set to $\alpha = 2$. Since the pathloss exponent in practice is usually larger than 2, this choice corresponds to a worst-case scenario in terms of PU interference. The parameters $\mu_k^{(n)+}$, $\mu_k^{(n)-}$ and $\sigma_k^{(n)}$ for the Bernstein approximations were chosen from [5, Table 1] using the known first- and second-order moments of the truncated channel gains. Specifically, the values of $\mu_k^{(n)+}$ and $\mu_k^{(n)-}$ are set as (cf. (4.8))

$$\mu_k^{(n)+} = \mu_k^{(n)-} = E\left\{ \frac{g_k^{(n)} - \beta_k^{(n)}}{\alpha_k^{(n)}} \middle| a_k^{(n)} \leq g_k^{(n)} \leq b_k^{(n)} \right\}. \tag{4.41}$$

Then, upon defining $\eta_k^{(n)} \triangleq E\left\{ \left(\frac{g_k^{(n)} - \beta_k^{(n)}}{\alpha_k^{(n)}} \right)^2 \middle| a_k^{(n)} \leq g_k^{(n)} \leq b_k^{(n)} \right\}$, and

$$q_{\mu,\eta}(t) \triangleq \begin{cases} \log\left(\frac{(1-\mu)^2 \exp\frac{t(\mu-\eta^2)}{1-\mu} + (\eta^2-\mu^2)\exp(t)}{1-2\mu+\eta^2} \right), & \text{if } t \geq 0 \\ \log\left(\frac{(1+\mu)^2 \exp\frac{t(\mu+\eta^2)}{1+\mu} + (\eta^2-\mu^2)\exp(-t)}{1+2\mu+\eta^2} \right), & \text{otherwise} \end{cases} \tag{4.42}$$

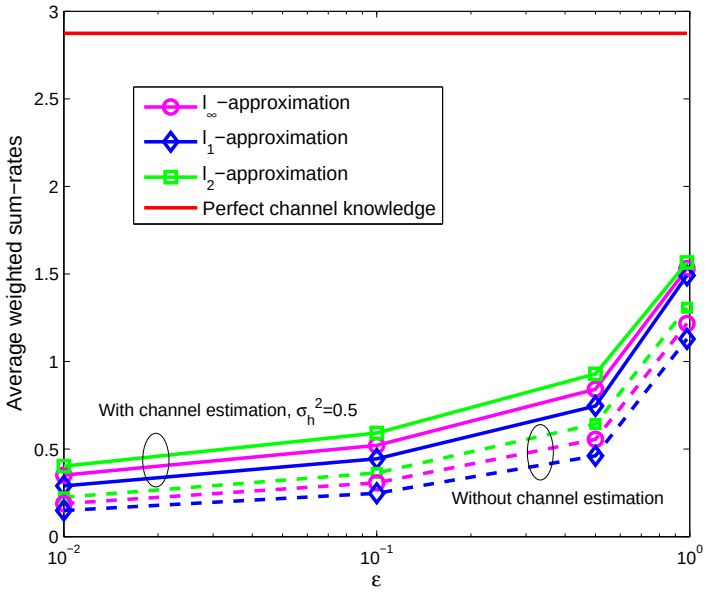

Figure 4.2: Average weighted sum-rates with and without channel estimation.

the values of $\sigma_k^{(n)}$ are obtained from solving

$$\sigma_k^{(n)} = \min\left\{c \geq 0 : q_{\mu_k^{(n)+},\eta_k^{(n)}}(t) \leq \mu_k^{(n)+}t + \frac{c^2t^2}{2}, \forall t\right\}. \tag{4.43}$$

Unless stated otherwise, the value of δ was set to $1-0.5\epsilon$, two CR users were experimented with $w_1 = 0.2$ and $w_2 = 0.8$, and the results were averaged over 80 realizations of $\tilde{g}_k^{(n)}$. The CR users were located equidistant from the CR BS throughout the tests.

Fig. 4.1 depicts the average weighted sum-rates for different values of ϵ without channel estimation for both Bernstein approximation-based and Gaussian approximation-based algorithms. The CR users are located equidistant from the PU. The solid line without markers is for the case when $\{g_k^{(n)}\}$ are perfectly known. In this case, the chance constraint (4.3) boils down to a deterministic constraint $\sum_{n\in\mathcal{N}} g_{k(n)}^{(n)} p^{(n)} < I_{\max}$, and thus the sum-rates do not depend on ϵ. The solid and dashed lines with markers correspond to the Bernstein approximation-based and the Gaussian approximation-based algorithms, respectively. The curves marked with squares, circles and diamonds were obtained by solving the ℓ_2-, ℓ_∞-, and ℓ_1-approximate problems, respectively. Note that in the case of the ℓ_2-approximate prob-

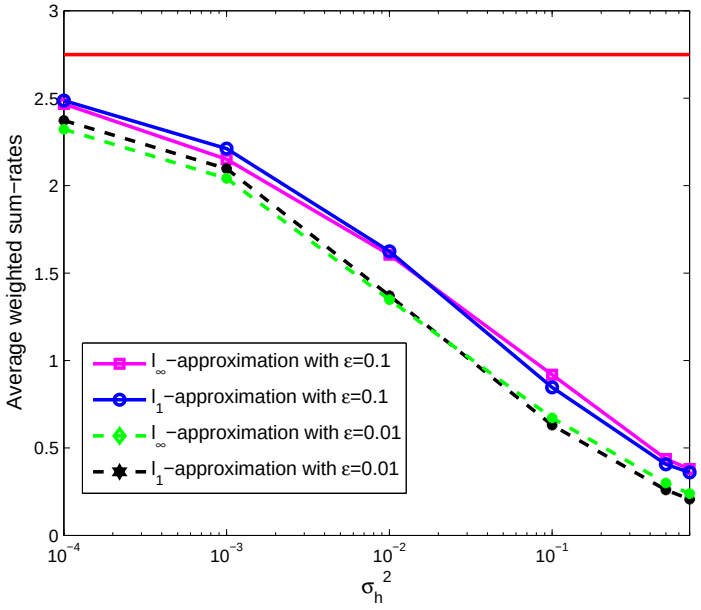

Figure 4.3: Average weighted sum-rates versus σ_h^2.

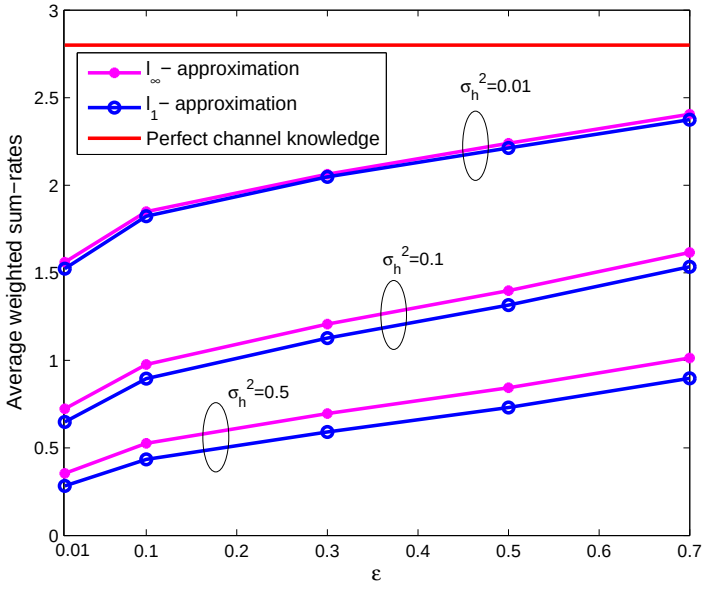

Figure 4.4: Average weighted sum-rates versus ϵ.

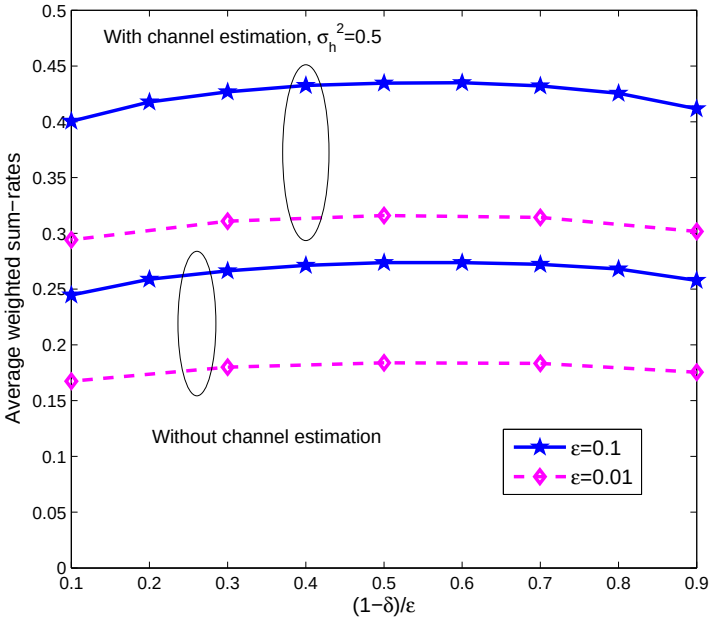

(a) CR users equidistant from the PU

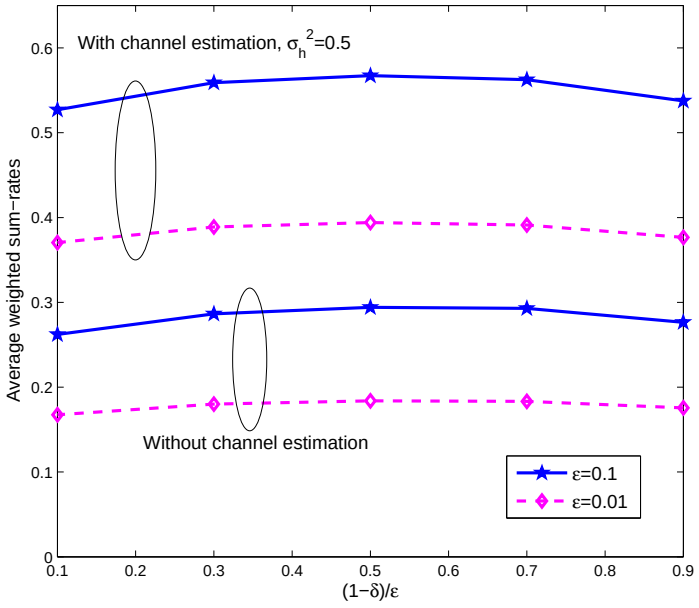

(b) CR user 1 twice farther from the PU than CR user 2

Figure 4.5: Average weighted sum-rates versus δ.

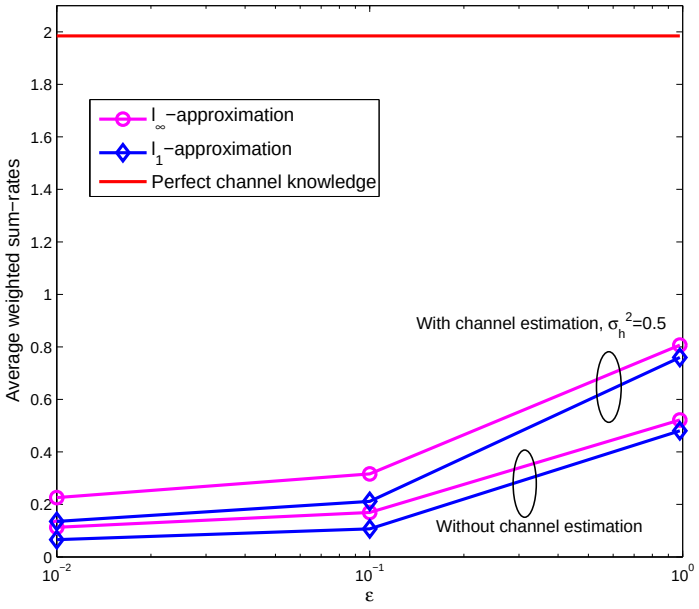

Figure 4.6: Average weighted sum-rates for $K = 6$ and $N = 16$.

lem, exhaustive search over $\mathbf{k}$ was performed, as the dual decomposition technique could not be applied. It can be observed that the average weighted sum-rates increase as ϵ increases, since larger ϵ renders the chance constraint more lenient. Also, it can be seen that the curves corresponding to the ℓ_∞- or the ℓ_1-approximate problems are very close to the ones from the ℓ_2-approximate problem, underlining the usefulness of the dual decomposition-based low-complexity solutions. Interestingly, the ℓ_∞-approximation seems to yield a slightly better performance than the ℓ_1-approximation with Bernstein approximation, while the performance differences are quite negligible in the Gaussian approximation case. However, as discussed in Remark 4.2, the ℓ_1-approximation incurs lower computational complexity than the ℓ_∞-approximation.

There is a large gap between the performance based on perfect channel knowledge and the robust RA performance. As can be seen, the Gaussian approximation yields much improvement in the weighted sum-rates, compared to Bernstein approximation. However, even the Gaussian approximation can achieve only a small portion of what can be achieved under perfect channel knowledge. This illustrates that the major portion in the perfor-

Table 4.1: Average run times.

ϵ	0.01	0.1	0.5
Suboptimal algorithm	7.4782 sec	6.0122 sec	6.1220 sec
Dual method with ℓ_∞-approximation	3.7597 sec	3.6138 sec	3.3216 sec
Dual method with ℓ_1-approximation	0.7312 sec	0.7102 sec	0.7060 sec

Table 4.2: Simulated values of $\Pr\{I < I_{\max}\}$ for Bernstein and the Gaussian approximations.

$1-\epsilon$	0.9	0.5	0.3
Bernstein approx. with ℓ_2 without channel est.	0.9995	0.9600	0.8925
Bernstein approx. with ℓ_∞ without channel est.	1	0.9720	0.9526
Bernstein approx. with ℓ_1 without channel est.	0.9988	0.9600	0.9201
Bernstein approx. with ℓ_2 with channel est. ($\sigma_h^2 = 0.5$)	0.9967	0.9155	0.8234
Bernstein approx. with ℓ_∞ with channel est. ($\sigma_h^2 = 0.5$)	0.9998	0.9662	0.9226
Bernstein approx. with ℓ_1 with channel est. ($\sigma_h^2 = 0.5$)	0.9997	0.9655	0.8988
Gaussian approx. with ℓ_2 without channel est.	0.7785	0.6981	0.6718
Gaussian approx. with ℓ_∞ without channel est.	0.8310	0.7266	0.6982
Gaussian approx. with ℓ_1 without channel est.	0.8575	0.7602	0.7217

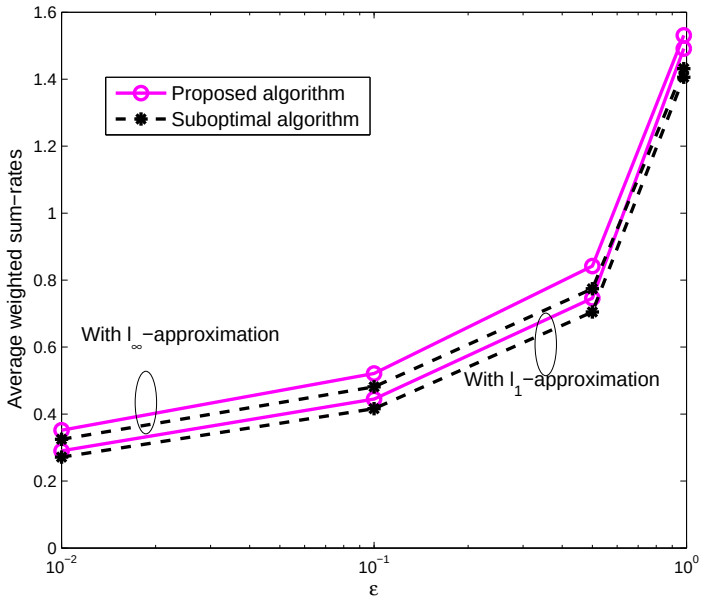

Figure 4.7: Comparison with suboptimal algorithm.

mance degradation may be attributed to the uncertainty in the channel, rather than the conservatism in Bernstein approximation.

The said gap can be alleviated by employing channel estimation, as shown in Fig. 4.2 for $\sigma_h^2 = 0.5$. The figure depicts the case where user 1 is twice farther from the PU than user 2. Among the curves obtained with channel estimation, the performance-complexity trade-offs similar to what appeared in the case without channel estimation are observed.

Fig. 4.3 shows the average weighted sum-rate performance as σ_h^2 is varied when both CR users are in the same distance from the PU. Two sets of curves corresponding to $\epsilon = 0.1$ and $\epsilon = 0.01$ are presented. It is seen that as the channel estimation accuracy improves (smaller σ_h^2), the performance of the RA algorithms also increases. As was discussed in Remark 4.1, the gap will eventually close as σ_h^2 vanishes. Similar trends are observed in Fig. 4.4, where the sum-rate performance versus ϵ is plotted with different values of σ_h^2, all with user 1 located twice farther away from the PU than user 2 is.

The sensitivity of the weighted sum-rate performance to the choice of δ is examined in Fig. 4.5 for $\epsilon = 0.01$ and 0.1 for two different network topologies. It is seen that the

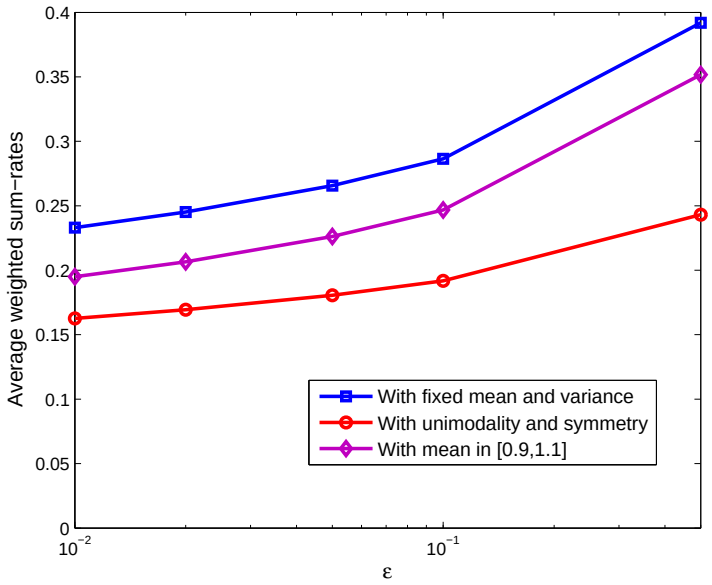

Figure 4.8: The case of unknown p.d.f.

performance is maximized at about $\delta = 1 - 0.5\epsilon$ and is quite robust to the choice of δ. Interestingly, such an observation seems to hold regardless of the experimented network topologies and whether channel estimation is performed.

We also tested the case with $K = 6$ CR users with $\{w_k\}$ set to $[0.1, 0.2, 0.3, 0.2, 0.1, 0.1]$ using $N = 16$ subcarriers. Fig. 4.6 plots the weighted sum-rates averaged over 40 realizations of $\tilde{g}_k^{(n)}$. Due to the prohibitive complexity of exhaustive search required for the ℓ_2-approximate problem, only the results for the ℓ_∞- and the ℓ_1-approximate problems are reported. The overall trend remains unchanged from the two-user case.

To highlight the effectiveness of the dual decomposition-based approach, the performance of the suboptimal algorithm is compared to the proposed algorithms under channel estimation with $\sigma_h^2 = 0.5$ in Fig. 4.7 for the two-user case with CR user 1 twice farther from the PU than CR user 2.

The suboptimal algorithm is seen to be inferior to the proposed dual method-based algorithm both for the ℓ_∞- and the ℓ_1-approximate problems, although the gaps are small. On the other hand, the algorithms differ much in terms of computational complexity. Table 4.1 presents the average run times for the algorithms, where the experiments were done using

a 2.13-GHz Intel CPU with 2 GB of RAM. It can be seen that the suboptimal algorithm takes much longer than the proposed algorithms until convergence. In fact, the suboptimal algorithm spent a lot of time to solve the convex subproblems, while the number of iterations were actually small.

To confirm that the interference constraint (4.3) is satisfied by the proposed methods, actual values of $\Pr\{I < I_{\max}\}$ are listed in Table 4.2 for the case with CR users equidistant from the PU, for different target values $1-\epsilon$. It is clearly seen that the interference constraint is enforced conservatively with Bernstein approximation. (Although the achieved values of $\Pr\{I < I_{\max}\}$ are often quite off from the prescribed target $(1-\epsilon)$, this should not be interpreted as severe suboptimality of the proposed algorithms, because the performance must be ultimately gauged in terms of the weighted sum rates; see Fig. 2 and the associated discussion in this section.) However, it is seen that the Gaussian approximation approach does not always yield a solution feasible for the chance constraint, especially when ϵ is small. Therefore, the modest performance degradation as was seen in Fig. 4.1 may be thought of as the price to pay for guaranteed feasibility while maintaining tractability and accommodating a large class of distributions for uncertain parameters.

To illustrate the performance obtained when the channel *p.d.f.* is bounded but not known precisely, the average weighted sum-rate curves are plotted in Fig. 4.8 when the CR-to-PU channel gains belong to a bounded interval $[0, 7.38]$ for both CR users. The curve with circle markers represents the case where the support as well as the unimodality and the symmetry information are used. The curve with the diamonds corresponds to the case where the information that the mean lies in $[0.9, 1.1]$ was used in addition to the support information. The curve with the squares depicts the case of using the known mean and variance in addition to the support information. It can be seen that the performance is improved by employing more prior knowledge on the distribution.

4.5 Summary

Weighted sum-rate maximization of an OFDMA CR uplink was considered, where the power loading and the user assignment over individual subcarriers are performed while

ensuring that the interference power experienced at the PU location is less than a prescribed threshold. Since the channel gains between CR transmitters and PU receivers often cannot be estimated accurately, the PU interference constraint was cast as a chance constraint. As the resulting optimization problem is intractable, two layers of approximations were introduced. First, a convex conservative surrogate of the chance constraint was employed using Bernstein approximation, to bypass the need to analytically represent the chance constraint, even without precise knowledge of the distribution of uncertain channel gains. Secondly, due to the combinatorial complexity of searching for the optimal user assignment, approximation involving the ℓ_1- or the ℓ_∞-norms were employed so that the OFDMA RA problems possess separable structures, and can be tackled in the dual domain. Although such approximations indeed introduce conservatism, this is a side-effect often shared by a broad class of robust optimization approaches, and arguably constitutes the price paid to obtain guaranteed feasible solutions to chance-constrained OFDMA CR RA problems at an affordable complexity. Algorithms based on the dual decomposition method were developed for the cases with and without channel estimation. Numerical tests showed that the proposed algorithms outperformed a benchmark suboptimal algorithm in terms of both weighted sum-rate performance and computational complexity. It was also shown that the performance degradation due to the approximation introduced for enforcing the separability is rather insignificant.

Chapter 5

Resource Allocation for OFDMA CR under Channel Uncertainty in Downlink

In this chapter, an OFDMA CR network downlink operating in a spectrum underlay set-up is addressed. A weighted sum rate maximization problem is formulated for a CR base station (BS) that transmits to a set of CR mobile stations (MSs), while respecting a strict interference constraint to protect PUs when the channel estimate between the CR-BS and the PU receiver contains uncertainty. It turns out that the interference constraint can be converted to a second-order cone constraint, which is convex. However, the overall optimization problem is still non-convex in general due to the combinatorial search necessary for subcarrier assignment. It is well known that when an OFDMA RA problem has a separable structure, the duality gap vanishes as the number of subcarriers grows large [35, 43]. To induce such a separable structure, a tight linear approximation for the interference constraint is introduced at a modest (polynomial) increase in the problem dimension. The approximated problem can then be readily solved using the dual decomposition method, which leads to a near-optimal, computationally efficient algorithm. The material in this chapter draws from [29], [30].

5.1 Modeling and Problem Statement

Consider a CR-BS allocating resources to K CR-MSs (users) employing OFDMA using N subcarriers. The channel gain $h_k^{(n)} \geq 0$ between the CR-BS and the k-th CR-MS for each $k \in \mathcal{K} := \{1, 2, \ldots, K\}$, and each subcarrier $n \in \{1, 2, \ldots, N\}$ is assumed to have been acquired accurately via conventional channel estimation techniques. Suppose also that during the sensing phase, the CR-BS has detected the presence of an active PU. Let $p^{(n)}$ denote the transmit-power loaded on subcarrier n, and $P_{\max}^{(n)}$ the maximum transmit-power allowed on subcarrier n. Vectors $\mathbf{p}$ and $\mathbf{P}_{\max}$ collect $\{p^{(n)}\}$ and $\{P_{\max}^{(n)}\}$, respectively. Also, let $k(n) \in \mathcal{K}$ represent the index of the user served on subcarrier n, and define $\mathbf{k} := [k(1), \ldots, k(N)]^T$.

Rather than employing ideal Gaussian signaling, practical discrete constellations are adopted. Thus, the received signal for user k on subcarrier n is modeled as

$$y_k^{(n)} = \sqrt{h_k^{(n)} p^{(n)}} x_k^{(n)} + v_k^{(n)} \tag{5.1}$$

where $x_k^{(n)}$ is the unit-average-power input signal on subcarrier n drawn from a practical constellation of user k, where the inputs for different users and subcarriers are assumed to be independent. Random variables $\{v_k^{(n)}\}$ represent independent and identically distributed (i.i.d.) complex Gaussian noise with mean 0 and variance 1. The mutual information for user k on subcarrier n is denoted as $\mathcal{I}_k^{(n)}(\gamma) := I\left(x_k^{(n)}; \sqrt{\gamma} x_k^{(n)} + v_k^{(n)}\right)$, where γ represents the received signal power-to-noise power ratio (SNR). Let w_k denote the positive weight of user $k \in \mathcal{K}$. Then, a relevant RA objective is to maximize a weighted sum of mutual information $\sum_{n=1}^{N} w_{k(n)} \mathcal{I}_{k(n)}^{(n)}(h_k^{(n)} p^{(n)})$ of the CR system, while adhering to a transmit-power constraint, and a PU interference constraint.

To model the PU interference constraint, let $g^{(n)} \geq 0$ denote the channel gain from the CR-BS to the PU receiver on subcarrier n. Unlike the channels between CR transceivers, it is difficult to estimate $\{g^{(n)}\}$ precisely, due to the lack of cooperation from the PU system. Thus, $\{g^{(n)}\}$ are assumed uncertain.

In this work, a deterministic robust optimization approach is adopted. Specifically, it is assumed that the uncertainty in vector $\mathbf{g} := [g^{(1)}\ g^{(2)}\ \ldots\ g^{(N)}]^T$ can be captured by an

ellipsoidal uncertainty region given by

$$\mathcal{G} := \left\{ \bar{\mathbf{g}} + \Delta\mathbf{g} : \Delta\mathbf{g}^T \mathbf{C}_g^{-1} \Delta\mathbf{g} \leq \Omega^2 \right\} \tag{5.2}$$

where $\bar{\mathbf{g}}$ is the nominal value of $\mathbf{g}$, $\Delta\mathbf{g}$ the deviation from the nominal value, $\mathbf{C}_g$ a symmetric positive definite matrix, and $\Omega \geq 0$ a given constant. Then, a robust interference constraint guarantees tolerable interference to the PU system for all possible $\mathbf{g} \in \mathcal{G}$; that is,

$$\sum_{n=1}^{N} g^{(n)} p^{(n)} \leq I_{\max} \text{ for all } \mathbf{g} \in \mathcal{G}. \tag{5.3}$$

which was shown to be equivalent to

$$\mathbf{p} \in \mathcal{C} := \left\{ \mathbf{p} \middle| I_{\max} - \bar{\mathbf{g}}^T \mathbf{p} \geq \Omega \sqrt{\mathbf{p}^T \mathbf{C}_g \mathbf{p}} \right\} \tag{5.4}$$

which is a second-order cone constraint [5]. Then, the following optimization problem is of interest:

$$\text{(P1)} \qquad \max_{0 \preceq \mathbf{p} \preceq \mathbf{P}_{\max}, \mathbf{k} \in \mathcal{K}^N} \sum_{n=1}^{N} w_{k(n)} \mathcal{I}_{k(n)}^{(n)} (h_k^{(n)} p^{(n)}) \tag{5.5}$$

$$\text{subject to } \sum_{n=1}^{N} p^{(n)} \leq P_{\max} \tag{5.6}$$

$$\bar{\mathbf{g}}^T \mathbf{p} - I_{\max} + \Omega \sqrt{\mathbf{p}^T \mathbf{C}_g \mathbf{p}} \leq 0. \tag{5.7}$$

Note that (P1) is convex provided $K = 1$, i.e., for a single-user system. In the general case of multiple users with $K > 1$, (P1) is non-convex due to the combinatorial assignment of users on each subcarrier.

When an OFDMA RA problem has a separable structure, in which the Lagrangian dual can be decomposed into per-subcarrier subproblems, it can be shown that the duality gap vanishes as the number of the subcarriers increases [6, 43]. This implies that the problem can be solved near-optimally in polynomial time for sufficiently large N. However, due to the coupling of $p^{(n)}$ belonging to different subcarriers n in (5.7), (P1) does not possess this separable structure. The novel approach here is to enforce such a structure by approximating (5.7) by a set of linear constraints. To this end, a general result that approximates second-order cone constraints by polyhedral constraints is employed, which is outlined next.

5.2 Polyhedral Approximation of Second-Order Cones

Motivated by the availability of efficient large-scale linear program (LP) solvers, a second-order cone program was tackled via an approximate LP in [4]. To this end, it was shown that the second-order Lorentz cone

$$\mathcal{L}^N := \left\{(y_0, \mathbf{y}) \in \mathbb{R} \times \mathbb{R}^N : ||\mathbf{y}|| \leq y_0\right\} \tag{5.8}$$

admits a polyhedral approximation of accuracy δ, comprising variables and constraints whose number is polynomial in N and $\log(1/\delta)$; see also [20] for a refinement of this result. Here, we briefly recap the idea behind this approximation.

Direct construction of a polyhedral approximation circumscribing $\mathcal{L}^N$ in the $(N+1)$-dimensional space is bound to have its number of facets growing exponentially with the dimension N, which implies that it needs an exponentially growing number of linear inequalities to define. The key idea is to reduce the number of inequalities by lifting the polyhedron to a higher-dimensional space by introducing additional variables, and considering its projection onto the $(N+1)$-dimensional subset. Since a projection of a higher-dimensional polyhedral set can significantly multiply the number of facets, this approach yields a relaxation that is "efficient" in the sense that it is very tight, yet it is defined using a relatively small number of constraints and extra variables.

The first step is to decompose the $(N+1)$-dimensional Lorentz cone $\mathcal{L}^N$ to a number of 3-dimensional Lorentz cones using the "tower of variables" concept. Suppose for simplicity that $N = 2^d$ for some integer d. Then, by introducing a vector of $N/2$ new variables $\boldsymbol{\rho}^{(1)} := \left[\rho_1^{(1)}, \rho_2^{(1)}, \ldots, \rho_{\frac{N}{2}}^{(1)}\right]^T$, where the superscript $^{(\ell)}$ in $\boldsymbol{\rho}^{(\ell)}$ denotes the ℓ-th layer of the "tower," the cone $\mathcal{L}^N$ can be equivalently written as

$$\begin{aligned}\mathcal{L}^N = \Bigg\{&(y_0, \mathbf{y}) \in \mathbb{R} \times \mathbb{R}^N : \exists \boldsymbol{\rho}^{(1)} \in \mathbb{R}^{\frac{N}{2}},\ \sum_{n=1}^{N} {\rho_i^{(1)}}^2 \leq y_0^2, \\ &y_{2i-1}^2 + y_{2i}^2 \leq {\rho_i^{(1)}}^2,\ i = 1, 2, \ldots, \frac{N}{2}\Bigg\} \qquad (5.9)\\ = \Big\{&(y_0, \mathbf{y}) \in \mathbb{R} \times \mathbb{R}^N : \exists \boldsymbol{\rho}^{(1)} \in \mathbb{R}^{\frac{N}{2}},\ (y_0, \boldsymbol{\rho}^{(1)}) \in \mathcal{L}^{\frac{N}{2}}, \\ &(\rho_i^{(1)}, y_{2i-1}, y_{2i}) \in \mathcal{L}^2,\ i = 1, 2, \ldots, \frac{N}{2}\Big\}. \qquad (5.10)\end{aligned}$$

Decomposing further the $\left(\frac{N}{2}+1\right)$-dimensional Lorentz cone in (5.10) by applying the idea repeatedly, one obtains eventually $(N-1)$ three-dimensional second-order cone constraints via $(N-2)$ new variables $\boldsymbol{\rho}^{(\ell)} := \left[\rho_1^{(\ell)}, \ldots, \rho_{\frac{N}{2^\ell}}^{(\ell)}\right]^T$, $\ell = 1, 2, \ldots, d-1$.

The remaining task is to approximate $\mathcal{L}^2$ using a polynomial number of variables and constraints. Consider a polyhedral δ-relaxation Π_δ^N of $\mathcal{L}^N$ with $\delta > 0$ in the sense that

$$\mathcal{L}^N \subset \Pi_\delta^N \subset \mathcal{L}_\delta^N := \left\{(y_0, \mathbf{y}) \in \mathbb{R} \times \mathbb{R}^N : ||\mathbf{y}|| \leq (1+\delta) y_0\right\}. \tag{5.11}$$

Then, for an integer q with

$$\delta = \frac{1}{\cos\left(\frac{\pi}{2^q}\right)} - 1 \tag{5.12}$$

it can be shown that the set of points $(y_0, y_1, y_2) = (\alpha_{q+1}, \alpha_0, \beta_0)$ satisfying the following set of linear constraints is a δ-relaxation of $\mathcal{L}^2$ [4], [20]:

$$\alpha_{i+1} = \alpha_i \cos\left(\frac{\pi}{2^i}\right) + \beta_i \sin\left(\frac{\pi}{2^i}\right), \quad i = 0, 1, \ldots, q \tag{5.13}$$

$$\beta_{i+1} \geq \left|\beta_i \cos\left(\frac{\pi}{2^i}\right) - \alpha_i \sin\left(\frac{\pi}{2^i}\right)\right|, \quad i = 0, \ldots, q-1 \tag{5.14}$$

where $\boldsymbol{\alpha} := [\alpha_1, \alpha_2, \ldots, \alpha_q]^T$ and $\boldsymbol{\beta} := [\beta_1, \ldots, \beta_q]^T$ are extra variables introduced to "lift" the approximation to a higher-dimensional space. Thus, $2q$ extra variables have been introduced to form $(q+1)$ equality constraints and $2q$ inequality constraints. One can further reduce the number of variables and constraints by eliminating $\boldsymbol{\alpha}$ and β_q using the equalities (5.13). The resulting set of linear constraints contains $(q-1)$ extra variables and only $2q$ linear inequality constraints.

Overall, using δ_ℓ-relaxations for the cones in the ℓ-th layer, a polyhedral δ-relaxation of $\mathcal{L}^N$ can be obtained as

$$\begin{aligned}\Pi_\delta^N := \Big\{&(y_0, \mathbf{y}) = (\rho_1^{(d)}, \boldsymbol{\rho}^{(0)}) \in \mathbb{R} \times \mathbb{R}^N : \exists \boldsymbol{\rho}^{(1)}, \ldots, \boldsymbol{\rho}^{(d-1)}, \\ &(\rho_i^{(\ell)}, \rho_{2i-1}^{(\ell-1)}, \rho_{2i}^{(\ell-1)}) \in \Pi_{\delta_\ell}^2,\ i = 1, \ldots, \frac{N}{2^\ell}, \ell = 1, \ldots, d\Big\}\end{aligned} \tag{5.15}$$

where $\delta = \prod_{\ell=1}^d (1+\delta_\ell) - 1$ holds. Thus, the overall approximation introduces $v(N) := (N-2) + \sum_{\ell=1}^d (q_\ell - 1)\frac{N}{2^\ell}$ extra variables, and $c(N) := \sum_{\ell=1}^d \frac{N \cdot q_\ell}{2^{\ell-1}}$ inequality constraints. Given the overall accuracy requirement δ, $\{\delta_\ell\}$ were optimized in [20], and can be obtained by plugging in $q = q_\ell = \lceil \frac{\ell+1}{2} \rceil - \lfloor \log_4 \left(\frac{16}{9}\pi^{-2} \log(1+\delta)\right) \rfloor$ to (5.12).

5.3 Resource Allocation Algorithms

5.3.1 Algorithm Based On Lagrangian Dual

In order to obtain a feasible solution to the original robust RA problem, the set of linear constraints approximating (5.4) must be tighter than the original constraint (5.4). Thus, for a given small positive constant δ, consider a tightened constraint set given by

$$\mathcal{C}' := \left\{ \mathbf{p} \middle| \frac{I_{\max} - \bar{\mathbf{g}}^T \mathbf{p}}{(1+\delta)\Omega} \geq \sqrt{\mathbf{p}^T \mathbf{C}_g \mathbf{p}} \right\}. \tag{5.16}$$

Then, a δ-relaxed lifted polyhedral approximation of the form

$$\mathcal{C}'_\delta := \left\{ \mathbf{p} \middle| \exists \mathbf{q} \in \mathbb{R}^{n_q}, \mathbf{A}\mathbf{p} + \mathbf{B}\mathbf{q} \preceq \mathbf{b} \right\} \tag{5.17}$$

exists, where $\mathbf{A} \in \mathbb{R}^{n_c \times N}$, $\mathbf{B} \in \mathbb{R}^{n_c \times n_q}$, and $\mathbf{b} \in \mathbb{R}^{n_c}$ are obtained from the procedure outlined in Sec. 5.2, and $\mathbf{q} \in \mathbb{R}^{n_q}$ is the vector of additional variables, with $n_c = c(N)$ and $n_q = v(N)$. From (5.11), it can be seen that

$$\mathcal{C}' \subset \mathcal{C}'_\delta \subset \mathcal{C} \tag{5.18}$$

holds. Therefore, the following optimization problem is a conservative surrogate for (P1):

$$\text{(P2)} \qquad \max_{\mathbf{p},\mathbf{q},\mathbf{k} \in \mathcal{K}^N} \sum_{n=1}^{N} w_{k(n)} \mathcal{I}^{(n)}_{k(n)}(h^{(n)}_{k(n)} p^{(n)}) \tag{5.19}$$

$$\text{subject to } \sum_{n=1}^{N} p^{(n)} \leq P_{\max} \tag{5.20}$$

$$0 \leq p^{(n)} \leq P^{(n)}_{\max}, \quad n = 1, 2, \ldots, N \tag{5.21}$$

$$\mathbf{A}\mathbf{p} + \mathbf{B}\mathbf{q} \preceq \mathbf{b}. \tag{5.22}$$

Problem (P2) is again non-convex. However, it can be shown that the duality gap vanishes asymptotically as $N \to \infty$ [12, 35, 63]. A precise statement and its proof can be found in the Appendix. Therefore, (P2) can be solved efficiently using the dual method. Introducing dual variables $\lambda \geq 0$ and $\boldsymbol{\mu} := [\mu_1, \mu_2, \ldots, \mu_{n_c}]^T \succeq \mathbf{0}$, the (partial) Lagrangian

is

$$L(\mathbf{p},\mathbf{q}) = \sum_{n=1}^{N} w_{k(n)}\mathcal{I}_{k(n)}^{(n)}(h_{k(n)}^{(n)}p^{(n)}) - \lambda\left(\sum_{n=1}^{N} p^{(n)} - P_{\max}\right) - \boldsymbol{\mu}^T(\mathbf{A}\mathbf{p}+\mathbf{B}\mathbf{q}-\mathbf{b}) \tag{5.23}$$

$$= \sum_{n=1}^{N}\left\{w_{k(n)}\mathcal{I}_{k(n)}^{(n)}(h_{k(n)}^{(n)}p^{(n)}) - (\lambda+\boldsymbol{\mu}^T\mathbf{A}(:,n))p^{(n)}\right\} + \lambda P_{\max} - \boldsymbol{\mu}^T\mathbf{B}\mathbf{q} + \boldsymbol{\mu}^T\mathbf{b} \tag{5.24}$$

where $\mathbf{A}(:,n)$ denotes the n-th column of matrix $\mathbf{A}$. Upon defining

$$L_n(p^{(n)},k) := w_k\mathcal{I}_k^{(n)}(h_k^{(n)}p^{(n)}) - (\lambda+\boldsymbol{\mu}^T\mathbf{A}(:,n))p^{(n)} \tag{5.25}$$

the dual function is given by

$$D(\lambda,\boldsymbol{\mu}) = \sup_{\mathbf{0}\preceq\mathbf{p}\preceq\mathbf{P}_{\max},\mathbf{q},\mathbf{k}\in\mathcal{K}^N} L(\mathbf{p},\mathbf{q}) \tag{5.26}$$

$$= \begin{cases} \sup\limits_{\mathbf{0}\preceq\mathbf{p}\preceq\mathbf{P}_{\max},\mathbf{k}\in\mathcal{K}^N} \sum\limits_{n=1}^{N} L_n(p^{(n)},k(n)) + \lambda P_{\max} + \boldsymbol{\mu}^T\mathbf{b}, \\ \qquad\qquad\qquad\qquad\qquad\qquad \text{if } \mathbf{B}^T\boldsymbol{\mu}=\mathbf{0} \\ \infty, \qquad\qquad\qquad\qquad\qquad\qquad \text{otherwise} \end{cases} \tag{5.27}$$

and thus the dual optimization problem boils down to

$$\inf_{\lambda,\boldsymbol{\mu}} D(\lambda,\boldsymbol{\mu}) \tag{5.28}$$

$$\text{subject to } \lambda\geq 0,\ \boldsymbol{\mu}\succeq\mathbf{0},\ \mathbf{B}^T\boldsymbol{\mu}=\mathbf{0}. \tag{5.29}$$

It is interesting to note that the auxiliary variables $\mathbf{q}$ introduced for the lifted polyhedral relaxation do not need to be determined in order to obtain the dual function. Moreover, it is immediate that the optimization in (5.27) can be decomposed into individual tones, thanks to the transformation of the nonlinear cone constraint into multiple linear ones, so that the interference contributions due to individual $p^{(n)}$ can be separately assessed.

Specifically, for each subcarrier $n\in\{1,2,\ldots,N\}$

$$\max_{0\leq p^{(n)}\leq P_{\max}^{(n)},k(n)\in\mathcal{K}} L_n(p^{(n)},k(n)) \tag{5.30}$$

needs to be solved. It is revealing to interpret (5.25) from an economic perspective, as balancing the payoff due to an achievable rate and the cost incurred for causing interference, where $\boldsymbol{\mu}$ contains the prices associated with different facets of the polyhedral model. If $k(n) = k \in \mathcal{K}$, the optimal power loading can be obtained by taking the derivative of $L_n(p^{(n)}, k)$ w.r.t. $p^{(n)}$, and setting it to zero. To this end, one needs the derivative of the mutual information $\mathcal{I}_k^{(n)}$. Since it is not straightforward to obtain the mutual information of an arbitrary input distribution in closed form and compute its derivative, a fundamental relationship between the derivative of mutual information and the nonlinear minimum mean-square error (MMSE) can be utilized [23].

Specifically, let $\mathsf{MMSE}_k^{(n)}(h_k^{(n)}p^{(n)})$ denote the MMSE for estimating $x_k^{(n)}$ given $y_k^{(n)}$ based on model (5.1). Then, it is known that

$$\frac{d}{dp^{(n)}}\mathcal{I}_k^{(n)}(h_k^{(n)}p^{(n)}) = h_k^{(n)}\mathsf{MMSE}_k^{(n)}(h_k^{(n)}p^{(n)}). \tag{5.31}$$

Using (5.31), it can be shown that the optimal power loading $p^{*(n)}[k]$ is given by

$$p^{*(n)}[k] = \begin{cases} P_{\max}^{(n)}, & \text{if} \quad \lambda + \boldsymbol{\mu}^T\mathbf{A}(:,n) < 0 \\ \left[\frac{1}{h_k^{(n)}}\mathsf{MMSE}_k^{(n)^{-1}}\left(\frac{\lambda+\boldsymbol{\mu}^T\mathbf{A}(:,n)}{w_k h_k^{(n)}}\right)\right]_0^{P_{\max}^{(n)}}, & \\ \qquad\qquad \text{if } 0 \le \frac{\lambda+\boldsymbol{\mu}^T\mathbf{A}(:,n)}{w_k h_k^{(n)}} \le 1 & n = 1, 2, \ldots, N \\ 0, \quad \text{otherwise,} & \end{cases} \tag{5.32}$$

where $\mathsf{MMSE}_k^{(n)^{-1}}(\cdot)$ is the inverse function of $\mathsf{MMSE}_k^{(n)}(\gamma)$, and $[\cdot]_a^b := \min\{\max\{0, a\}, b\}$. Thus, the optimal user allocation $\mathbf{k}^*$ and power loading $\mathbf{p}^*$ are given, respectively, by

$$k^*(n) \in \arg\max_{k\in\mathcal{K}} L_n(p^{*(n)}[k], k), \quad n = 1, 2, \ldots, N \tag{5.33}$$

$$p^{*(n)} = p^{*(n)}[k^*(n)], \quad n = 1, 2, \ldots, N. \tag{5.34}$$

The optimal solution of (5.28)–(5.29) can be obtained via iterative optimization methods for non-differentiable objectives, such as the subgradient method or the ellipsoid method. To ensure $\mathbf{B}^T\boldsymbol{\mu} = \mathbf{0}$ as required in (5.29), $\boldsymbol{\mu}$ is parametrized by $\boldsymbol{\theta} \in \mathbb{R}^{n_\theta}$ as $\boldsymbol{\mu} = \mathbf{Z}\boldsymbol{\theta}$, where

Table 5.1: Algorithm for solving (P2).

1: Initialize $\boldsymbol{\Sigma}$ and $\boldsymbol{\nu} := [\lambda, \boldsymbol{\theta}^T]^T$. Set tolerance τ
2: Repeat
3: If $\lambda < 0$, set $\mathbf{d} = -\boldsymbol{i}_1$ (first canonical basis)
4: Or, if $\mathbf{Z}(i,:)\boldsymbol{\theta} < 0$ for some $i \in \{1, 2, \ldots, n_c\}$, set $\mathbf{d} = [0 \ -\mathbf{Z}(i,:)]^T$
5: Otherwise:
6: Find $\mathbf{k}^*$ and $\mathbf{p}^*$ from (5.33)–(5.34)
7: Set $\mathbf{d}$ equal to (5.35)
8: If $\sqrt{\mathbf{d}^T\boldsymbol{\Sigma}\mathbf{d}} < \tau$, stop
9: Perform the ellipsoid update:
10: $\mathbf{d} \leftarrow \mathbf{d}/\sqrt{\mathbf{d}^T\boldsymbol{\Sigma}\mathbf{d}}$
11: $\boldsymbol{\nu} \leftarrow \boldsymbol{\nu} - \boldsymbol{\Sigma}\mathbf{d}/(n_\theta + 2)$
12: $\boldsymbol{\Sigma} \leftarrow \frac{(n_\theta+1)^2}{(n_\theta+1)^2-1}\left(\boldsymbol{\Sigma} - \frac{2}{n_\theta+2}\boldsymbol{\Sigma}\mathbf{d}\mathbf{d}^T\boldsymbol{\Sigma}\right)$

the columns of $\mathbf{Z}$ constitute the basis vectors of the null space of $\mathbf{B}^T$. It can be shown that

$$-\begin{bmatrix} \sum_{n=1}^{N} p^{*(n)} - P_{\max} \\ \mathbf{Z}^T(\mathbf{A}\mathbf{p}^* - \mathbf{b}) \end{bmatrix} \tag{5.35}$$

is a subgradient of $D(\lambda, \mathbf{Z}\boldsymbol{\theta})$ w.r.t. $[\lambda \ \boldsymbol{\theta}^T]^T$. The overall procedure for solving (P2) using the ellipsoid method is presented in Table 5.1, where $\mathbf{Z}(i,:)$ is the i-th row of $\mathbf{Z}$ for $i = 1, 2, \ldots, n_c$.

It is of interest to examine the complexity of the algorithm in Table 5.1. The overall complexity can be characterized by multiplying the complexity per iteration by the number of iterations needed. The number of iterations needed for the ellipsoid method to converge grows as the square of the number of optimization variables [8]. The number of variables in the proposed algorithm equals $(n_\theta + 1)$, where $n_\theta = n_c - \text{rank}(\mathbf{B}^T)$. Note that $\text{rank}(\mathbf{B}^T) \leq \min(n_c, n_q) = n_q$ since $v(N) < c(N)$. On the other hand, it can be shown that the values of n_q and n_c both grow as $\mathcal{O}(N \log \frac{1}{\delta})$ for $\delta \leq \frac{1}{2}$ [20]. Therefore, the value of n_θ also grows at most as $\mathcal{O}(N \log \frac{1}{\delta})$. It can thus be deduced that the required number of iterations for

our algorithm grows as $\mathcal{O}(N^2(\log \frac{1}{\delta})^2)$.

It turns out that the number of operations per iteration grows as $\mathcal{O}(N^2(\log \frac{1}{\delta})^2)$ as well, leading to the overall complexity order of $\mathcal{O}(N^4(\log \frac{1}{\delta})^4)$. The per-iteration complexity can be verified as follows. In line 4 of Table 5.1, $\mathcal{O}(n_c n_\theta)$ operations are needed. In line 6, $\mathcal{O}(n_c N)$ operations are necessary to compute the powers on all subcarriers using (5.34), where the dominant component is the calculation of $\boldsymbol{\mu}^T\mathbf{A}$. Once the values of $\boldsymbol{\mu}^T\mathbf{A}$ are stored, $L_n(p^{*(n)}[k], k)$ must be evaluated KN times to find the maximizing k per (5.33). In line 7, $\mathcal{O}(n_c N + n_c n_\theta)$ operations are necessary. In lines 8–12, the dominant calculation is the computation of $\boldsymbol{\Sigma}\mathbf{d}$, which takes $\mathcal{O}(n_\theta^2)$ operations. Therefore, the overall per-iteration complexity with large N and small δ grows as $\mathcal{O}(N^2(\log \frac{1}{\delta})^2)$.

5.3.2 Suboptimal Algorithm

To benchmark performance of the proposed near-optimal scheme, a simple suboptimal algorithm based on alternating minimization is also considered. Note that with the subcarrier allocation $\mathbf{k}$ fixed, the optimization problem (P1) with regard to only $\mathbf{p}$ is a convex problem. Also, with $\mathbf{p}$ fixed, solving for $\mathbf{k}$ is straightforward since the problem naturally decouples across subcarriers, and boils down to choosing on each subcarrier n the user that yields the maximum contribution to the objective. Iterating these two steps will monotonically increase the objective, which can be stopped when no further increase is made. It is noted that this algorithm can be thought of as an extension of the algorithm in [52] to the OFDMA case, since the latter can be employed as a subroutine (after appropriate adaptation to cope with practical constellations). The procedure can be described in pseudocode as follows.

- Step 1: Initialize $\mathbf{p}$, e.g., set $p^{(n)} = P_{\max}/N$ for $n = 1, 2, \ldots, N$.
- Step 2: Set $k(n) = \arg\max_k w_k \mathcal{I}_k^{(n)}(h_k^{(n)} p^{(n)})$ for $n = 1, 2, \ldots, N$.
- Step 3: With $\mathbf{k}$ fixed, solve (P1) only over $\mathbf{p}$ using convex optimization techniques (or by using an adapted version of the algorithm in [52].)
- Step 4: If the objective is not increased, stop; otherwise, go to Step 2.

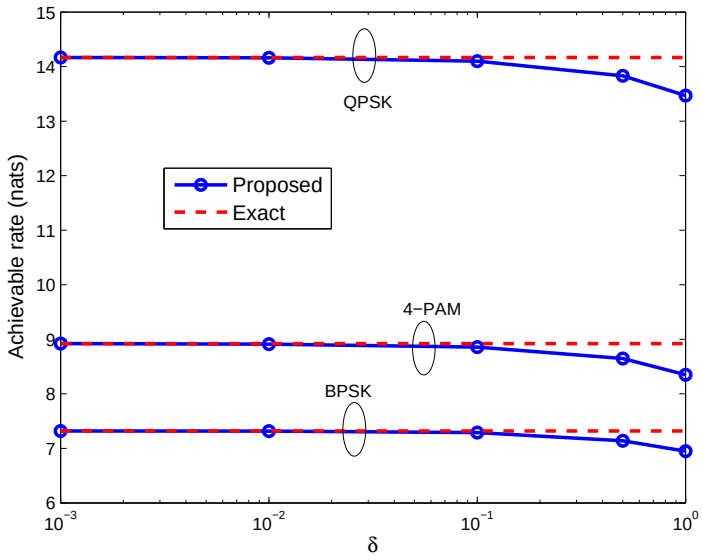

Figure 5.1: Achievable rates for a single-user case.

5.4 Numerical Tests

The proposed RA algorithm is verified via numerical tests. A Rayleigh-faded, 4-path channel is simulated. The pathloss exponent is set to $\alpha = 2$. Assuming Gaussian-distributed $\mathbf{g}$, we set $\Omega = Q^{-1}(\epsilon)$ for small $\epsilon > 0$. The covariance of the channel estimation error follows the model in [60]. Unless stated otherwise, the values of $P_{\max} = 10^2$ and $I_{\max} = 1$ were used with unit-power channel coefficients and additive noise.

In order to validate the polyhedral approximation of the second-order cone constraint, the single-user case is first examined. Recall that when $K = 1$, the original problem (P1) is convex, which can be easily solved using generic convex optimization software for optimal power allocation across subcarriers. The solid lines with circle markers in Fig. 5.1 represent the sum rates in nats obtained by solving (P2) with $\epsilon = 0.1$ for various values of δ, where $N = 16$ subcarriers were used. Recall that when δ is small, the polyhedral approximation for the interference constraint is tight. Results using three different practical constellations are shown, namely, QPSK, 4-PAM, and BPSK constellations. Also shown in dashed lines are the optimal sum rates obtained by solving (P1) directly. It can be seen that the rate

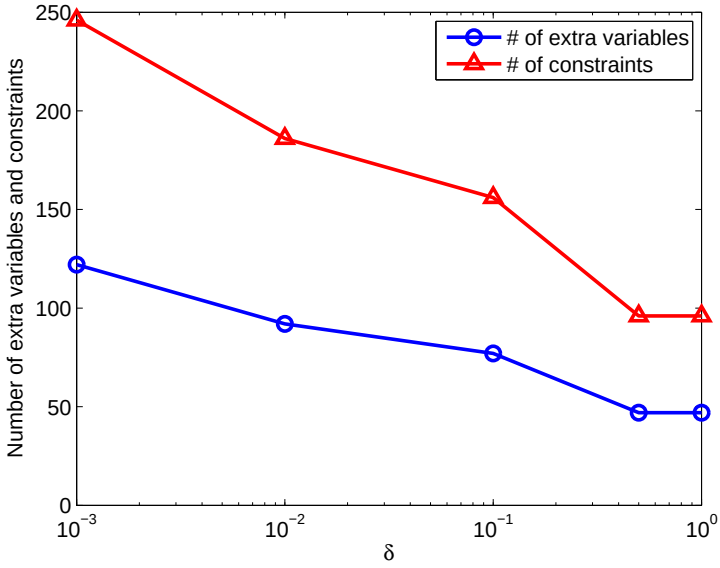

Figure 5.2: Number of constraints and extra variables.

performances from (P2) are indistinguishable from those of (P1) when $\delta \leq 0.1$.

As was discussed in Sec. 5.2, decreasing δ incurs increase in the number of optimization variables and constraints. Fig. 5.2 depicts the number of extra variables introduced for the polyhedral approximation as well as the number of constraints, as δ is varied. It can be observed that as δ is decreased by orders of magnitude, the corresponding growth in the problem complexity is rather mild.

In the multi-user case with $K > 1$, (P1) becomes hard due to the combinatorial search for optimal subcarrier assignment. Exhaustive search would require enumerating K^N different assignments, and solving a (convex) power allocation problem per (P1) for each of the assignments. Fig. 5.3 shows the case of $K = 2$ users, with user 2 located four times farther than user 1 from the CR-BS. Equal weights of $w_1 = w_2 = 0.5$ were used. User 1 employed a BPSK constellation and user 2 QPSK, and the number of subcarriers $N = 8$. Two sets of curves corresponding to $\epsilon = 0.1$ and $\epsilon = 0.01$ are presented in Fig. 5.3 in solid and dashed lines, respectively. In each set, the line with circle markers represents the weighted sum rate obtained using the proposed algorithm, and the line without markers corresponds to the results from exhaustive search. In addition, the results from the suboptimal algorithm

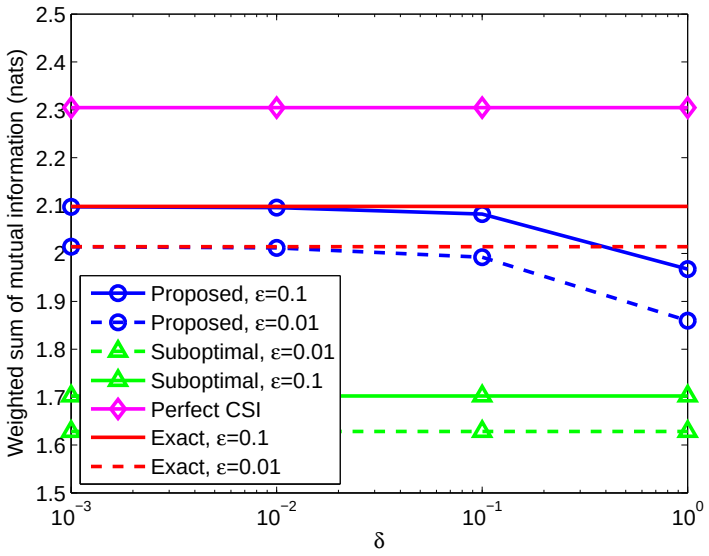

Figure 5.3: Weighted sum rates when $K = 2$.

in Sec. 5.3.2 are depicted as the lines with triangle markers, and the rate achievable under perfect channel state information on the interfering channel with diamond markers. It can be seen that the proposed algorithm approaches the performance of exhaustive search with sizeable improvement relative to that of the suboptimal heuristic, although the loss due to channel uncertainty is evident.

Fig. 5.4 depicts the weighted sum rates for the same set-up as used for Fig. 5.3, but with user 2 employing QPSK or 4-PAM modulations. The value of $\delta = 0.1$ was used and the values of ϵ were varied. The lines with square markers and the ones with circle markers correspond to the results of exhaustive search and the proposed method, respectively. It can be verified that the proposed method can achieve near-optimal performance at a moderate value of δ. Also, as expected, the rate performance improves as ϵ grows larger, as this amounts to more lenient interference constraints.

The case with $K = 3$ CR users were also tested and shown in Fig. 5.5 for $\epsilon = 0.1$ and $\epsilon = 0.01$. The distances of users 2 and 3 from the CR-BS were four times that of user 1, and the input constellations for user 1, 2, and 3 were set to BPSK, 4-PAM, and QPSK, respectively. Equal weights were used. The value of $I_{\max}$ was set to 10 and $N = 8$

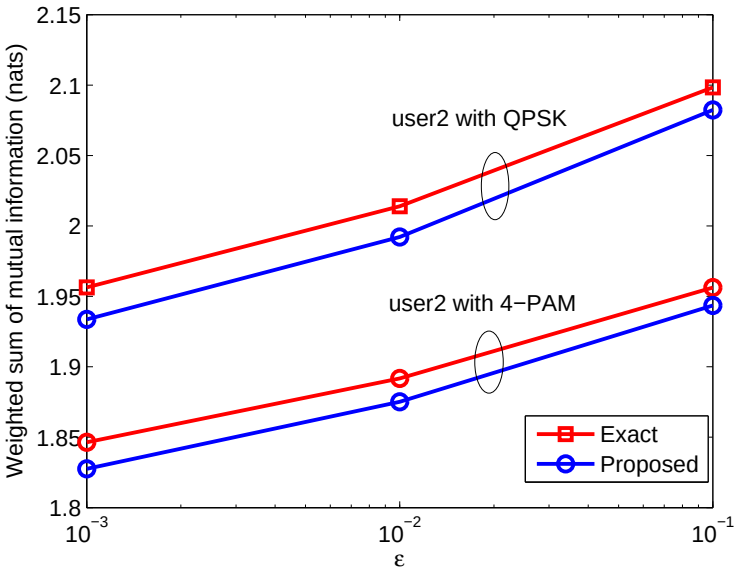

Figure 5.4: Weighted sum rates versus ϵ.

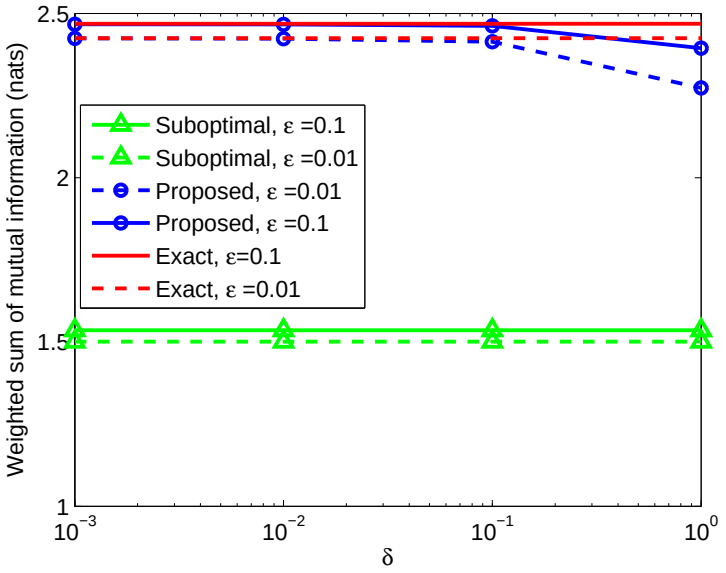

Figure 5.5: Weighted sum rates when $K = 3$.

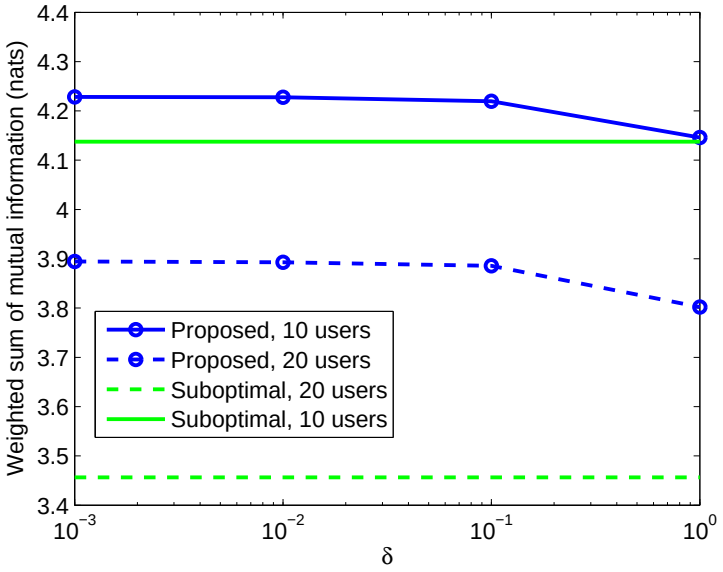

Figure 5.6: Weighted sum rates when $K = 10$ and $K = 20$.

Table 5.2: Run times of RA algorithms in seconds.

		$\delta = 0.01$	$\delta = 0.1$	$\delta = 1$
$N = 32$	proposed	758	473	336
$K = 10$	suboptimal	180.		
$N = 8$	proposed	18.1	14.2	12.2
$K = 3$	suboptimal	2.74		

subcarriers (or subbands) were employed. The results from the proposed and the suboptimal algorithms as well as the exhaustive search are presented. The overall trend is quite similar to the two-user case.

The proposed algorithm was tested for larger values of K. Fig. 5.6 depicts the cases with $K = 10$ and $K = 20$, where $N = 32$ and $\epsilon = 0.1$ were used. Due to prohibitive computational complexity associated with exhaustive search, only the results from the proposed and the suboptimal methods are plotted. Again, it can be seen that the achieved weighted sum rates saturate with $\delta \leq 0.1$, implying that they have reached the optimal values.

To get a rough idea on the practical implementation complexity of the algorithms,

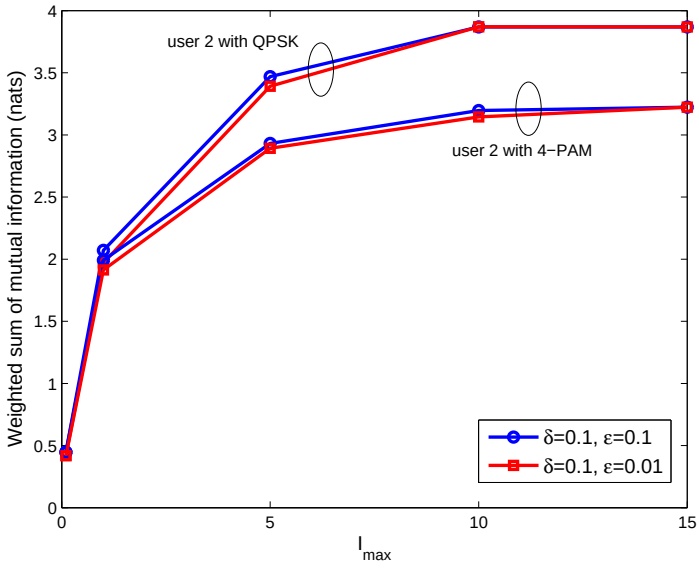

Figure 5.7: Weighted sum rates versus $I_{\max}$.

actual run times of the proposed and the benchmark algorithms are presented in Table 5.2 for the cases with $N = 8$ and $N = 32$ using $\tau = n_\theta \times 10^{-3}$. A 2.3 GHz Intel processor with 6 GB of RAM was used. Since the convex optimization subroutine called by the suboptimal algorithm was implmented in a native code, while the proposed algorithm was run in Matlab, which is interpreter-based, the suboptimal algorithm may be at a slight advantage. Nonetheless, it can be seen that our algorithm is quite competitive.

To assess the sensitivity of the rate performance to the PU interference constraint, the weighted sum rates are plotted against the value of $I_{\max}$ in Fig. 5.7 for $\delta = 0.1$ with $N = 8$ and $K = 2$. As $I_{\max}$ is increased, the CR can allocate more power to serve the CR users, yielding a higher total rate. Once $I_{\max}$ becomes large enough, the total power constraint becomes the bottleneck, which explains the leveling of the curves at high $I_{\max}$ in Fig. 5.7. On the other hand, when $I_{\max}$ is very small, the use of higher order modulation does not seem to be warranted.

To characterize the performance gain of specifically accounting for practical modulation constellations, the rates achievable using the power and subcarrier allocation based on traditional Gaussian coding are compared to the rates from the proposed design. The same

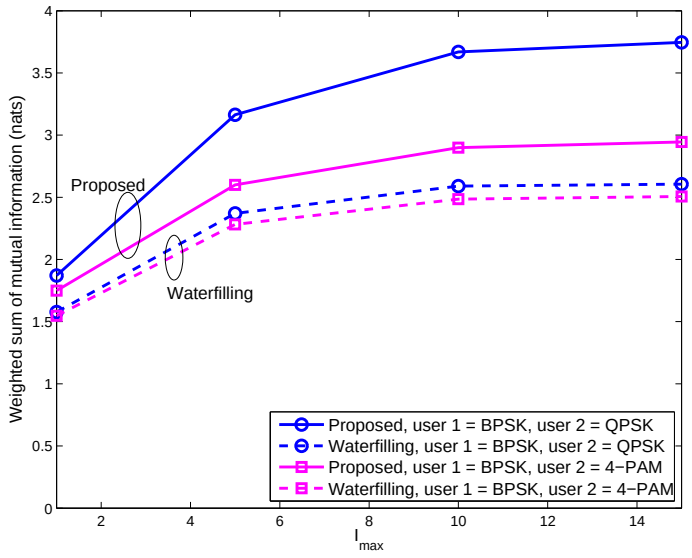

Figure 5.8: Performance comparison to algorithm with water-filling.

set-up as in Fig. 5.3 is used with $K = 2$ and $\epsilon = 0.01$. The solid lines in Fig. 5.8 represent the case where user 2 uses QPSK modulation, while the dashed lines the case with 4-PAM. The circle markers signify the proposed method in which the mercury/water-filling is used, whereas the square markers correspond to the method with the water-filling. It can be seen that regardless of the constellation, the proposed formulation yields superior performance.

5.5 Summary

A weighted sum rate maximization problem was formulated for a CR system employing OFDMA. Due to the uncertainty present in the CR-to-PU channel, a robust interference constraint with an ellipsoidal uncertainty set was imposed to protect the PU system, which is equivalent to a second-order cone constraint. When only one CR user is served by the BS, the optimization problem is convex. When multiple users are present, due to the combinatorial search for optimal subcarrier assignment, the problem is non-convex and hard to solve. In fact, since the second-order cone constraint lacks separable structure, the optimization variables are coupled across all subcarriers. Therefore, a polyhedral approximation was

introduced to break the coupling. The dual method could then be employed to decompose the overall problem into per-subcarrier sub-problems, which can be easily solved. Since the complexity of the polyhedral approximation scales modestly (polynomially) in the number of subcarriers, the overall algorithm can efficiently find the near-optimal power loading and subcarrier assignment. Numerical tests verified the efficiency of the novel algorithm.

5.6 Appendices

Appendix: Duality gap of (P2)

Here, a claim related to the duality gap of (P2) is proved. To this end, we will invoke [6, Proposition 5.26], which considers problems of the following form:

$$\text{(P3)} \qquad \min \sum_{i=1}^{I} f_i(\mathbf{x}_i) \tag{5.36}$$

$$\text{subject to } \mathbf{x}_i \in \mathcal{X}_i \tag{5.37}$$

$$\sum_{i=1}^{I} \mathbf{h}_i(\mathbf{x}_i) \leq \boldsymbol{\gamma} \tag{5.38}$$

where $\mathcal{X}_i \subset \mathbb{R}^{d_i}$, $\boldsymbol{\gamma} \in \mathbb{R}^m$, $f_i : \mathcal{X}_i \to \mathbb{R}$ and $\mathbf{h}_i : \mathcal{X}_i \to \mathbb{R}^m$. Then, it was shown in [6] that under conditions

c1) There exists at least one feasible solution to (P3).

c2) For each i, the set $\{\mathbf{x}_i, \mathbf{h}_i(\mathbf{x}_i), f_i(\mathbf{x}_i) | \mathbf{x}_i \in \mathcal{X}_i\}$ is compact.

c3) For each i, given any $\tilde{\mathbf{x}}_i \in *(\mathcal{X}_i)$, there exists $\mathbf{x}_i \in \mathcal{X}_i$ such that $\mathbf{h}_i(\mathbf{x}_i) \leq \tilde{\mathbf{h}}_i(\tilde{\mathbf{x}}_i)$, where $*(\cdot)$ denotes the convex hull operator, and

$$\tilde{\mathbf{h}}_i(\tilde{\mathbf{x}}) := \inf \left\{ \sum_{j=1}^{d_i+1} \pi^j \mathbf{h}_i(\mathbf{x}^j) \middle| \tilde{\mathbf{x}} = \sum_{j=1}^{d_i+1} \pi^j \mathbf{x}^j,\ \mathbf{x}^j \in \mathcal{X}_i,\ \sum_{j=1}^{d_i+1} \pi^j = 1,\ \pi^j \geq 0 \right\} \tag{5.39}$$

the duality gap can be upper-bounded by $(m+1) \max_{i \in \{1,2,\ldots,I\}} \rho_i$, where

$$\rho_i \leq \sup \{ f_i(\mathbf{x}_i) | \mathbf{x}_i \in \mathcal{X}_i \} - \inf \{ f_i(\mathbf{x}_i) | \mathbf{x}_i \in \mathcal{X}_i \}. \tag{5.40}$$

Thus, as long as $\max_i \rho_i$ grows sublinearly in i, the duality gap of (P3) normalized by I vanishes as $I \to \infty$. In other words, provided that the optimal objective of (P3) is proportional in I, the fraction of the duality gap to the objective goes to zero as I grows.

This result is applicable to (P2). For this, set $I = N + 1$, and let $\mathbf{x}_n := (k(n), p^{(n)})$ for $n = 1, 2, \ldots, N$, and $\mathbf{x}_{N+1} := \mathbf{q}$. Then, $\mathcal{X}_n := \mathcal{K} \times [0, P_{\max}^{(n)}]$ for $n = 1, \ldots, N$. Without loss of generality, $\mathbf{q}$ can be confined to a convex and compact set $\mathcal{Q}$, and let $\mathcal{X}_{N+1} :=$

$\mathcal{Q}$. Furthermore, let $f_n(\mathbf{x}_n) := w_{k(n)}\mathcal{I}^{(n)}_{k(n)}(h^{(n)}_{k(n)}p^{(n)})$ for $n = 1,\ldots,N$, $f_{N+1}(\mathbf{x}_{N+1}) = 0$, $\mathbf{h}_n(\mathbf{x}_n) := [1, \mathbf{A}(:,n)^T]^T p^{(n)}$ for $n = 1,\ldots,N$, $\mathbf{h}_{N+1}(\mathbf{x}_{N+1}) := [\mathbf{0}^T, \mathbf{B}^T]^T\mathbf{q}$, and $\boldsymbol{\gamma} = [P_{\max}, \mathbf{b}^T]^T$. Then, conditions c1) and c2) are readily satisfied. It is also trivial to verify that c3) is met, since $\mathbf{h}_n(\mathbf{x}_n)$ for $n = 1,\ldots,N$, is constant with respect to $k(n)$, and also linear in $p^{(n)}$. Therefore, a duality gap over-estimate of (P2) is given by

$$(n_c + 2) \max_{n\in\{1,2,\ldots,N\}} \max_{k\in\mathcal{K}} w_k \mathcal{I}^{(n)}_k (h^{(n)}_k P^{(n)}_{\max}) \tag{5.41}$$

which is related to the highest-order constellation employed by the OFDMA users, and is thus finite. Therefore, the ratio of the duality gap of (P2) to the optimal objective approaches zero as N grows large.

Chapter 6

Summary and Future Directions

This thesis presented algorithms for optimal resource management under uncertainty in smart grid networks and cognitive radio (CR) networks. In addition, online algorithms were devised to learn the temporal variations and the dynamics of these networks.

6.1 Thesis Summary

While EVs are expected to provide environmental and economical benefit, judicious coordination of EV charging is necessary to prevent overloading the distribution grid. Leveraging the smart grid infrastructure, the utility company can adjust the electricity price intelligently for individual customers to elicit desirable load curves. In this context, Chapter 2 of this thesis addresses the problem of predicting the EV charging behavior of the consumers at different prices, which is a prerequisite for optimal price adjustment. The dependencies on price responsiveness among consumers are captured by a conditional random field (CRF) model. To account for temporal dynamics potentially in a strategic setting, the framework of online convex optimization (OCO) was adopted to develop an efficient online algorithm for tracking the CRF parameters. Such information is essential for setting the electricity prices in real time to coordinate EV charging. The probabilities with which individual EV consumers charge their vehicles when presented with real-time prices were obtained based on the CRF model. The CRF model was then applied as an input to a stochastic

profit maximization problem for real-time price setting. The performance of the proposed algorithms was corroborated using simulated and semi-real data.

Then, in Chapter 3, the problem of learning the consumers' charging behavior with missing data was pursued. A CRF-based model for capturing the probabilities with which individual EV consumers charge their vehicles was considered. It was assumed that the collected charging data from individual customers include misses, as it is natural to expect errors and misses in the charging data collected from the network of consumers. Then, instead of neglecting the misses or filling them with all possible values as in EM-based algorithms, an estimate of the misses was obtained. Incorporating the estimates and without explicit models for temporal dynamics of consumption behavior of consumers, an online algorithm for learning the consumers dependency network parameters and elasticity was developed. The performance of the proposed algorithm was verified by numerical tests using synthetic and semi-real data.

In the context of wireless CR communication networks, resource management was addressed in Chapters 4 and 5. Since CRs do not receive explicit support from the PUs, acquiring accurate channel estimates is often challenging. Therefore, one needs to ensure that the interference constraint is effected robustly against channel uncertainty. In Chapter 4, resource allocation for the uplink of OFDMA-based CR systems was pursued. The weighted sum-rate was maximized over subcarrier assignment as well as over power loading per CR user, while protecting primary user (PU) systems. However, due to the lack of explicit support from PU systems, the channels from CR users to the PU may not be accurately acquired. Motivated by this, the PU interference constraint was posed as a chance constraint, for which conservative convex approximation based on Bernstein method was employed for tractability. In particular, to mitigate the combinatorial complexity incurred for optimal subcarrier assignment, a separable structure was pursued, and the dual decomposition method was adopted to obtain near-optimal solutions. Numerical tests verify that the proposed algorithms yield higher weighted sum-rate at lower computational complexity than a benchmark algorithm.

Chapter 5 addresses a resource allocation problem for a CR base station (BS) commu-

nicating with multiple CR mobile stations (MSs) in the downlink, which relies on OFDMA. Practical finite-alphabet constellations were adopted and total weighted achievable rate was maximized. To protect the incumbent PU system operating over the same frequency band, the interference inflicted to the PU receiver must be regulated. Since the channel gain estimates from the CR-BS to the PU receiver are typically uncertain in practice, a robust interference constraint with an ellipsoidal uncertainty set was imposed to protect the PU system, which is equivalent to a second-order cone constraint. When only one CR user is served by the BS, the optimization problem is convex. When multiple users are present, due to the combinatorial search for optimal subcarrier assignment, the problem is non-convex and hard to solve. In fact, since the second-order cone constraint lacks separable structure, the optimization variables are coupled across all subcarriers. To circumvent the resulting computational hurdle, a tight polyhedral approximation of the second-order cone was introduced to break the coupling. The dual method could then be employed to decompose the overall problem into per-subcarrier sub-problems, which can be easily solved. As the rate does not grow without bound even when the transmit-power is increased, a mercury/water-filling step is used rather than the conventional water-filling step. The dual problem is solved using the relationship between the minimum mean-square error (MMSE) and the derivative of mutual information [23]. Since the complexity of the polyhedral approximation scales modestly (polynomially) in the number of subcarriers, the overall algorithm can efficiently find the near-optimal power loading and subcarrier assignment. Numerical tests verified the efficiency of the novel algorithm.

It is worth noting that the proposed approaches in Chapters 4 and 5 have potential to impact networks beyond the particular ones treated, as they provide means to efficiently tackle a class of large-scale robust mixed-integer problems involving second-order cone constraints.

6.2 Ongoing Research and Future Directions

The work presented in this thesis only addresses certain aspects of learning and resource management in power and communication networks and opens up interesting directions for

a number of future research topics. In addition, it is shown that certain algorithms obtained for EV charging, can be tailored to CR networks. We outline some of the venues that we are currently pursuing.

6.2.1 OCO for Spectrum Sensing in CR Networks

The idea here is to tailor the online learning algorithms devised in Chapters 2 and 3 for efficient spectrum sensing in CR networks.

Consider an overlay cognitive scenario with one CR user and one PU coexisting in a geographical region where the CR user scans N bands for possible transmission opportunities. In most spectrum sensing techniques, binary hypothesis testing is performed per band $n \in N$ based on the assumption that the spectrum occupancy of the PU is independent across bands. However, this assumption is not valid in the presence of wideband PU signals, e.g., when PU is transmitting television signals. The issue is that the CR maps the PU band as multiple bands for its own transmission which in effect are correlated. The problem of spectrum sensing in the presence of correlated bands has been considered in [25].

Utilizing the OCO paradigm, we propose to track the probability of detection and false alarms while learning the occupancy dependencies across bands. Then, a CR learner tracks the possible correlations among bands and also PU strategies in spectrum occupancy which can later be used to adjust the sensing threshold, accordingly.

Consider N bands and let $\mathbf{s}^t := [s_1^t, ..., s_N^t]$ denote the true instantaneous PU activity over N bands and $\hat{\mathbf{s}}^t := [\hat{s}_1^t, ..., \hat{s}_N^t]$ the estimated PU activity by the CR receiver. With $\mathcal{S} \triangleq \{-1, 1\}$, $\{s_n^t \in \mathcal{S}\}_{n=1}^N$ and $\{\hat{s}_n^t \in \mathcal{S}\}_{n=1}^N$ indicate the true and estimated availability of band n at time t, i.e, s_n^t and $\hat{s}_n^t$ are 1 if the band is available and estimated to be available for CR activities, respectively, and -1 otherwise. When PU activities over different bands are correlated and due to the fact that spectrum occupancy changes over time, the PU activities can be fitted into a probabilistic spatio-temporal model using CRF.

Consider N bands and assume that the bands n and m are connected by an edge if their occupancy is dependent on each other with weights $\{\theta_{n,m}^t\}_{n,m \in V}$, thus forming the graph $G(V, E)$, where V and E represent the set of vertices and edges, respectively. Here,

it is assumed that there are no self-loops in the graph, i.e., $\theta^t_{n,m} = 0$. In addition, $\{\theta^t_n\}_{n\in V}$ captures the dependency of $\hat{s}^t_n$ on s^t_n. Letting $\boldsymbol{\theta}^t := [\theta^t_n, n \in V; \theta^t_{n,m}, n, m \in V]$, the joint probability of bands occupancy using CRF model can thus be written as

$$P_{\boldsymbol{\theta}^t}(\hat{\mathbf{s}}^{\mathbf{t}}|\mathbf{s}^{\mathbf{t}}) = \frac{1}{Z(\boldsymbol{\theta}^t, \mathbf{s}^{\mathbf{t}})} \exp\{\sum_{n=1}^{N} \theta^t_n s^t_n \hat{s}^t_n + \sum_{n=1}^{N}\sum_{m=1}^{N} \theta^t_{n,m} \hat{s}^t_n \hat{s}^t_m\}. \tag{6.1}$$

The *pdf* in (6.1) represents the joint detection (or false-alarm) probability. The probability of false alarms and miss detection for each of the bands can then be obtained by marginalizing (6.1). As mentioned in Chapter 2, these marginal probabilities can be efficiently obtained using the BP algorithm.

The model parameters $\boldsymbol{\theta}^t$, can then be estimated sequentially by the online algorithm introduced in Chapter 2. Then, the problem of online parameter estimation amounts to tracking the probability of false alarms and miss detection, which can be further utilized for a more accurate occupancy detection and an adaptive threshold setting in energy detection-based spectrum sensing. On the other hand, the PU may change activities over the bands, adversarialy. Therefore, it is important for the online algorithm to accommodate the strategic change of band occupancy by the PU system. Clearly, in practice, the PU bands occupancies are also correlated across time. Advocating the OCO framework with minimal assumptions on the structure of temporal correlation of data (band's occupancy), while allowing for strategic band occupancy changes by the PU, an online algorithm with guaranteed performance is obtained. The instantaneous $P_{\boldsymbol{\theta}^t}(\hat{\mathbf{s}}^t|\mathbf{s}^t)$ can be further utilized in resource allocation in overlay scenario.

Dynamic learning of bands occupancy dependency network

In this theme, we propose an online algorithm based on the OCO framework. The forecaster is the CR user and the adversary is the PU. The loss represented by the negative log-likelihood function $\ell^t(\boldsymbol{\theta}^t) := -\log P_{\boldsymbol{\theta}^t}(\hat{\mathbf{s}}^t|\mathbf{s}^t)$ is not revealed to the CR user until the CR predicts $\hat{\boldsymbol{\theta}}^t$ and announces its estimate of bands occupancy, i.e., $\hat{\mathbf{s}}^t$, and the CR system becomes aware of the true state of the occupancy, i.e., $\mathbf{s}^t$ through a NACK(or ACK). Note that the chosen loss $\ell^t(\boldsymbol{\theta}^t)$ with $P_{\boldsymbol{\theta}^t}(\hat{\mathbf{s}}^t|\mathbf{s}^t)$ as in (6.1) is convex [40].

Similar to Chapter 2, $\hat{\boldsymbol{\theta}}^{t+1}$ is obtained using an online gradient descent by

$$\hat{\boldsymbol{\theta}}^{t+1} = \hat{\boldsymbol{\theta}}^{t} - \mu_t \nabla \ell^t(\hat{\boldsymbol{\theta}}^{t}). \tag{6.2}$$

As described in Chapter 2, the algorithm yields a regret bound that is sublinear in T.

The algorithm would have similar performance as discussed in the simulated test with synthetic data in Chapter 2. In addition, the algorithm proposed in Chapter 3 can accommodate the case with missing data.

The spectrum sensing improvement due to leverging the band correlation model, is another interesting future research direction.

6.2.2 OCO for Gaussian CRF in Smart Grid

So far charging decisions were modeled with discrete values using CRF. However, when modeling the aggregate load or the total consumption of consumers due to different types of load, it may be beneficial to resort to continuous CRFs which allow continuous output labels. A special case of continuous CRF, is the Gaussian CRF.

Consider the multivariate Gaussian CRF, where $p(\mathbf{b}^t|\boldsymbol{\rho}^t)$ is defined as

$$p_{\boldsymbol{\theta}^t,\Sigma^t}(\mathbf{b}^t|\boldsymbol{\rho}^t) = \frac{1}{Z(\boldsymbol{\rho}^t, \boldsymbol{\Sigma}^t, \theta^t)} e^{-\frac{1}{2}(\mathbf{b}^t - \boldsymbol{\mu}^t)(\boldsymbol{\Sigma}^t)^{-1}(\mathbf{b}^t - \boldsymbol{\mu}^t)} \tag{6.3}$$

where $Z(\boldsymbol{\rho}^t, \boldsymbol{\theta}^t, \boldsymbol{\Sigma}^t) := (2\pi)^{N/2}|\boldsymbol{\Sigma}^t|^{\frac{1}{2}}$ denotes the partition function. With $\bar{\boldsymbol{\mu}}^t \in \mathbf{R}^N$ capturing the average typical load of the consumers at time t , let $\boldsymbol{\mu}^t := \bar{\boldsymbol{\mu}}^t - \boldsymbol{\rho}^t \circ \boldsymbol{\theta}^t$ and $\circ$ represent the element-wise product of two vectors. Alternatively, one can connect (6.3) to a linear regression model as follows

$$\mathbf{b}^t = \mathbf{X}\boldsymbol{\theta}^t + \boldsymbol{\nu}^t \tag{6.4}$$

where $\mathbf{X}$ is a diagonal matrix and using MATLAB notation, it is denoted by $\mathbf{X} := \text{diag}(-\boldsymbol{\rho}^t)$ and $\boldsymbol{\nu}^t$ is jointly Gaussian with mean $\bar{\boldsymbol{\mu}}^t$ and covariance $\boldsymbol{\Sigma}^t$. Letting the inverse covariance matrix be defined as $\mathbf{C}^t := (\boldsymbol{\Sigma}^t)^{-1}$, then (6.3) can be rewritten as

$$p_{\boldsymbol{\theta}^t,\mathbf{C}^t}(\mathbf{b}^t|\boldsymbol{\rho}^t) = (2\pi)^{-N/2}|\mathbf{C}^t|^{\frac{1}{2}} e^{-\frac{1}{2}(\mathbf{b}^t - \boldsymbol{\mu}^t)\mathbf{C}^t(\mathbf{b}^t - \boldsymbol{\mu}^t)}. \tag{6.5}$$

The goal of the utility company is then to predict $\boldsymbol{\theta}^{t+1} \in \mathbf{R}^N$ and $\mathbf{C}^{t+1} \in \mathbf{R}^{N\times N}$ at time t. The missing edges in the graphical model correspond to zero entires in the inverse covariance matrix which suggest an ℓ_1-norm penalty term in estimating $\mathbf{C}^t$. In addition, it is natural to assume that only a few consumers may change their price-responsiveness over time, thus promoting sparsity in $\boldsymbol{\theta}^t$. Then, the problem can be formulated as

$$\{\hat{\boldsymbol{\theta}}^{t+1}, \hat{\mathbf{C}}^{t+1}\} = \arg \min_{\boldsymbol{\theta}, \mathbf{C}\succ \mathbf{0}} \quad \ell^t(\boldsymbol{\theta}, \mathbf{C}) + \lambda_1 \|\boldsymbol{\theta}\|_1 + \lambda_2 \|\mathbf{C}\|_{1,*} \tag{6.6}$$

where $\ell^t(\boldsymbol{\theta}, \mathbf{C}) := -\log p_{\boldsymbol{\theta},\mathbf{C}}(\mathbf{b}^t|\boldsymbol{\rho}^t)$, $\|\mathbf{C}\|_{1,*}$ denotes the element wise ℓ_1-norm on off-diagonal elements of $\mathbf{C}$, and $\mathbf{C} \succ \mathbf{0}$ ensures that $\mathbf{C}$, the inverse covariance matrix, is positive definite.

Dynamic learning the dependency network and load elasticity

It should be noted that regular OMD involves linearization of the objective function. However, when dealing with composite objective functions, where there are regularizers such as the ℓ_1-norm in the objective function, one should avoid linearizing the penalty terms as the subgradient of the penalty term may not carry the merit of the regularizer. For instance, in the proposed problem, the linearized ℓ_1-norm may not result in sparse solution of $\boldsymbol{\theta}$ and $\mathbf{C}$ in (6.6). The remedy is to use composite objective mirror descent (COMID). Future research directions include devising efficient algorithms and regret analyses.

6.2.3 Periodicity in Consumption Behavior

It should be noted that there are periodic patterns in the charging behavior of consumers across different days of the week. Accounting for the periodicity in consumption behavior and proposing efficient and scalable modeling and algorithms offers an interesting extension to Chapter 2.

6.2.4 Distributed Online Learning Algorithm

The proposed online learning algorithm for predicting the consumption behavior of consumers, and real-time price setting require centralized computations. However, in general it may be of interest to introduce distributed online algorithms for price setting schemes and dependency learning.

Bibliography

[1] R. Aggarwal, M. Assaad, C. E. Koksal, and P. Schniter, "Joint Scheduling and Resource Allocation in the OFDMA Downlink: Utility Maximization Under Imperfect Channel-State Information," *IEEE Trans. Sig. Proc.*, vol. 59, pp. 5589–5604, Nov. 2011.

[2] S. M. Almalfouh and G. L. Stüber, "Interference-aware radio resource allocation in OFDMA-based cognitive radio networks," *IEEE Trans. Veh. Technol.*, vol. 60, pp. 1699–1713, May 2011.

[3] M. Bagnoli and T. Bergstrom, "Log-concave probability and its applications," *Econometric Theory*, vol. 26, pp. 445–469, 2005.

[4] A. Ben-Tal and A. Nemirovski, "On polyhedral approximations of the second-order cone," *Math. Oper. Res.*, vol. 26, pp. 193–205, May 2001.

[5] A. Ben-Tal and A. Nemirovski, "Selected topics in robust convex optimization," *Math. Prog., Ser. B*, vol. 112, pp. 125–158, 2008.

[6] D. P. Bertsekas, *Constrained Optimization and Lagrange Multiplier Methods*. Belmont, MA: Athena Scientific, 1996.

[7] P. Billingsley, *Probability Measure*. New York: J. Wiley & Sons, 3rd ed., 1995.

[8] S. Boyd, "Ellipsoid method." `http://www.stanford.edu/class/ee364b/lectures/ellipsoid_method_notes.pdf`, 2008.

[9] R. C. Bradley, "Basic properties of strong mixing conditions. A survey and some open questions," *Probability Surveys*, vol. 2, pp. 107–144, 2005.

[10] A. Castaño-Martínez and F. López-Blázquez, "Distribution of a sum of weighted central chi-square variables," *Communications in Statistics - Theory and Methods*, vol. 34, no. 3, pp. 515–524, 2005.

[11] A. Castaño-Martínez and F. López-Blázquez, "Distribution of a sum of weighted non-central chi-square variables," *Test*, vol. 14, no. 2, pp. 397–415, 2005.

[12] R. Cendrillon, W. Yu, M. Moonen, J. Verlinden, and T. Bostoen, "Optimal multiuser spectrum balancing for digital subscriber lines," *IEEE Trans. Wireless Commun.*, vol. 54, pp. 922–933, May 2006.

[13] K. Clement-Nyns, E. Haesen, and J. Driesen, "The impact of charging plug-in hybrid electric vehicles on a residential distribution grid," *IEEE Trans. Power Syst.*, vol. 25, pp. 371–380, Jan. 2010.

[14] E. Dall'Anese, S.-J. Kim, G. B. Giannakis, and S. Pupolin, "Power control for cognitive radio networks under channel uncertainty," vol. 10, pp. 3541–3551, Dec. 2011.

[15] E. Dall'Anese, S.-J. Kim, G. B. Giannakis, and S. Pupolin, "Power control for cognitive radio networks under channel uncertainty," vol. 10, pp. 3541–3551, Dec. 2011.

[16] J. Davies and K. Kurani, "Moving from assumption to observation: Implications for energy and emissions impacts plug-in hybrid electric vehicles," *Energy Policy*, vol. 62, pp. 550–560, Nov. 2013.

[17] S. Deilami, A. Masoum, P. Moses, and M. Masoum, "Real-time coordination of plug-in electric vehicle charging in smart grids to minimize power losses and improve voltage profile," *IEEE Trans. Smart Grid*, vol. 2, pp. 456–467, May 2011.

[18] L. Gan, U. Topcu, and S. H. Low, "Optimal Decentralized Protocol for Electric Vehicle Charging," in *Proc. of 50th IEEE Conf. on Decision and Control and European Control Conf.*, Orlando, FL, Dec. 2011.

[19] L. Gan, U. Topcu, and S. H. Low, "Stochastic distributed protocol for electric vehicle charging with discrete charging rate," in *Proc. of PES General Meeting*, San Diego, California, pp. 1–8, 2012.

[20] F. Glineur, "Computational experiments with a linear approximation of second-order cone optimization," Tech. Rep. 0001, Service de Mathématique et de Recherche Opérationnelle, Faculté Polytechnique de Mons, Mons, Belgium, Nov. 2000.

[21] A. Goldsmith, S. A. Jafar, I. Marić, and S. Srinivasa, "Breaking spectrum gridlock with cognitive radios: An information theoretic perspective," *Proc. IEEE*, vol. 97, pp. 894–914, May 2009.

[22] V. Gomez, M. Chertkov, S. Backhaus, and H. Kappen, "Learning Price-Elasticity of Smart Consumers in Power Distribution Systems," in *Proc of IEEE Intl. Conf. on Smart Grid Commun.*, Tainan City, Taiwan, Nov. 2012.

[23] D. Guo, S. Shamai, and S. Verdú, "Mutual information and minimum mean-square error in Gaussian channels," *IEEE Trans. Info. Theory*, vol. 51, pp. 1261–1283, Apr. 2005.

[24] E. Hazan, A. Agarwal, and S. Kayle, "Logarithmic regret algorithms for online convex optimization," *Journal of Machine Learning*, vol. 69, pp. 169–192, Dec. 2007.

[25] K. Hossain and B. Champagne, "Wideband Spectrum Sensing for Cognitive Radios With Correlated Subband Occupancy," *IEEE Signal Processing Letters*, vol. 18, pp. 35–38, Jan. 2011.

[26] D. Huang, Z. Shen, C. Miao, and C. Leung, "Resource allocation in MU-OFDM cognitive radio systems with partial channel state information," *EURASIP J. Wireless Commun. Netw.*, Apr. 2010.

[27] J. Huang, V. G. Subramanian, R. Agrawal, and R. A. Berry, "Downlink scheduling and resource allocation for OFDM systems," vol. 8, pp. 288–296, Jan. 2009.

[28] International Energy Agency, "Technology roadmap electric and plug-in hybrid electric vehicles." `http://www.iea.org/publications/freepublications/publication/EV_PHEV_Roadmap.pdf`, 2011.

[29] S.-J. Kim, N. Y. Soltani, and G. B. Giannakis, "Resource allocation for OFDMA cognitive radios under channel uncertainty," in *Proc. of Intl. Conf. on Acoustics, Speech and Signal Processing*, Prague, Czech Republic, pp. 3188–3191, May 2011.

[30] S.-J. Kim, N. Y. Soltani, and G. B. Giannakis, "Resource Allocation for OFDMA Cognitive Radios under Channel Uncertainty," *IEEE Trans. Wireless Commun.*, vol. 12, pp. 3578–3587, July 2013.

[31] H. Kushner and G. Yin, *Stochastic Approximation Algorithms and Applications*. Springer-Verlag, 2nd ed., 2003.

[32] J. Lafferty, A. McCallum, and F. Pereira, "Conditional random fields: Probabilistic models for segmenting and labeling sequence data," in *Proc. of Intl. Conf. on Mach. Learning*, Williamstown, MA, Jun.-Jul. 2001.

[33] R. Liu, L. Dow, and E. Liu, "A Survey of PEV Impacts on Electric Utilities," in *Proc. of Innovative Smart Grid Technologies*, Anaheim, CA, pp. 1–8, Jan. 2011.

[34] A. Lozano, A. M. Tulino, and S. Verdú, "Optimum Power Allocation for Multiuser OFDM with Arbitrary Signal Constellations," *IEEE Trans. Commun.*, vol. 56, pp. 828–837, May 2008.

[35] Z.-Q. Luo and S. Zhang, "Dynamic spectrum management: complexity and duality," *IEEE J. Sel. Topics Sig. Proc.*, vol. 2, pp. 57–73, Feb. 2008.

[36] Z. Ma, D. Callaway, and I. Hiskens, "Decentralized charging control for large populations of plug-in electric vehicles," *IEEE Trans. Control Systems Technology*, vol. 21, pp. 67–78, Jan 2013.

[37] A. Nemirovski and A. Shapiro, "Convex approximations of chance constrained programs," *SIAM J. Optim.*, vol. 17, no. 4, pp. 969–996, 2006.

[38] K. Parks, P. Denholm, and T. Markel, "Costs and emissions associated with plug-in hybrid electric vehicle charging in the XCEL energy Colorado service territory," Tech. Rep. NREL/TP-640-41410, National Renewable Energy Lab., 2007.

[39] A. Putrus, P. Suwanapingkarl, D. Johnston, E. C. Bentley, and M. Narayana, "Impact of Electric Vehicles on Power Distribution Network," in *IEEE Vehicle Power and Propulsion Conf.*, Dearborn, MI, Sept. 2009.

[40] M. Raginsky, R. F. Marcia, S. Jorge, and R. Willett, "Sequential probability assignment via online convex programming using exponential families," in *Proc. of IEEE Intl. Symp. Info. Theory*, Seoul, Korea, Jun.-Jul. 2009.

[41] N. Ross, "Fundamentals of Stein's Method," *Probability Surveys*, vol. 8, pp. 210–293, 2011.

[42] P. K. Sen, "The mean-median-mode inequality and noncentral Chi square distributions.," *Sankhyā: The Indian Journal of Statistics*, vol. 51, pp. 106–114, 1989.

[43] K. Seong, M. Mohseni, and J. M. Cioffi, "Optimal resource allocation for OFDMA downlink systems," in *Proc. of the Intl. Symp. on Info. Theory*, Seattle, WA, pp. 1394–1398, Jul. 2006.

[44] S. Shalev-Shwartz, "Online learning and online convex optimization.," *Foundations and Trends in Machine Learning*, vol. 4, no. 2, pp. 107–194, 2011.

[45] J. Soares, H. Morais, T. Sousa, Z. Vale, and P. Faria, "Day-Ahead Resource Scheduling Including Demand Response for Electric Vehicles," *IEEE Trans. Smart Grid*, vol. 4, pp. 596–605, Mar. 2013.

[46] S. Sojoudi and S. H. Low, "Optimal charging of plug-in hybrid electric vehicles in smart grids," in *Proc. of IEEE PES General Meeting*, Detroit, MI, Jul. 2011.

[47] N. Y. Soltani and G. B. Giannakis, "Online Learning of Electric Vehicle Consumers' Charging Behavior with Missing Data," in *Proc. of 2nd IEEE Global Conference on Signal and Information Processing*, Atlanta, Georgia, Dec. 2014 (Submitted).

[48] N. Y. Soltani, S.-J. Kim, and G. B. Giannakis, "Chance-Constrained Optimization of Uplink Parameters for OFDMA Cognitive Radios," in *Proc. of Intl. Conf. on Acoustics, Speech and Signal Processing*, Kyoto, Japan, Mar. 2012.

[49] N. Y. Soltani, S.-J. Kim, and G. B. Giannakis, "Chance-Constrained Optimization of Uplink Parameters for OFDMA Cognitive Radios," *IEEE Trans. Wireless Commun.*, vol. 12, pp. 1098–1107, Mar. 2013.

[50] N. Y. Soltani, S.-J. Kim, and G. B. Giannakis, "Dynamic Learning of Consumer Elasticity in Charging Electric Vehicles," in *Proc. of 5th Intl. Workshop on Computational Advances in Multi-Sensor Adaptive Processing*, Saint Martin, Dec. 2013.

[51] N. Y. Soltani, S.-J. Kim, and G. B. Giannakis, "Real-Time Load Elasticity Tracking and Pricing for Electric Vehicle Charging," *IEEE Trans. Smart Grid*, submitted 2014.

[52] K. Son, B. C. Jung, S. Chong, and D. K. Sung, "Power allocation for OFDM-based cognitive radio systems under outage constraints," in *Proc. of the Intl. Conf. Commun.*, Cape Town, South Africa, May 2010.

[53] E. Sortomme, M. M. Hindi, S. D. J. MacPherson, and S. S. Venkata, "Coordinated charging of plug-in hybrid electric vehicles to minimize distribution system losses," *IEEE Trans. Smart Grid*, vol. 2, pp. 198–205, Mar. 2011.

[54] N. Srebro, K. Sridharan, and A. Tewari, "On the universality of online Mirror Descent," in *Proc. of Advances in Neural Information Processing Systems*, Granada, Spain, Dec. 2011.

[55] C. Sutton and A. McCallum, *An introduction to conditional random fields for relational learning.* Introduction to Statistical Relational Learning: MIT Press, 2006.

[56] P. Tarasak, "Optimal real-time pricing under load uncertainty based on utility maximization for smart grid," in *IEEE Intl. Conf. on Smart Grid Commun.*, Brussels, Belgium, pp. 321–326, Oct. 2011.

[57] M. J. Wainwright and M. I. Jordan, "Graphical Models, Exponential Families, and Variational Inference," *Foundations and Trends in Machine Learning*, vol. 1, no. 1–2, pp. 1–305, 2008.

[58] R. Wang, V. K. N. Lau, L. Lv, and B. Chen, "Joint cross-layer scheduling and spectrum sensing for OFDMA cognitive radio systems," *IEEE Trans. Wireless Commun.*, vol. 8, pp. 2410–2416, May 2009.

[59] I. Wong and B. L. Evans, "Resource allocation in the OFDMA downlink with imperfect channel knowledge," *IEEE Trans. Wireless Commun.*, vol. 57, pp. 232–241, Jan. 2009.

[60] Y. Yao and G. B. Giannakis, "Rate-maximizing power allocation in OFDM based on partial channel knowledge," *IEEE Trans. Wireless Commun.*, vol. 4, pp. 1073–1083, May 2005.

[61] J. S. Yedidia, W. T. Freeman, and Y. Weiss, "Bethe free energy, Kikuchi approximations, and belief propagation algorithms," Tech. Rep. TR-2001-16, Mitsubishi Electric Reseach Laboratories, May 2001.

[62] R. Yu, W. Yang, and S. Rahardja, "A Statistical Demand-Price Model with its Application in Optimal Real-Time Price," *IEEE Trans. Smart Grid*, vol. 3, no. 4, pp. 1734–1742, 2012.

[63] W. Yu and R. Lui, "Dual methods for nonconvex spectrum optimization for multicarrier systems," *IEEE Trans. Commun.*, vol. 54, pp. 1310–1322, Jul. 2006.

[64] Y. Zhang and C. Leung, "Resource allocation in an OFDM-based cognitive radio system," *IEEE Trans. Commun.*, vol. 57, pp. 1928–1931, Jul. 2009.

[65] Y. J. Zhang and A. M.-C. So, "Optimal spectrum sharing in MIMO cognitive radio networks via semidefinite programming," *IEEE J. Sel. Topics commun.*, vol. 29, pp. 362–373, Feb. 2011.

[66] Q. Zhao and B. M. Sadler, "A survey of dynamic spectrum access: signal processing, networking, and regulatory policy," *IEEE Signal Processing Mag.*, vol. 4, pp. 79–89, May 2007.

[67] G. Zheng, K.-K. Wong, and B. Ottersten, "Robust cognitive beamforming with bounded channel uncertainties," *IEEE Trans. Sig. Proc.*, vol. 57, pp. 4871–1881, Dec. 2009.

[68] C. Zhu and N. Nigro, "Plug-in Electric Vehicle Deployment in the Northeast: A Market Overview and Literature Review," tech. rep., Center for Climate and Energy Solution (C2ES), Sep 2012.

[69] M. Zinkevich, "Online convex programming and generalized infinitesimal gradient ascent," in *Proc. of the 20th Inl. Conf. Machine Learning*, Washington, DC, pp. 928–936, Aug. 2003.